PERSONALIZED 2D-SELECTIVE RF EXCITATION IN HIGH FIELD MRI

Brain Center
Rudolf Magnus

Ronald Mooiweer

Personalized 2D-selective RF excitation in high field MRI

Ronald Mooiweer

ISBN 978-94-6299-933-6

Printed by: Ridderprint BV

Cover art by: Maarten de Vries, illustratie-bureau.nl

Generous financial support by Philips Healthcare for the publication of this thesis is gratefully acknowledged. Financial support by the Dutch Heart Foundation for the publication of this thesis is gratefully acknowledged.

Personalized 2D-selective RF excitation in high field MRI

Gepersonaliseerde 2D-selectieve RF excitatie in hoog-veld MRI

(met een samenvatting in het Nederlands)

Proefschrift

ter verkrijging van de graad van doctor aan de Universiteit Utrecht op gezag van
de rector magnificus, prof.dr. G.J. van der Zwaan, ingevolge het besluit
van het college voor promoties in het openbaar te verdedigen op
dinsdag 15 mei 2018 des middags te 4.15 uur

door

Ronald Mooiweer
geboren op 20 september 1987 te Zwolle

Promotor:	Prof.dr. P. R. Luijten
Copromotoren:	Dr. J.H.M. Hoogduin
	Dr.Ir. C.A.T. van den Berg

Contents

Chapter 1 1
Introduction

Chapter 2 15
Fast 3D isotropic imaging of the aortic vessel wall by applicationof 2D spatially selective excitation and a new way of inversion recovery for black blood imaging

Chapter 3 33
Combining a reduced field of excitation with SENSE-based parallel imaging for maximum imaging efficiency

Chapter 4 51
Phase matched RF pulse design for imaging a reduced field of excitation with a fast TSE acquisition

Chapter 5 63
Ultra-high isotropic resolution imaging of the hippocampus through a reduced field of excitation

Chapter 6 81
Summary and general discussion

Chapter 7 91
Nederlandse samenvatting

List of publications 95

Acknowledgements 97

Curriculum vitae 99

Chapter 1

Introduction

Chapter 1

Magnetic resonance imaging

Magnetic resonance images are typically generated through the application of three types of magnetic fields: the main static magnetic field (B_0), pulsed gradient fields (G), and pulsed radiofrequency (RF) fields (B_1^+). Through the careful arrangement of the latter two time varying magnetic fields, pulse sequences can be generated: nuclear spins are excited, their signal is spatially encoded such that images can be created, and they can be manipulated to generate a desired contrast. This contrast allows magnetic resonance imaging (MRI) to differentiate between different types of tissue, both in normal and pathological states.

Slice selective excitation

Slice selective excitation is commonly used to limit spin excitation along one dimension, such that the remainder of the sequence can focus on encoding the signal in the two other spatial dimensions. To achieve this, an RF excitation pulse is activated simultaneously with a slice-selective gradient (**Figure 1**). In the original view on slice-selective excitation, spin excitation is confined along the direction of one of the gradients as it alters the local precession frequency. The only region that is excited is where the bandwidth of the pulse RF pulse overlaps with the gradient-induced resonance frequency range.

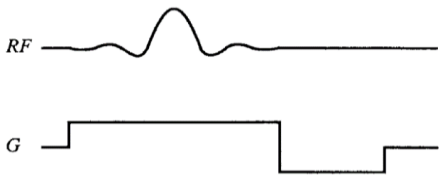

Figure 1. *Typical slice selective excitation pulse. A gradient lobe of opposite polarity and half the surface area of the slice selective gradient is used to rephase the magnetization. Image reproduced with permission of the rights holder, copyright © 1989 Elsevier Inc. [1].*

Transmit k-space

Pauly and coworkers redefined thinking about spin excitation by introducing the *transmit* k-space in 1989 [1]. In the transmit k-space approach, excitation patterns are created by depositing energy, using RF pulses, at different spatial frequencies, which are defined through simultaneously applied gradients. This is analogous to *imaging* k-space, where data originating from different spatial frequencies is collected and combined to create an image.

The spatial distribution of magnetization (**Equation 1**) follows from the Bloch equations when certain simplifications are applied: small tip angles ($M_z(t) \approx M_0$) are assumed and the relaxation effects from spin-lattice (T_1) and spin-spin (T_2) interactions are ignored. The magnetization is described as a complex value: $M_{xy} = M_x + iM_y$. This and all following equations in this chapter are described as seen from the rotating frame of reference.

$$M_{xy}(\mathbf{x}) = i\gamma M_0 \int_0^T B_1(t) e^{i\mathbf{x}\cdot\mathbf{k}(t)} dt. \qquad \text{(Eq. 1)}$$

Here γ is the gyromagnetic ratio, M_0 the equilibrium magnetization, T the time duration of the RF pulse, $B_1(t)$ the (amplitude of the) RF waveform, and $\boldsymbol{x}$ the spatial location vector. The location in transmit k-space at time t is defined by the time-integrated gradients **G** from t until the end of the pulse T:

$$\mathbf{k}(t) = -\gamma \int_t^T \mathbf{G}(\tau) d\tau. \quad \text{(Eq. 2)}$$

Transmit k-space can be understood from considering the spin magnetization vector $\boldsymbol{M} = [M_x\ M_y\ M_z]$, which experiences RF excitaiton at time t. Before t, the magnetization is in its equilibrium position M_0, and thus any gradients that are applied before that moment will not affect the spin distribution. As soon as the magnetization has been moved away from M_0, it will be affected by the gradients, explaining why the integral runs from t until the end of the pulse T. Owing to the linearity of the system in the small tip angle regime, the magnetization that results from the entire pulse of RF and gradients is then found by integrating over all time-steps dt in which RF energy is deposited at different k-space frequencies. An example of transmit k-space traversal for a slice selective pulse is shown in **Figure 2**.

Magnetization design

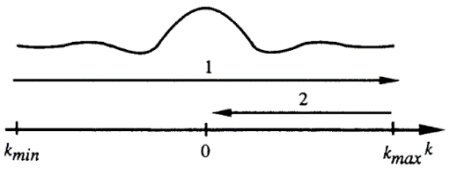

Figure 2. *Slice selection in the k-space approach. 1: During the application of the RF pulse, k-space is traversed from negative to positive frequencies. 2: The refocusing lobe ensures that the center of k-space is visited halfway through the symmetric RF pulse. Image reproduced with permission of the rights holder, copyright © 1989 Elsevier Inc. [1].*

Further analysis led Pauly and coworkers to describe the magnetization equation completely in the k-space domain, using a weighting function $W(\mathbf{k})$ and sampling function $S(\mathbf{k})$:

$$M_{xy}(\mathbf{x}) = i\gamma M_0 \int_{\mathbf{K}} W(\mathbf{k}) S(\mathbf{k}) e^{i\mathbf{x}\cdot\mathbf{k}} d\mathbf{k}, \quad \text{(Eq. 3)}$$

with

$$W(\mathbf{k}(t)) = \frac{B_1(t)}{|\gamma \mathbf{G}(t)|}, \quad \text{(Eq. 4)}$$

and

$$S(\mathbf{k}) = \int_0^T \{\, {}^3\delta(\mathbf{k}(t) - \mathbf{k}) |\dot{\mathbf{k}}(t)| \}\, dt. \quad \text{(Eq. 5)}$$

The sampling function follows from a chosen trajectory through transmit k-space, such as an echo-planar or spiral trajectory. The trajectory should meet certain conditions similar to imaging k-space, such as covering k-space uniformly and densely enough to prevent aliasing. If we choose an analytically defined target magnetization pattern $M_{xy}(\mathbf{x})$, we can use an inverse Fourier transform to determine what the weighting function should be for a given

transmit k-space trajectory. As the gradient waveform is also determined via the chosen k-space trajectory, and we can identify the corresponding time-varying shape of the RF pulse through:

$$B_1(t) = W\big(\mathbf{k}(t)\big)\,|\gamma \mathbf{G}(t)|. \qquad \text{(Eq. 6)}$$

2D spatially selective excitation

Not only does the k-space approach to excitation allows for more creative excitation patterns than slices, it opens up the way to create excitation pulses that are spatially selective in more than one dimension. Most notable is two-dimensional spatially selective excitation (2D SSE, **Figure 3**), where an RF pulse is used together with two orthogonal gradient pulses [2]. By localizing the excitation in two dimensions, and thus the region from which signal is generated, the encoding burden on the rest of the acquisition scheme is reduced. It might be possible with 2D SSE to shorten pulse sequences or to reduce artifacts related to obtaining short pulse sequences using other acceleration techniques. Inherent to the small tip angle approximation used in this method, excitation amplitudes are limited to tip angles up to 90°, and the technique is thus not suitable to create inversion or refocusing pulses.

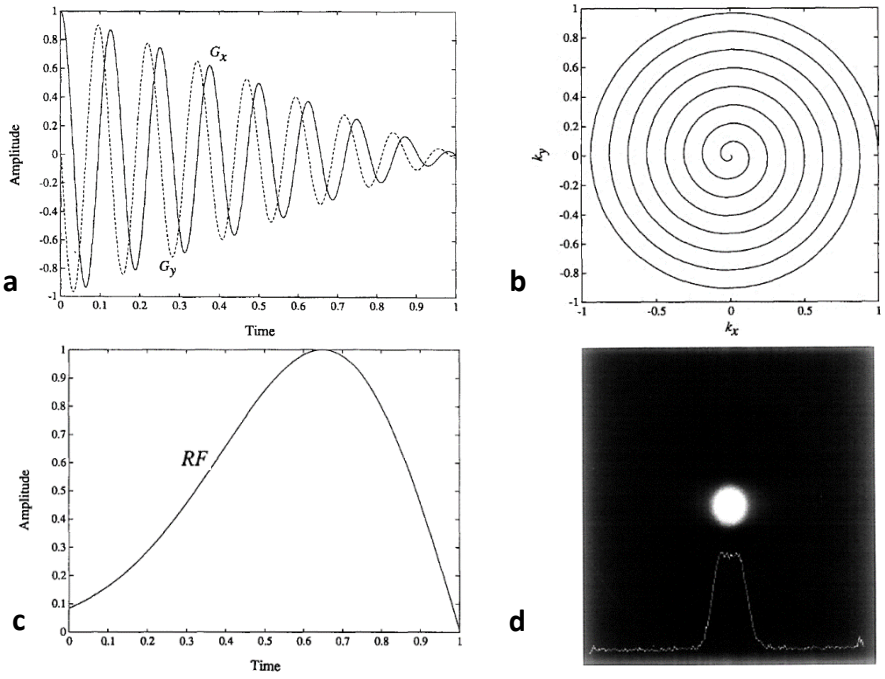

***Figure 3**. 2D SSE **a)** Gradient waveforms, describing the spiral-in transmit k-space trajectory in **b)**. Together with the RF waveform **c)** this produces a 2D SSE, of which an image and line profile are shown in **d)**. Images reproduced with permission of the rights holder, copyright © 1989 Elsevier Inc. [1].*

Numerically solving the discretized excitation equation

Further advancement in the design of multidimensional selective excitation pulses came from Yip and coworkers in 2005 [3]. By discretizing the excitation equation (**Equation 7**), with time steps matching the RF pulse samples, the problem can be written as a matrix equation (**Equation 8**). The entries in the encoding matrix **A** are filled according to **Equation 9**, and the RF waveform **b** can now be solved numerically (**Equation 10**) instead of analytically. The conjugate-gradient (CG) method [4] known from image reconstruction was used for the iterative optimization. A regularization has been introduced, controlled by regularization factor β. The regularization limits the amplitude of the RF waveform **b**, thereby limiting the RF power (**b**' **b**) and tissue heating (via the specific absorption rate (SAR)). The regularization also stabilizes the design problem, as the matrix **A** is typically ill-conditioned [5].

$$M_{xy}(\mathbf{x}) \approx i\gamma M_0 \sum_{j=0}^{N_t-1} b_j \, e^{i\mathbf{x}\cdot\mathbf{k}(t_j)+i\Delta\omega(\mathbf{x})[t_j-T]}\Delta t, \qquad \text{(Eq. 7)}$$

$$\mathbf{m} \approx \mathbf{A}\mathbf{b}, \qquad \text{(Eq. 8)}$$

$$a_{i,j} = i\gamma M_0 e^{i\mathbf{x}_i\cdot\mathbf{k}(t_j)+i\Delta\omega(\mathbf{x}_i)[t_j-T]}\Delta t, \qquad \text{(Eq. 9)}$$

$$\hat{\mathbf{b}} = \underset{\mathbf{b}}{\operatorname{argmin}}\{\|\mathbf{A}\mathbf{b}-\mathbf{d}\|_{\mathbf{W}}^2 + \beta\mathbf{b}'\mathbf{b}\}. \qquad \text{(Eq. 10)}$$

Additional improvement was made by taking into account local offsets in the resonance frequency Δω(**x**), which can be measured using a separate dual-echo gradient echo sequence (B_0 map). This matches the initially proposed k-space trajectory to what is actually achieved. So-called 'don't-care' regions were also introduced: through location-specific weighting (**w**) of the cost function of the numerical optimization, the weight of all locations outside a region of interest can be set to zero. In this way the air-containing voxels outside the body can be disregarded, further improving the fidelity of the targeted excitation pattern inside the region of interest, see **Figure 4**.

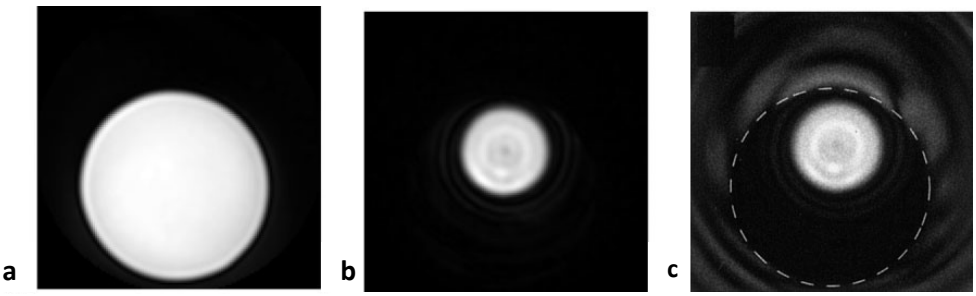

***Figure 4**. 2D SSE with iterative pulse design and ROI specification, phantom experiment. **a)** default excitation, **b)** 2D SSE, **c)** Bloch simulation of 2D SSE, the area outside the phantom (dashed circle) was specified as don't-care region for the numerical optimization. Images reproduced with permission of the rights holder, copyright © 2005 Wiley-Liss, Inc. [3].*

Parallel transmit and ultra high field MRI: renewed interest

As MRI scanners are manufactured with stronger main magnetic fields (offering increased magnetization), the effective RF field (and thus the resulting flip angle) becomes increasingly inhomogeneous inside the imaging objects. Parallel excitation using multiple transmit coils simultaneously (PTX) was invented to counteract this spatial inhomogeneity [6,7]. By taking into account the different coil sensitivities, and transmitting a unique waveform on every coil, the length of 2D SSE pulses could also be shortened compared single channel excitation [8]. Again, this technique on the transmit side has an earlier counterpart on the receive side: sensitivity encoded parallel imaging acceleration (SENSE) [9], explaining the other name for PTX: transmit SENSE.

Parallel transmit pulse design

Grissom and coworkers expanded the numerical pulse design method optimization with PTX [10]. The linearity of the system in the small tip angle regime allows the contributions of each transmit coil to be summed, taking into account the spatial sensitivity ($s(\mathbf{x})$) of each coil (labeled r).

$$m(\mathbf{x}) = i\gamma m_0 \sum_{r=1}^{R} s_r(\mathbf{x}) \int_0^T b_r(t)\, e^{i\gamma \Delta B_0(\mathbf{x})(t-T)} e^{i\mathbf{x}\cdot\mathbf{k}(t)} dt. \qquad \text{(Eq. 11)}$$

In the discretized form of the magnetization equation, the elements making up the encoding matrix **A** remain the same as in **Equation 9**, but the matrix **A** is concatenated for each transmit coil, and a diagonal matrix **D** is included that contains the coil sensitivity values (**Equation 12**). Inherent to this method, instead of calculating one RF waveform, separate waveforms $\mathbf{b_r}$ are calculated for each transmit coil, to be transmitted simultaneously.

$$\mathbf{m} = [\mathbf{D}_1\mathbf{A} \ldots \mathbf{D}_R\mathbf{A}] \begin{bmatrix} \mathbf{b}_1 \\ \vdots \\ \mathbf{b}_R \end{bmatrix} = \mathbf{A}_{full}\mathbf{b}_{full}. \qquad \text{(Eq. 12)}$$

This work has been hugely influential in the PTX community, as it was the first method that allowed PTX and transmit SENSE to be used in a simple way: PTX pulses could now calculated in the spatial domain rather than in the frequency domain [8]. All previous improvements such as local off-resonance correction and inclusion of 'don't-care' regions were now also available to PTX pulse design.

Time efficient pulse design

The latest developments in multidimensional RF pulse design that are used in this thesis were described by Sbrizzi and coworkers in 2011 [5]. A technique known from numerical linear algebra was adapted for the calculation of several pulses with different regularization factors *simultaneously*: multi shift conjugate gradients for least squares (mCGLS) [11]. This speeds up the process as generally the optimal regularization factor is not known beforehand, but rather chosen based on an L-curve that shows excitation error versus pulse amplitude. Also, a second regularization term is introduced that acts on the time differential of the RF waveform. This has a practical advantage as it promotes smooth waveforms, which are more

likely to be generated accurately by the RF amplifiers. The numerical optimization in its final form is now:

$$\hat{\mathbf{b}} = \underset{\mathbf{b}}{\operatorname{argmin}}\{\|\mathbf{Ab} - \mathbf{d}\|_2^2 + \beta\|\mathbf{b}\|_2^2 + \eta\|\mathbf{Db}\|_2^2\}, \qquad \text{(Eq. 13)}$$

with **D** the finite differences second derivative operator:

$$\mathbf{D} = \frac{1}{\Delta_t^2}\begin{pmatrix} -2 & 1 & 0 & 0 & \cdots \\ 1 & -2 & 1 & 0 & \cdots \\ 0 & 1 & -2 & 1 & \cdots \\ 0 & 0 & 1 & -2 & \cdots \\ \vdots & \vdots & \vdots & \vdots & \ddots \end{pmatrix}. \qquad \text{(Eq. 14)}$$

An example of 2D SSE using this latest method for RF pulse design is given in **Figure 5**. As the pulses are numerically optimized for personalized excitation targets and don't-care regions, and including measured field maps, these are truly *tailored* excitation pulses.

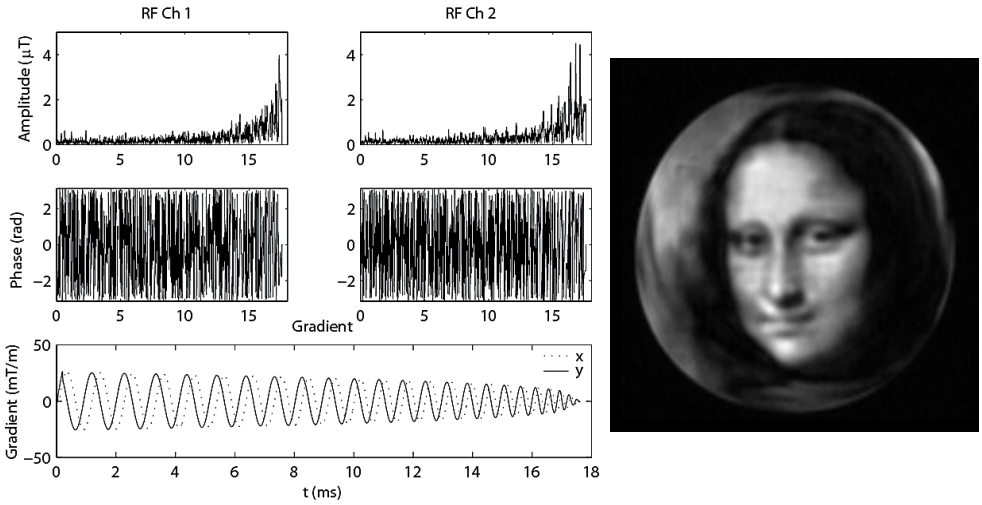

Figure 5. *Mona Lisa's portrait recreated using the mCGLS pulse design method [5]. Dual channel PTX was used, and a homogeneously doped phantom was imaged. Reproduced work from 'Mona Lisa's Magnetic Resonance', Mooiweer et al., Great Italian Art and Food Challenge, ISMRM Milan (2014).*

Applications of 2D SSE thus far

Several advantages have been identified in the earliest studies where 2D SSE has been applied in MR angiography. A rectangular 2D SSE was shown to improve angiographic contrast in the abdomen through reduced saturation outside the FOV [12]. In MR angiography of the coronary artery, a 2D SSE allowed for better imaging using a shortened 3D zonal EPI sequence [13]. In both cases, 3D imaging with 2D SSE was compared to 2D imaging with slice-selective excitation.

Later, 2D SSE was used to improve 2D imaging of the heart [14] and to reduce blurring in single shot fast spin echo sequences, [15,16]. Additionally, the SAR levels were reduced since less 180 degree refocusing pulses were needed in turbo spin echo (TSE) sequences and a shorter scan time was reported. It must be noted, however, that several reported advantages such as shorter scan times and related effects of reduced read out lengths, are not specific to 2D SSE, and might also be achieved by other methods such as such as parallel imaging acceleration [9,17,18]. None of these studies were seriously continued, and these initial applications of 2D SSE remained isolated.

A more persisting use of 2D SSE has been in EPI-based functional imaging (e.g. fMRI and DWI), where the benefits of limiting the excited area are more obvious. In these sequences a slice is completely encoded following one excitation, with single shot echo planar imaging (ss-EPI). As T_2 decay reduces the signal intensity along the length of the acquisition, the resulting

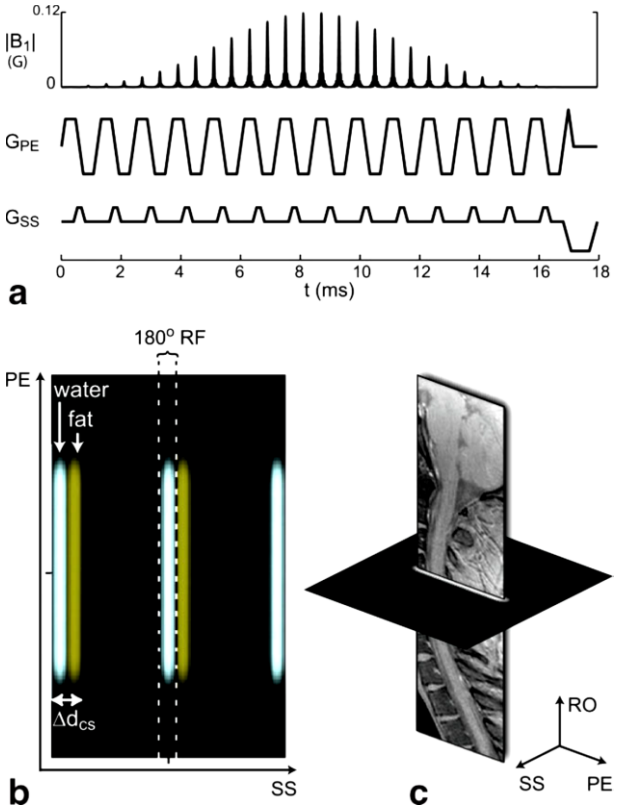

***Figure 6**. Echo planar 2D SSE with slice selective refocusing. **a)** RF pulse amplitude (|B_1|) and gradients, where 'phase encoding' gradients (G_{PE}) and 'slice selective' gradients are used to distinguish to fast and slow encoding direction respectively. **b**) A simulation shows aliasing of the excitation pattern in the slow encoding direction, with excitation displacement between water and fat due to the chemical shift (Δd_{cs}). Only one of the aliases of the water signal is selected to lead to signal generation, via a refocusing pulse (180° RF). **c)** A 2D image can now be generated with a single shot EPI sequence of reduced length. Image reproduced with permission of the rights holder, copyright © 2008 Wiley-Liss, Inc. [23].*

images are often blurred in ss-EPI. Additional geometrical distortions emerge from phase accrual due to susceptibility-induced local off resonances. With 2D SSE, a slice can be acquired faster, blurring can be reduced, and susceptibility-related artifacts can be avoided [19–23]. Fat suppression in ss-EPI sequences can also be improved, as 2D SSE provides additional control over the direction of chemical shift in the excitation [21,23]. In these applications, refocusing pulses are often used for additional selectivity and the 2D SSE pulses are usually not individually tailored. See **Figure 6** for an example.

An alternative way to limit the excitation in 2D is to use 1D selective excitation and 1D selective refocusing at orthogonal angles [24]. This method, referred to as inner volume imaging (IVI), lacks most of the flexibility that personalized 2D SSE offers and, again, does not allow pure gradient echo imaging. Expanded to 3D selection, this method is often used in spectroscopy [25]. Here, the unavailability of a frequency encoded readout makes spatial localization of the acquisition more challenging.

Aim of the thesis

The aim of this thesis is to study 2D SSE for structural imaging at (ultra) high field (UHF), with a particular 3D imaging strategy that fully encodes the excited volume from 2D SSE. The two directions in which the field of excitation is limited are encoded using phase encoding, such that the unrestricted 3rd dimension can be encoded using frequency encoding (**Figure 7**). This approach has already been suggested in 1989 [26], but has not been developed further.

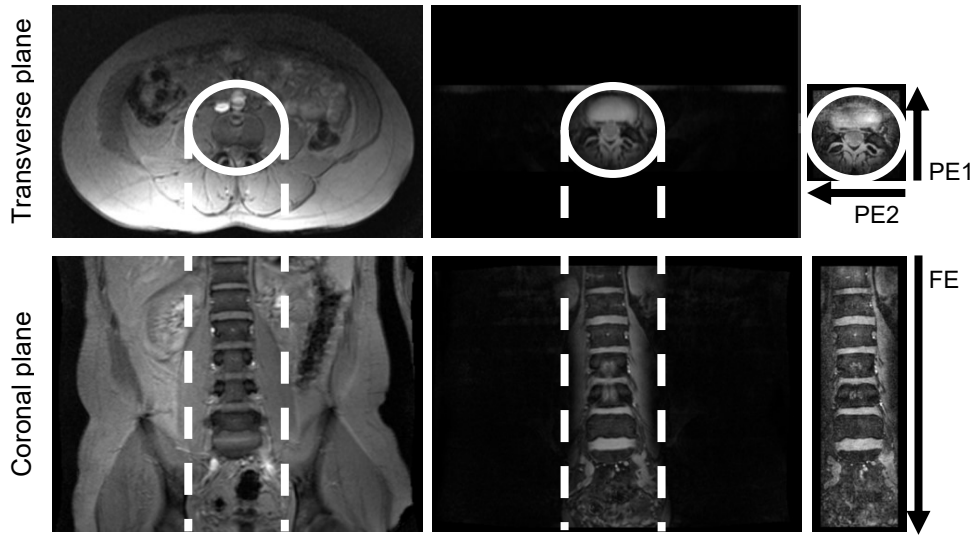

***Figure 7**. Example of 2D SSE with a 3D acquisition (**right column**), lumbar spine. A 2D SSE (**white circle**) is created in the transverse plane, with no excitation selection in the orthogonal direction (feet-head, **dashed white lines**). A 3D acquisition can be planned such that both phase encoding direction (PE1, PE2) benefit from the limited excitation field in the transverse plane, and the frequency encode direction (FE, 'read out') coincides with the nonselective direction (i.e. coronal or sagittal scan orientation).*

The immediate incentive for investigating 2D SEE has been the installation of a 7 T scanner in Utrecht, for multiple reasons:

- A major benefit of UHF is that the higher signal to noise ratio (SNR) allows imaging with increased resolution. Higher resolution requires a longer scan time, 2D SSE could reduce this.
- On the other hand, 2D SSE can reduce the available SNR in an image compared to a full 3D acquisition as less samples result in lower noise averaging. UHF offers a higher signal level to start from, ameliorating this effect.
- The transmit field at 7T is strongly inhomogeneous. 2D SSE pulses can create a homogeneous excitation locally, even when a single transmit coil is used, as transmit sensitivity information is taken into account in the design of the pulses.
- Parallel transmit systems are often installed at 7T scanners, enabling 2D SSE pulse shortening through transmit SENSE.

In particular, we hope to achieve: 1) 3D imaging at high isotropic resolution, 2) avoiding artifacts by strategically targeting the 2D SSE to exclude artifact-generating tissues. Numerically designed, field-informed, 2D SSE pulses are considered, that are calculated based on spiral k-space trajectories. Spiral transmit k-space trajectories are chosen as they can reduce the field of excitation indiscriminately in the two dimensions. In contrast, echo-planar k-space trajectories are defined along a fast and a slow k-space traversing speed. In the fast direction, a sharp excitation profile can be created, similar to slice-selection, but the selection fidelity of the second dimension is far more limited, such that additional refocusing selection is needed. Spiral excitation pulses can be used without additional pulses, possibly replacing all excitation pulses in a (gradient echo) sequence. Furthermore, in echo-planar pulses the center of k-space coincides with the center of the pulse, meaning that the shortest echo time is limited to at least half the pulse length. With trajectories that spiral inwards, the pulse ends in the center of k-space and no re-phasing is needed, allowing a short echo time.

Outline of the thesis

The aorta covers a small area on a transverse slice through the body, but is long in the feet head dimension, matching the intended application geometry of 2D SSE. Moreover, the standard imaging method was 2D, with anisotropic voxels sizes (largest along the length of the aorta) and gaps between the slices. In Chapter 2, a new approach to 3D imaging the vessel wall of the aorta was developed with the use of 2D SSE. This required re-thinking of the black-blood methods and adapting the pulse design strategy to the particular task at hand. Field maps that are obtained in the body often contain (motion) artifacts, and considering the large vertical range that we intended to image the aorta, the values obtained on one two-dimensional slice are not likely to be representative for the whole volume. Instead, an average representative value was chosen which was used for all voxels inside the region of pulse design. Improved image quality of the vessel wall was shown, compared an optimized 3D protocol with conventional excitation, mostly owing to the suppression of motion artifacts originating from the abdomen. This study was conducted at 3T.

In Chapter 3 the interplay between 2D SSE and parallel imaging is studied. The standard way of adapting an existing sequence to incorporate 2D SSE has always been to reduce the field

of view (rFOV) according to the excitation area. An rFOV is also used in parallel imaging acceleration, but aliasing artifacts are avoided through the use of receive coil sensitivity information. A greater flexibility can be obtained if 2D SSE and SENSE are combined into rSENSE.

Whereas initially gradient-echo based sequences are considered, in Chapter 4 the application of 2D SSE for TSE sequences is studied. 3D TSE with variable refocusing angles is often used for 7T imaging. Although our small-tip angle based pulse design method restricts us from calculating 2D selective refocusing pulses, the 3D TSE sequence can easily be combined with 2D SSE by only replacing the excitation pulse; the highly efficient non-selective refocusing pulses of variable flip angle can remain unchanged. This combination of custom excitation with standard refocusing pulses forces us to keep a close eye on the CPMG conditions. We describe how excitation pulses can be designed using the information that is available from B_1^+ mapping, such that they are compatible with default nonselective refocusing pulses for TSE imaging.

In the Chapter 5 we revisit our initial goal: improving structural imaging at 7T, by reporting on ultra-high resolution imaging of the hippocampus. The excitation pattern was designed to avoid possible artifacts originating from outside the hippocampus, such as the brain stem. Care was also taken to benchmark the 2D SSE approach against conventional methods. The study showed that 0.35mm isotropic voxels are possible by using 2D SSE, in scan time of only 10 minutes. For this, the flexibility of the rSENSE method as described in chapter 3 was exploited.

The results of this thesis are summarized in Chapter 6 and a general discussion is provided.

References

1. Pauly J, Nishimura D, Macovski A. A k-space analysis of small-tip-angle excitation. J. Magn. Reson. 1989;81:43–56. doi: 10.1016/0022-2364(89)90265-5.

2. Bottomley PA, Hardy CJ. Two-dimensional spatially selective spin inversion and spin-echo refocusing with a single nuclear magnetic resonance pulse. J. Appl. Phys. 1987;62:4284–4290. doi: 10.1063/1.339103.

3. Yip C, Fessler J a, Noll DC. Iterative RF pulse design for multidimensional, small-tip-angle selective excitation. Magn. Reson. Med. 2005;54:908–917. doi: 10.1002/mrm.20631.

4. Sutton BP, Noll DC, Fessler JA. Fast, iterative image reconstruction for MRI in the presence of field inhomogeneities. IEEE Trans. Med. Imaging 2003;22:178–188. doi: 10.1109/TMI.2002.808360.

5. Sbrizzi A, Hoogduin H, Lagendijk JJ, Luijten P, Sleijpen GLG, van den Berg C a T. Time efficient design of multi dimensional RF pulses: Application of a multi shift CGLS algorithm. Magn. Reson. Med. 2011;66:879–885. doi: 10.1002/mrm.22863.

6. Katscher U, Börnert P. Parallel RF transmission in MRI. NMR Biomed. 2006;19:393–400. doi: 10.1002/nbm.1049.

7. Zhu Y. Parallel excitation with an array of transmit coils. Magn. Reson. Med. 2004;51:775–784. doi: 10.1002/mrm.20011.

8. Katscher U, Börnert P, Leussler C, van den Brink JS. Transmit SENSE. Magn. Reson. Med. 2003;49:144–150. doi: 10.1002/mrm.10353.

9. Pruessmann KP, Weiger M, Scheidegger MB, Boesiger P. SENSE: sensitivity encoding for fast MRI. Magn. Reson. Med. 1999;42:952–62.

10. Grissom W, Yip C, Zhang Z, Stenger VA, Fessler J a, Noll DC. Spatial domain method for the design of RF pulses in multicoil parallel excitation. Magn. Reson. Med. 2006;56:620–629. doi: 10.1002/mrm.20978.

11. van den Eshof J, Sleijpen GLG. Accurate conjugate gradient methods for families of shifted systems. Appl. Numer. Math. 2004;49:17–37. doi: 10.1016/j.apnum.2003.11.010.

12. Alley MT, Pauly JM, Sommer FG, Pelc NJ. Angiographic Imaging with 2D RF Pulses. Magn. Reson. Med. 1997;37:260–267. doi: 10.1002/mrm.1910370220.

13. Yang GZ, Gatehouse PD, Keegan J, Mohiaddin RH, Firmin DN. Three-dimensional coronary MR angiography using zonal echo planar imaging. Magn. Reson. Med. 1998;39:833–42.

14. Abd-Elmoniem KZ, Barmet C, Stuber M. Free-breathing inner-volume black-blood imaging of the human heart using two-dimensionally selective local excitation at 3 T. Magn. Reson. Med. 2012;68:822–829. doi: 10.1002/mrm.23305.

15. Finsterbusch J. Fast-spin-echo imaging of inner fields-of-view with 2D-selective RF excitations. J. Magn. Reson. Imaging 2010;31:1530–7. doi: 10.1002/jmri.22196.

16. Yuan J, Zhao T-C, Tang Y, Panych LP. Reduced field-of-view single-shot fast spin echo imaging using two-dimensional spatially selective radiofrequency pulses. J. Magn. Reson. Imaging 2010;32:242–248. doi: 10.1002/jmri.22204.

17. Sodickson DK, Manning WJ. Simultaneous acquisition of spatial harmonics (SMASH): Fast imaging with radiofrequency coil arrays. Magn. Reson. Med. 1997;38:591–603. doi: 10.1002/mrm.1910380414.

18. Griswold M a, Jakob PM, Heidemann RM, Nittka M, Jellus V, Wang J, Kiefer B, Haase A. Generalized autocalibrating partially parallel acquisitions (GRAPPA). Magn. Reson. Med. 2002;47:1202–1210. doi: 10.1002/mrm.10171.

19. Rieseberg S, Frahm J, Finsterbusch J. Two-dimensional spatially-selective RF excitation pulses in echo-planar imaging. Magn. Reson. Med. 2002;47:1186–1193. doi: 10.1002/mrm.10157.

20. Samson RS, Lévy S, Schneider T, Smith AK, Smith SA, Cohen-Adad J, Wheeler-Kingshott CAMG. ZOOM or Non-ZOOM? Assessing spinal cord diffusion tensor imaging protocols for multi-centre studies. PLoS One 2016;11:1–14. doi: 10.1371/journal.pone.0155557.

21. Banerjee S, Nishimura DG, Shankaranarayanan A, Saritas EU. Reduced field-of-view DWI with robust fat suppression and unrestricted slice coverage using tilted 2DRF excitation. Magn. Reson. Med. 2016;1676:1668–1676. doi: 10.1002/mrm.26405.

22. Finsterbusch J. Functional neuroimaging of inner fields-of-view with 2D-selective RF excitations. Magn. Reson. Imaging 2013;31:1228–1235. doi: 10.1016/j.mri.2013.03.005.

23. Saritas EU, Cunningham CH, Lee JH, Han ET, Nishimura DG. DWI of the spinal cord with reduced FOV single-shot EPI. Magn. Reson. Med. 2008;60:468–473. doi: 10.1002/mrm.21640.

24. Feinberg D, Hoenninger JC, Crooks L, Kaufman L, Watts J, Arakawa M. Inner volume MR imaging: technical concepts and their application. Radiology 1985;156:743–747. doi: http://dx.doi.org/10.1148/radiology.156.3.4023236.

25. Bottomley PA. Spatial Localization in NMR Spectroscopy in Vivo. Ann. N. Y. Acad. Sci. 1987;508:333–348. doi: 10.1111/j.1749-6632.1987.tb32915.x.

26. Hardy CJ, Cline HE. Spatial localization in two dimensions using NMR designer pulses. J. Magn. Reson. 1989;82:647–654. doi: 10.1016/0022-2364(89)90230-8.

Chapter 2

Fast 3D isotropic imaging of the aortic vessel wall by application of 2D spatially selective excitation and a new way of inversion recovery for black blood imaging

This chapter has been published as:

Mooiweer, R., Sbrizzi, A., El Aidi, H., Eikendal, A. L.M., Raaijmakers, A., Visser, F., van den Berg, C. A.T., Leiner, T., Luijten, P. R. and Hoogduin, H. (2016*), Fast 3D isotropic imaging of the aortic vessel wall by application of 2D spatially selective excitation and a new way of inversion recovery for black blood imaging*. Magn Reson Med, 75: 547–555.

Abstract

Purpose: Aortic vessel wall imaging requires large coverage and a high spatial resolution, which makes it prohibitively time-consuming for clinical use. This work explores the feasibility of imaging the descending aorta in acceptable scan time, using 2D spatially selective excitation and a new way of inversion recovery for black blood imaging.

Methods: The excitation pattern and field of view in a 3D gradient echo sequence are reduced in two dimensions, following the aorta's anisotropic geometry. Black blood contrast is obtained by partially inverting the bloods magnetization in the heart at the start of the cardiac cycle. Imaging is delayed until the inverted blood has filled the desired part of the aorta. The flip angle and delay are determined such that the blood signal is nulled upon arrival in the aorta.

Results: Experiments on eight volunteers showed that the descending aortic vessel wall could be imaged over more than 15 cm at a maximal resolution of 1.5x1.5x1.5mm^3 in less than 5 minutes minimal scan time.

Conclusion: This feasibility study demonstrates that time-efficient isotropic imaging of the descending aorta is possible by using 2D spatially selective excitation for motion artifact reduction and a new way of inversion recovery for black blood imaging.

Introduction

Atherosclerosis is an inflammatory condition affecting the large and medium sized arteries and remains one of the most common causes of death worldwide (1). Its clinical sequelae affect millions of people every year. Plaque formation plays an essential role in the atherosclerotic pathophysiological pathway. Since plaque formation is a gradual process, timely detection and treatment is an important aim of prevention programs. MRI is a powerful tool for studying atherosclerosis (2,3). The aorta and the carotid arteries are strongly susceptible to atherosclerosis. Therefore appropriate, time-efficient sequences to image these vessels are highly desirable. The following specific properties define an adequate protocol for vessel wall characterization: sufficient spatial resolution, sufficient signal-to-noise ratio (SNR) and a field of view (FOV) that covers a large part of the vessel. Blood signal suppression, in short 'black blood' (BB), is also required to increase contrast between blood and vessel wall (2,4) and to prevent overestimation of vessel wall thickness due to slow flowing blood (5).

The current standard in MR based aortic wall visualization is Turbo Spin Echo (TSE) imaging combined with a dual inversion recovery (DIR) prepulse to obtain BB (6). Typically, high in-plane spatial resolution (1.0 x 1.0 mm^2) is used in combination with a much coarser slice thickness (5 mm, necessary to achieve adequate SNR) and gaps between the slices to accommodate imperfect slice profiles. Probing the atherosclerotic burden of the entire descending aorta would be very time-consuming using DIR TSE. Alternatively, several 3D imaging methods have been described where high resolution isotropic voxels allow for inspection of the vessel wall in any arbitrary direction (7). T1-SPACE is a 3D TSE sequence that shows promising image quality but requires over 30 minutes to image the entire descending aorta (8,9). The use of diffusion sensitizing gradients in 3D sequences has been demonstrated in the aorta (10), carotid arteries (11) and the heart (12). However, the diffusion sensitizing gradients can lead to some signal losses because of T2 decay and true diffusion effects. In addition, Roes et al (13) have described a 3D acquisition of the aorta using DIR combined with Turbo Field Echo (TFE) imaging, but the slab thickness of 2 cm makes it impractical for imaging the entire descending aorta.

Imaging time of the aorta can be shortened by choosing a reduced field of view (rFOV) to match the vessel's area on a transverse plane. This can be achieved by limiting the signal generating area, either by orthogonal excitation and refocusing pulses (14) or by two-dimensional spatially selective excitation pulses (2D SSE) (15–17). The rFOV approach has been employed to shorten scan times of DIR TSE and other sequences (18–22). However, the amount of longitudinal information is still limited because of the slice selective imaging sequences that are being used.

We propose a 3D gradient echo sequence that is specifically optimized for the aorta's anisotropic geometry. Two-dimensional spatially selective RF pulses are used to create a column-like excitation profile around the aorta, facilitating a rFOV with frequency encoding ("read out") along the longitudinal direction and phase encoding in the other two directions. Scan time reduction by using this rFOV is one of the possible advantages of 2D SSE. Another possible advantage of 2D SSE is that mobile tissue structures, which would otherwise lead to motion artifacts, can now be avoided in excitation, alleviating the need for breathing motion compensating techniques.

We also present a BB method that can be combined with the 3D acquisition. The BB method is based on saturating the magnetization of blood at the time of acquisition. Saturation is applied, not as it is typically done in a slice above and below the targeted imaging slice (23,24), but in a volume encompassing the heart's left ventricle. The saturating pre-pulse is applied at the beginning of each cardiac cycle before the left ventricular blood is ejected into the aorta. The rFOV is acquired in the diastolic phase when the blood bolus has reached the descending aorta, resulting in BB contrast. In this phase of the heart cycle the flow through the aorta is slow, so the vessel wall is not expected to show pulsating motion which could lead to artifacts. The proposed sequence, together with the reduced acquisition geometry, is referred to as 3D BB rFOV. The aim of this study is to test the feasibility of the proposed 3D BB rFOV sequence to image the descending aorta in a time-efficient manner.

Methods

Subjects

With approval of the Medical Ethics committee of the University Medical Center Utrecht, eight healthy volunteers without ferromagnetic implants were recruited and scanned. Four of the subjects were male, four female, and the average age was 25 (± 2) years. Written informed consent was obtained from all subjects.

MRI system

All scans were performed on a commercially available 3T multi-transmit MR system (Achieva, software release 3.2.1, Philips Healthcare, Best, The Netherlands), with a maximum gradient amplitude of 40 mT/m and maximum gradient slew rate of 200 mT/m/ms. Subjects were positioned between the anterior and posterior elements of a 32-channel phased array cardiac receiver coil (Philips). The scanner software was extended with an external RF and gradient waveform interface, which was used to load the subject specific pulses. First order B_0 shim correction was performed on a volume of 100 x 100 x 300 mm^3 around the descending aorta.

2D spatially selective pulse design

A flow chart of the pulse design process is shown in **Figure 1a**. In order to design an RF and gradient pulse combination that excites the desired 2D profile, B_0 and B_1^+ information together with the subject's geometry are needed. Therefore, maps of the local B_0 offsets (delta TE: 2.3 ms, scan time: 18 s) and B_1^+ efficiency (dual TR method (25), TR extension: 80 ms, scan time: 74 s[7]) were acquired of a transverse slice in the abdomen. In the pulse design process however, both the field maps were assumed to be uniform in the transverse plane since only one 2D spatially selective pulse is used to excite a 3D volume. The average value of the field maps measured in the aorta and direct surroundings was used for the whole transverse plane, to minimize excitation errors in the area of interest. A mask indicating the subject's torso was drawn on the first echo image of the B_0 map; the area outside this mask is not incorporated in the pulse design. The position of the aorta in the transverse plane was determined from transverse localizer images extending from the heart to the abdomen. An area covering these positions was specified as the target magnetization profile (**Figure 1b**).

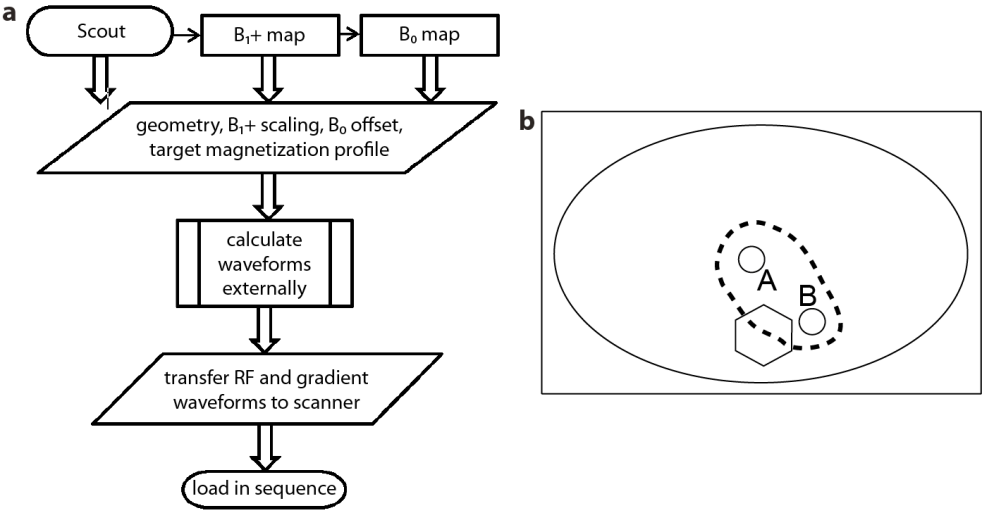

***Figure 1**. **a**: Flow chart of the pulse design process. **b**: Schematic overview of magnetization profile determination. Black box: full FOV, oval: outline of the body and mask for pulse design, hexagon: spine, circles: superposition of: A, aorta in the most caudal localizer scan and B, aorta in the most cranial localizer scan, dashed line: target magnetization profile.*

A spiral-in transmit k-space trajectory was designed within hardware limitations of the gradient system, with a maximum spatial frequency of 3 rad/cm to result in a pulse length of approximately 8 ms. High spatial frequencies of the target magnetization profile were filtered out by a two-dimensional Tukey window. The remaining profile was apodized in the frequency domain to match the extent of the transmit k-space trajectory.

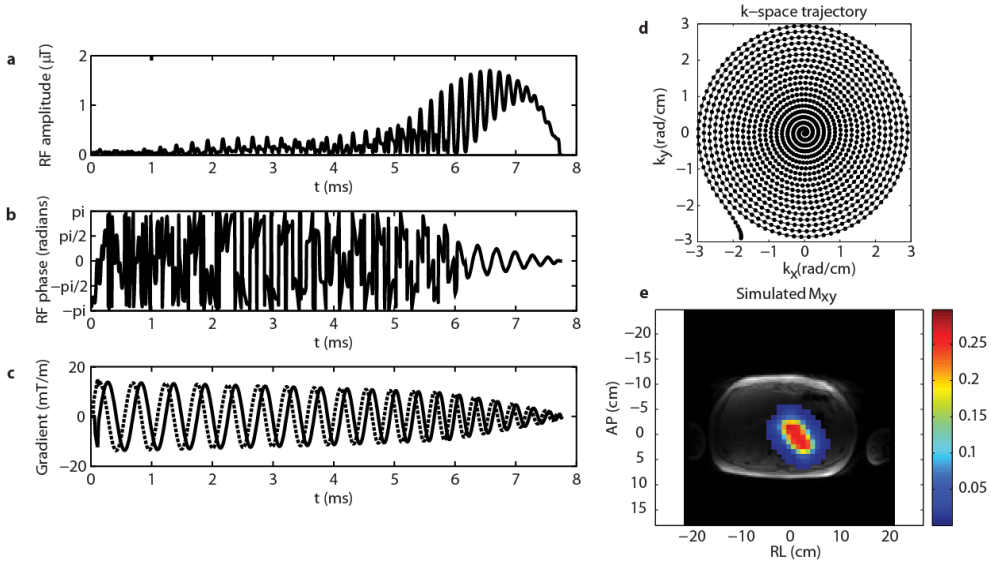

***Figure 2**. RF amplitude (**a**) and phase (**b**), and gradients (**c**) that result in the desired transmit k-space trajectory (**d**) and simulated transverse magnetization profile (**e**). The color filling representing the zero value in (**e**) was omitted to show the underlying anatomical scan.*

2D SSE RF pulses (FA = 15˚) were calculated following the method described in (26), a typical example is shown in **Figure 2**. The gradient trajectories were pre-compensated for short-term eddy currents (typical time constant 43 µs) that are not corrected for in the scanner software. Individual pulse design processes took about 2 minutes using MATLAB (R2014a, The MathWorks, Inc., Natick, Massachusetts, United States) on a computer with a 2.5 GHz dual core processor and 8 GB RAM.

Determining the rFOV geometry

The effect of the 2D SSE pulses was assessed on a low resolution (3.0 x 3.0 x 3.0 mm^3) gradient echo scan of the entire torso (scan time ≅ 2.5 minutes). The rFOV was planned on this large FOV scan, taking into account the obtained excitation profile. The subject specific rFOV dimensions are listed **in Table 1**.

Subject	rFOV (FH, AP, RL) (mm)	Voxel size (FH, AP, RL) (mm)	TFE factor	Startup echoes	TR	BB delay (ms)	Minimal acquisition time
1	425, 138, 99	1.50, 1.53, 1.50	30	25	16	400	4:14
2	425, 138, 99	1.50, 1.84, 1.50	25	25	16	400	3:54
3	425, 138, 99	1.50, 1.84, 1.50	25	25	17	425	4:14
4	425, 138, 99	1.50, 1.84, 1.50	25	25	17	425	4:14
5	425, 138, 80	1.50, 1.84, 1.50	25	25	16	400	3:26
6	425, 138, 80	1.50, 1.72, 1.50	20	25	16	400	3:45
7	425, 138, 80	1.50, 1.56, 1.50	25	25	16	400	4:13
8	425, 138, 99	1.50, 1.50, 1.50	14	20	16	320	4:33

***Table 1**. Parameters of the 3D BB rFOV scans for 8 volunteers. Inter subject variations in rFOV and heart rate required subject specific timing properties, resulting into slight variations in voxel sizes. The actual acquisition time can be larger than the minimal acquisition time due to heart rate irregularities.*

Timing of the rFOV 3D BB TFE scan: 3D BB

BB in the aorta for a 3D acquisition was achieved by nulling the longitudinal magnetization of the blood bolus in the aorta when the excitation pulses are applied for imaging. The sequence timing and geometry is illustrated in **Figure 3**. A saturation slab on the heart is timed directly after the R-wave is detected by electrocardiography (ECG) since the moments after the R-wave coincide with the isovolumetric contraction of the ventricles and a large volume of blood is present in the left ventricle for saturation. The magnetization-saturated blood coming from the left ventricle will replace the blood in the descending aorta approximately 400 ms after the R-wave (27,28). From this time on, images of the aorta are acquired using TFE. The required interval between the saturation slab and TFE train is realized by adding 25 dummy startup echoes before the actual TFE train. Bloch simulations showed that the low flip angle (FA), 2D RF excitation pulses in the startup echoes do not significantly influence M_z regrowth of the blood (data not shown). The saturation pulse intensity is increased to the empirically derived FA of 216˚. This FA was found to result in the best BB contrast after evaluating different flip angles (168, 192, 216 and 240˚). This increased FA was needed to pre-compensate for T1 recovery of the blood during the interval (assuming a blood T1 of 1650 ms at 3T (29)) and to

take into account the local transmit efficiency. In fact, the saturation pulse can be viewed as a partial inversion pulse that leads to signal saturation at the time of imaging.

Based on the ECG-detected heart rate, small changes in the number of startup echoes and the TFE factor were made. The individually adapted acquisition parameters are listed in Table 1. While an isotropic resolution of 1.5 x 1.5 x 1.5 mm^3 was demanded, subject specific geometries and timing parameters resulted in up to 23% larger voxel sizes in the AP direction. The fixed scan parameters were: sagittal slice orientation, multi shot TFE, profile order: low-high, TR: shortest (16 - 17 ms), ECG trigger delay: shortest, TE: 2.3 ms, FA: 15˚, reconstructed voxel sixe: 1.5 mm, SENSE: 1x1. Fat suppression was achieved by globally applying a Spectral Presaturation with Inversion Recovery (SPIR) pulse before the spatial saturation pulse for BB. Also, as part of the standard 3D gradient echo scan protocol, oversampling with a factor 1.4 is applied in the slice direction (left-right).

Additional scans

To show that the combination of 2D SSE and 3D BB is needed to generate useful images, two additional scans were performed in which one of the techniques was not used. First, instead of the 2D SSE pulse, a standard slice selective excitation pulse was chosen. Accordingly, the FOV was extended to cover the complete AP span of the subjects. In RL direction the number of sagittal slices was chosen to tightly fit the aorta. Second, in one subject an ECG-triggered 3D TFE rFOV scan with and without saturation slab was made to illustrate the effect of the 3D BB method.

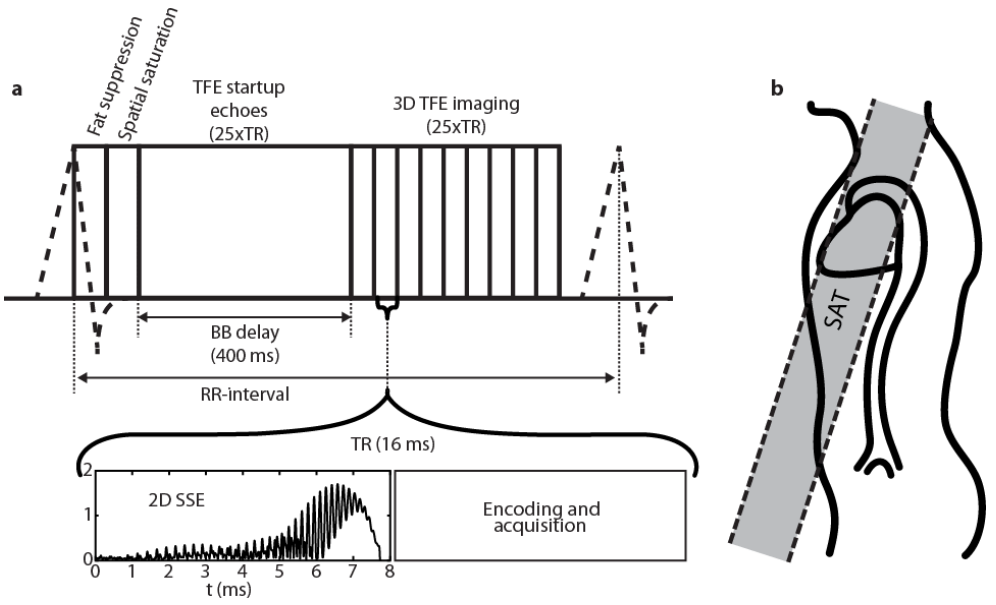

***Figure 3**. **a**: timing of the 3D BB rFOV sequence with respect to the ECG signal. **b**: Positioning of the spatial saturation slab (SAT), sketched in the sagittal plane.*

For five out of eighth subjects, higher spatial resolution images of 1.0 x 1.0 x 1.0 mm^3 were also obtained using the 3D BB rFOV sequence. The aim of these scans was to investigate whether a higher resolution scan would improve vessel wall delineation with still acceptable SNR. Theoretically the SNR is expected to be almost half that of the 1.5 mm scans ($SNR_{1mm3} = SNR_{1.5mm3} / \sqrt{(1.5^3)}$).

Image Evaluation

The extent of the aorta that can be imaged with BB properties is determined by the length of the blood bolus that is ejected by the left ventricle and underwent magnetization saturation in the heart. To quantitatively assess the extent over which BB contrast was achieved, the average signal intensity from the lumen was measured for every transverse reformatted slice containing the descending aorta. This average intensity was normalized to the average intensity of the vessel wall to take into account absolute signal fluctuations related to coil sensitivities. Vessel wall and lumen contours were determined using VesselMASS (Medis specials, Leiden, The Netherlands) (30). Contours were manually drawn in the first and last slice that depicted the aorta and every 11^{th} slice in between. Interpolation was used to determine the contours in the remaining slices.

For every subject, transverse reformatted images of the vessel wall at 16.5 mm intervals were visually scored by 3 observers (HA, AE, TL). All images were anonymized and presented in random order to the observers. The marks were as follows (31,32): 1: undistinguishable aortic wall, 2: partially visible aortic wall (<50% of circumference) but with incomplete borders, 3: partially visible aortic wall (50% – 75% of circumference) and distinguishable from the lumen and surrounding; 4: mostly distinguishable aortic vessel wall with only small portions (<25%) of the vessel wall not visible, and 5: the aortic vessel wall is completely visible with sharply defined borders. Images scored 4 or higher were considered to be of adequate quality for potential future clinical applications (31).

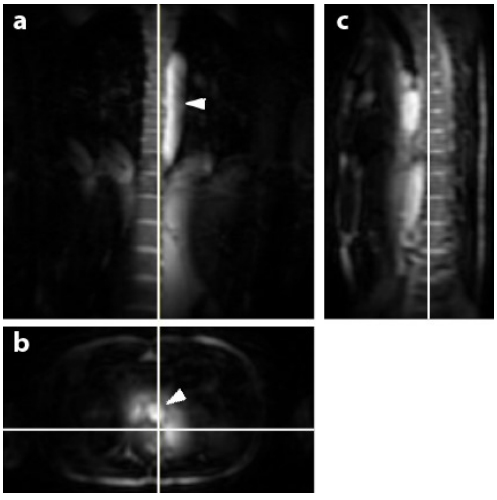

***Figure 4**. Low resolution 3D full FOV scan showing the 2D excitation pattern in the coronal (**a**), transverse (**b**) and sagittal (**c**) plane. The transverse image was reformatted at the height of the B0 and B1+ maps used for pulse design and the locations of the coronal and sagittal scans are marked in all three images. Arrowheads point to the aorta.*

Results

The typical excitation pattern of the 2D SSE pulses is shown in **Figure 4**, in a low resolution scan across the entire torso. A large signal intensity difference between the region of interest (in the center of the transverse image, around the descending aorta) and the rest of the FOV can be observed. A typical example of a 3D BB scan without 2D SSE and rFOV is shown in **Figures 5a** and **5b**. Noticeable motion artifacts are present in these images. To illustrate the effect of the saturation prepulse, **Figures 5c** and **5d** show transverse reformatted slices of the 3D BB rFOV scans without and with saturation for BB contrast. In the former case, the distinction between blood and vessel wall can hardly be made, while in the latter case the BB contrast allows for vessel wall characterization.

3D BB rFOV datasets were successfully acquired in all 8 subjects. Examples are summarized in **Figure 6**, where transverse reformatted images are shown of all volunteers. Clear depiction of the aortic vessel wall can be observed in most images. Several images, mostly in the lower, abdominal, regions show substantial signal intensity in the aortic lumen.

Image analysis

Figure 7 shows the image evaluation on BB and vessel wall visibility for all subjects. Slices with an intensity ratio of 0.5 or lower corresponded well with manually observed adequate blood to vessel wall contrast. An average number of 118 ± 18 slices of the descending aorta could successfully be imaged with BB contrast, with a minimum of 91 and a maximum of 134 slices per subject. This corresponds to 17.7 ± 2.7 cm.

The vessel wall scoring to assess the SSE fidelity follows the trend of the lumen intensity ratio. In the most caudal sections of the aorta the vessel wall visibility is low and the blood signal is high. Furthermore, vessel wall imaging quality locally degrades around 120 cm from the aortic arch. This position corresponds to the level of the thoracic diaphragm. Over all subjects, 63% ± 14% of the slices presented to the experts were scored to be of adequate quality by all

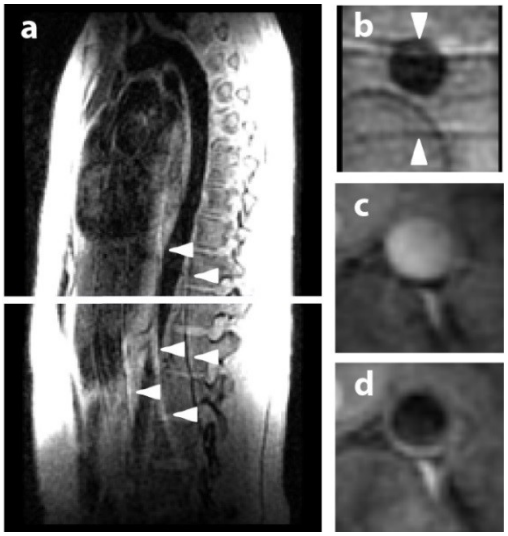

***Figure 5**. Scans showing the effects on vessel wall imaging of a full FOV in combination with the 3D BB method (**a**,**b**), of a rFOV without 3D BB (**c**), and of both the 3D BB and rFOV methods combined (**d**). Subfigures **b**, **c**, and **d** are transverse reformatted and cropped images, with the location of **b** marked with a line in **a**. Arrowheads point to motion artifacts in the sagittal (**a**) and transverse (**b**) slices of the full FOV scan. The images in **c** and **d** show a different subject than **b**, yet at a similar anatomical location.*

observers. Interpolating this ratio to the 179 ± 20 transverse slices containing the descending aorta leads to an average number of 112 ± 30 (min 70, max 165) slices per subject that are suitable for evaluation.

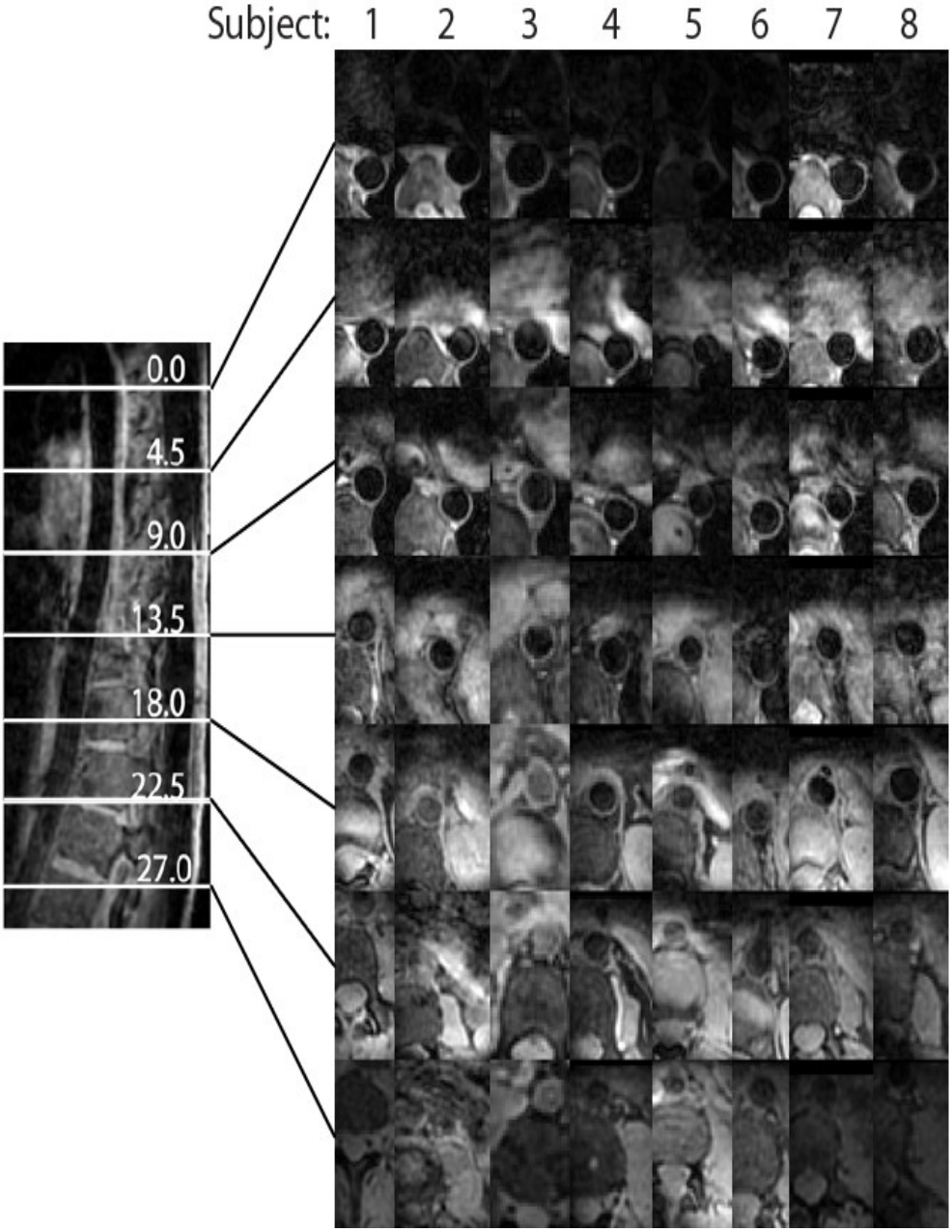

***Figure 6**. Reduced field of view images of the aortic vessel wall for all volunteers (**1**-**8**, left to right). Cross sections of the original sagittal scans are shown with 4.5 cm interval (top to bottom) as marked in the sagittal scan on the left. The images are cropped tightly around the aorta.*

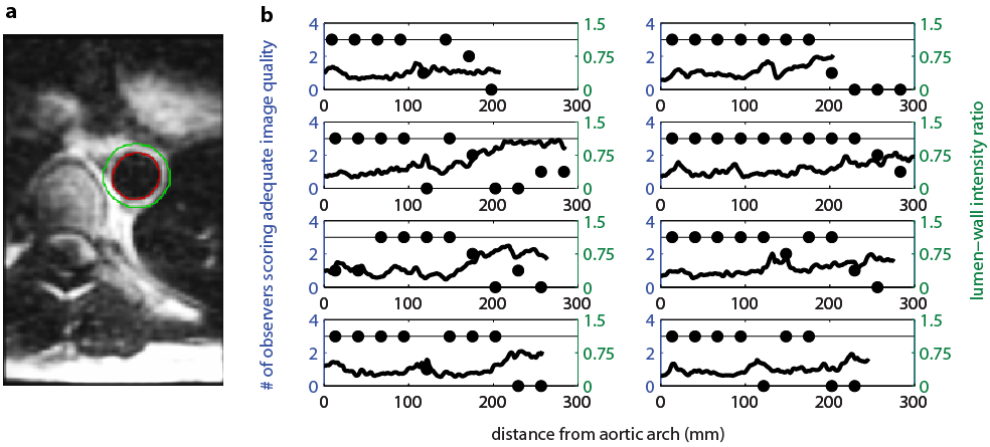

***Figure 7**. **a**: Example of vessel wall contour definition in VesselMASS. Red contour: demarcation of the lumen, green contour: demarcation of the outer edge vessel wall. **b**: Number of observers scoring adequate image quality (black circles) and the ratio of average signal level of the lumen to that of the vessel wall for all subjects (black continuous line). The horizontal black line is a guide to the eye at the vertical position of all three observers scoring adequate image quality.*

High spatial resolution scans

For five out of eight subjects an additional acquisition was made at a higher spatial resolution of 1.0 x 1.0 x 1.0 mm^3, as shown in **Figure 8**. The increased spatial resolution can be appreciated in the sharper depiction of the aortic vessel wall as compared to **Figure 6**, but this comes at the expense of a slightly higher noise level.

Discussion

The 2D SSE pulses performed robustly in practice. Even though spatial B_0 and B_1^+ field variations were not taken into account and the pulses were calculated on one transverse slice only, no obvious signal folding back from excitation outside the rFOV was observed. At the longitudinal extremities of the FOV, blurring of the excitation profile due to B_0 offset and signal loss due to B_1^+ reduction are expected. Still, a high number of transverse slices with adequate vessel wall visibility could be observed. The reduced image quality around 12 cm below the aortic arch is thought to be due to B_0-variations near the diaphragm, amplified by breathing effects. This may be counteracted by imaging only in the expiration phase of the breathing cycle, at the expense of a significantly increased scan time. Another point is that the usage of subject specific pulses requires more preparation steps than using regular excitation pulses. This process costs time, but integrating it with the scanner software could reduce it.

Fat suppression is necessary because the 2D SSE pulses are designed for the resonance frequency of water rather than fat. Because of the additional delay needed for BB, between the prepulses and the acquisition, the effectiveness of the fat suppressing prepulse is expected to be reduced. Nonetheless, no significant fold back artifacts from fat signal outside the rFOV were observed.

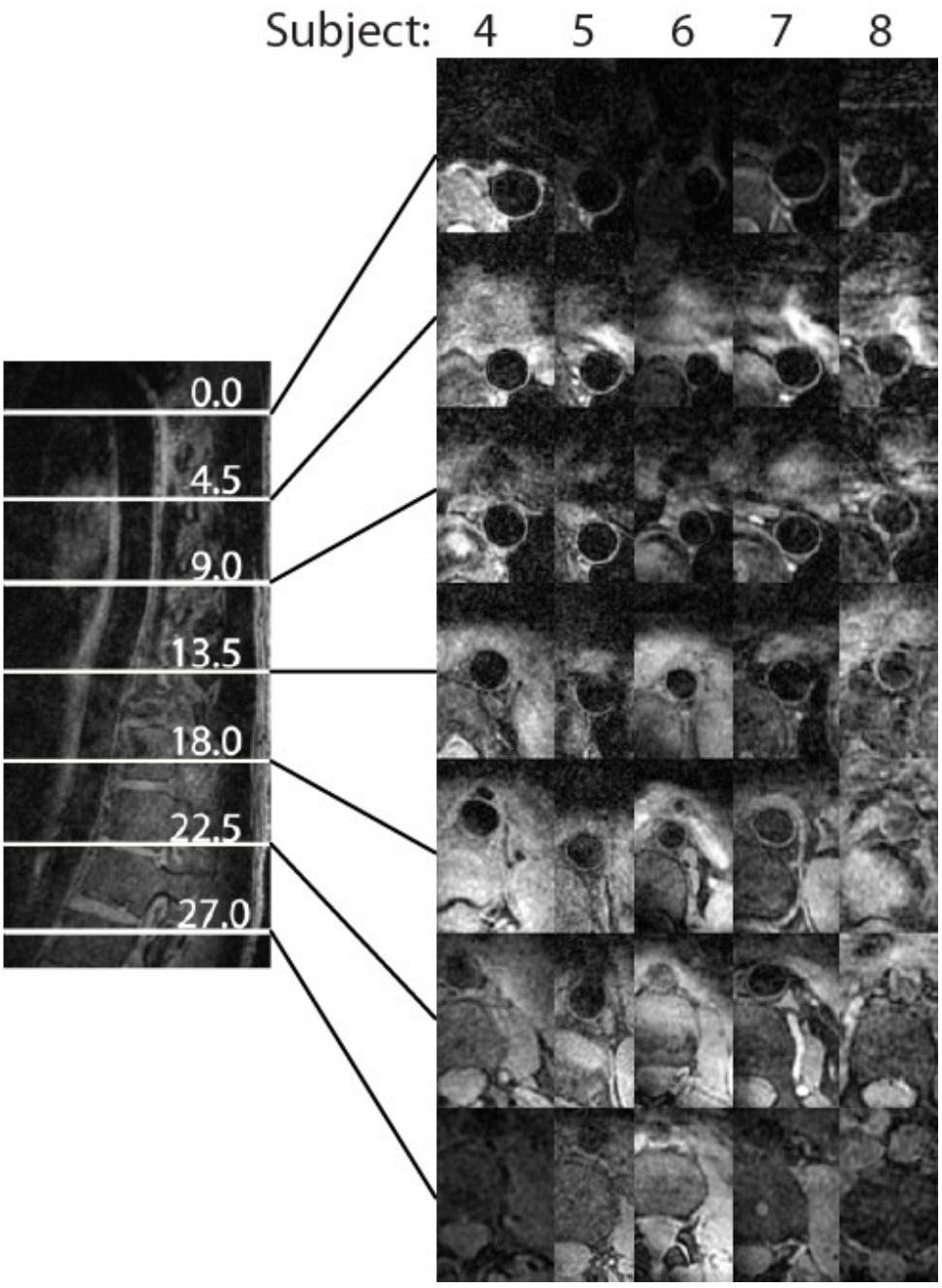

***Figure 8**. Reduced field of view images of the aortic vessel wall for five volunteers (**4**-**8**, left to right) at 1 mm³ resolution. Cross sections of the original sagittal scans are shown with 4.5 cm interval (top to bottom) as marked in the sagittal scan on the left. The images are cropped tightly around the aorta. Divergent from the 3D BB rFOV protocol, the scans in subject 4 and 5 were acquired using SENSE factor 1.5 in AP and RL directions and 2 signal averages.*

From the image quality analysis, 112 ± 30 slices of 1.5 mm thickness per subject were found to be of adequate image quality. Although some slices had to be discarded, in principle this technique offers inspection of the vessel wall over a contiguous volume. Images were acquired with an average minimum scan time of 4:04 minutes, corresponding to 2.2 ± 0.7 seconds per transverse slice. The reported minimal scan time does not take into account additional time required (up to 50%) due to non-perfect detection of the R-wave (with irregular heart rates). Still, the coverage of 3D BB rFOV is much larger and with greater longitudinal detail than what the conventional techniques can achieve in the same scan time (DIR TSE: 9 slices of 5 mm thickness in 5 minutes, zoom-DIR/QIR: 33 slices of 5 mm thickness at 11 heartbeats per slice). Only SPACE imaging is approaching the efficiency of 3D BB rFOV imaging. While Mihai et al. still need 30 minutes for 3D imaging the entire descending aorta (8), Dragonu et al. recently showed imaging of the entire aorta at 1 mm^3 isotropic resolution in 8:17 minutes ± 1:48 minutes (33). However, this was done using a T2-weighted sequence, while T1-weighting is desired for plaque analysis.

The 3D BB method by partial inversion in the heart can provide BB contrast in a large part of the aorta: on average 118 ± 18 slices of 1.5 mm thickness per subject. This method could be combined with a wide variety of sequences, but is inherently limited by the blood volume ejected into the aorta. It would be interesting to see the performance of this technique in populations with suspected or known atherosclerotic disease. If the displacement of partially inverted blood is larger than the imaging volume after 400 ms, no difference in black blood properties is to be expected compared to healthy volunteers. However, when the displacement of the bolus does not reach the end of the imaging volume at the start of the acquisition a smaller portion of the aorta is expected to be imaged with black blood properties. If the cardiac output is sufficiently large, the BB delay can be increased (with corresponding higher FA) to improve the BB coverage. For future clinical application of the proposed method, automatic computation of the inversion delay time based on heart rate could be added to the scanner software. If so desired, the 2D rFOV with a 3D read out can also be combined with other black blood techniques.

The minimal TR available in the proposed sequence was higher (16 - 17 ms) than necessary to take into account the encoding gradients durations and SAR levels. In fact, a TR shorter than twice the excitation pulse duration was not allowed. This is probably a limitation imposed by the gradient duty cycle model of the scanner. Shorter pulses could increase the efficiency of the sequence, for instance these could be achieved by using Transmit SENSE (34). However, shortening the TR will result in a lower signal level and a different effective contrast mechanism for which the vessel wall depiction quality has not been evaluated.

The motion artifacts present in the 3D BB scans without 2D SSE and rFOV can typically be avoided by using frequency encoding in the AP direction. However, this would lead to a longer scan time of about 8 minutes. By using 2D SSE these motion artifacts can be avoided and efficient imaging with frequency encoding in the longitudinal direction can be achieved. Compared to the sagittal acquisition with frequency encoding in the AP direction to avoid motion artifacts, the rFOV approach is roughly 2 times faster.

The currently investigated 3D BB rFOV sequence does not yield enough SNR to facilitate 1 mm isotropic resolution, as was demonstrated by the high spatial resolution scans. Signal

averaging or moderately increasing the rFOV can be employed to increase the SNR. However, this comes at the expense of an increased scan time.

A limitation of this study is the low number of participants. Before clinical implementation, this sequence should be tested in a larger number of participants. Also, a direct comparison between the proposed technique and other 3D BB methods is recommended. These studies are conducted preferably in patients with proven atherosclerosis, to evaluate the BB effectiveness under the physiological conditions in which the vessel wall imaging sequences are to be employed. The images presented in this paper are T1 weighted. Although T1 is the most important contrast mechanism in plaque detection and analysis, further studies on this subject may require a multi-contrast approach to acquire more information on the plaque's composition. T2 weighted imaging can be achieved by changing sequence timing parameters, or by adding pre-pulses.

Conclusion

By using 2D spatially selective pulses, we have successfully imaged the descending aorta in 3D at isotropic resolution. A new way of inversion recovery for black blood imaging suitable for 3D imaging has been introduced which employs spatial saturation and the natural flow of blood. This BB technique provides sufficient contrast between the vessel wall and the lumen in the thorax, from the aortic arch to well below the diaphragm. The longitudinal coverage of the proposed method is larger and the longitudinal resolution is higher than currently available methods can obtain in the same scan time.

Acknowledgements

This study is part of the EU Artemis High Profile project.

References

1. Lloyd-Jones D, Adams RJ, Brown TM, et al. Heart disease and stroke statistics--2010 update: a report from the American Heart Association. Circulation 2010;121:e46–e215. doi: 10.1161/CIRCULATIONAHA.109.192667.

2. Gallino A, Stuber M, Crea F, et al. "In vivo" imaging of atherosclerosis. Atherosclerosis 2012;224:25–36. doi: 10.1016/j.atherosclerosis.2012.04.007.

3. Leiner T, Gerretsen S, Botnar R, Lutgens E, Cappendijk V, Kooi E, van Engelshoven J. Magnetic resonance imaging of atherosclerosis. Eur. Radiol. 2005;15:1087–99. doi: 10.1007/s00330-005-2646-8.

4. Fayad Z a., Nahar T, Fallon JT, Goldman M, Aguinaldo JG, Badimon JJ, Shinnar M, Chesebro JH, Fuster V. In Vivo Magnetic Resonance Evaluation of Atherosclerotic Plaques in the Human Thoracic Aorta : A Comparison With Transesophageal Echocardiography. Circulation 2000;101:2503–2509. doi: 10.1161/01.CIR.101.21.2503.

5. Wang J, Yarnykh VL, Hatsukami T, Chu B, Balu N, Yuan C. Improved suppression of plaque-mimicking artifacts in black-blood carotid atherosclerosis imaging using a multislice motion-sensitized driven-equilibrium (MSDE) turbo spin-echo (TSE) sequence. Magn. Reson. Med. 2007;58:973–81. doi: 10.1002/mrm.21385.

6. Jaffer F a. Age and Sex Distribution of Subclinical Aortic Atherosclerosis: A Magnetic Resonance Imaging Examination of the Framingham Heart Study. Arterioscler. Thromb. Vasc. Biol. 2002;22:849–854. doi: 10.1161/01.ATV.0000012662.29622.00.

7. Balu N, Yarnykh VL, Chu B, Wang J, Hatsukami T, Yuan C. Carotid plaque assessment using fast 3D isotropic resolution black-blood MRI. Magn. Reson. Med. 2011;65:627–37. doi: 10.1002/mrm.22642.

8. Mihai G, Chung Y-C, Merchant A, Simonetti OP, Rajagopalan S. T1-weighted-SPACE dark blood whole body magnetic resonance angiography (DB-WBMRA): initial experience. J. Magn. Reson. Imaging 2010;31:502–9. doi: 10.1002/jmri.22049.

9. Wong SK, Mobolaji-Iawal M, Arama L, Cambe J, Biso S, Alie N, Fayad Z a, Mani V. Atherosclerosis imaging using 3D black blood TSE SPACE vs 2D TSE. World J. Radiol. 2014;6:192–202. doi: 10.4329/wjr.v6.i5.192.

10. Koktzoglou I, Kirpalani A, Carroll TJ, Li D, Carr JC. Dark-blood MRI of the thoracic aorta with 3D diffusion-prepared steady-state free precession: initial clinical evaluation. AJR. Am. J. Roentgenol. 2007;189:966–72. doi: 10.2214/AJR.07.2428.

11. Makhijani MK, Hu HH, Pohost GM, Nayak KS. Improved blood suppression in three-dimensional (3D) fast spin-echo (FSE) vessel wall imaging using a combination of double inversion-recovery (DIR) and diffusion sensitizing gradient (DSG) preparations. J. Magn. Reson. Imaging 2010;31:398–405. doi: 10.1002/jmri.22042.

12. Srinivasan S, Hu P, Kissinger K V, Goddu B, Goepfert L, Schmidt EJ, Kozerke S, Nezafat R. Free-breathing 3D whole-heart black-blood imaging with motion sensitized driven equilibrium. J. Magn. Reson. Imaging 2012;36:379–86. doi: 10.1002/jmri.23662.

13. Roes SD, Westenberg JJM, Doornbos J, van der Geest RJ, Angelié E, de Roos A, Stuber M. Aortic vessel wall magnetic resonance imaging at 3.0 Tesla: a reproducibility study of respiratory navigator gated free-breathing 3D black blood magnetic resonance imaging. Magn. Reson. Med. 2009;61:35–44. doi: 10.1002/mrm.21798.

14. Feinberg D, Hoenninger JC, Crooks L, Kaufman L, Watts J, Arakawa M. Inner volume MR imaging: technical concepts and their application. Radiology 1985;156:743–747.

15. Pauly J, Nishimura D, Macovski A. A k-space analysis of small-tip-angle excitation. J. Magn. Reson. 1989;81:43–56. doi: 10.1016/0022-2364(89)90265-5.

16. Alley MT, Pauly JM, Sommer FG, Pelc NJ. Angiographic Imaging with 2D RF Pulses. MRM 1997:260–267.

17. Yang GZ, Gatehouse PD, Keegan J, Mohiaddin RH, Firmin DN. Three-dimensional coronary MR angiography using zonal echo planar imaging. Magn. Reson. Med. 1998;39:833–42.

18. Crowe L a, Gatehouse P, Yang GZ, Mohiaddin RH, Varghese A, Charrier C, Keegan J, Firmin DN. Volume-selective 3D turbo spin echo imaging for vascular wall imaging and distensibility measurement. J. Magn. Reson. Imaging 2003;17:572–80. doi: 10.1002/jmri.10294.

19. Yarnykh VL, Yuan C. Simultaneous outer volume and blood suppression by quadruple inversion-recovery. Magn. Reson. Med. 2006;55:1083–92. doi: 10.1002/mrm.20880.

20. Hussain T, Clough RE, Cecelja M, Makowski M, Peel S, Chowienczyk P, Schaeffter T, Greil G, Botnar R. Zoom imaging for rapid aortic vessel wall imaging and cardiovascular risk assessment. J. Magn. Reson. Imaging 2011;34:279–85. doi: 10.1002/jmri.22617.

21. Abd-Elmoniem KZ, Barmet C, Stuber M. Free-breathing inner-volume black-blood imaging of the human heart using two-dimensionally selective local excitation at 3 T. Magn. Reson. Med. 2012;68:822–9. doi: 10.1002/mrm.23305.

22. Peel S a, Hussain T, Cecelja M, Abbas A, Greil GF, Chowienczyk P, Spector T, Smith A, Waltham M, Botnar RM. Accelerated aortic imaging using small field of view imaging and electrocardiogram-triggered quadruple inversion recovery magnetization preparation. J. Magn. Reson. Imaging 2011;34:1176–83. doi: 10.1002/jmri.22785.

23. Felmlee JP, Ehman RL. Spatial presaturation: a method for suppressing flow artifacts and improving depiction of vascular anatomy in MR imaging. Radiology 1987;164:559–64. doi: 10.1148/radiology.164.2.3602402.

24. Edelman RR, Atkinson DJ, Silver MS, Loaiza FL, Warren WS. FRODO pulse sequences: a new means of eliminating motion, flow, and wraparound artifacts. Radiology 1988;166:231–6. doi: 10.1148/radiology.166.1.3336685.

25. Yarnykh VL. Actual flip-angle imaging in the pulsed steady state: a method for rapid three-dimensional mapping of the transmitted radiofrequency field. Magn. Reson. Med. 2007;57:192–200. doi: 10.1002/mrm.21120.

26. Sbrizzi A, Hoogduin H, Lagendijk JJ, Luijten P, Sleijpen GLG, van den Berg C a T. Time efficient design of multi dimensional RF pulses: application of a multi shift CGLS algorithm. Magn. Reson. Med. 2011;66:879–85. doi: 10.1002/mrm.22863.

27. Schnell S, Markl M, Entezari P, Mahadewia RJ, Semaan E, Stankovic Z, Collins J, Carr J, Jung B. k-t GRAPPA accelerated four-dimensional flow MRI in the aorta: Effect on scan time, image quality, and quantification of flow and wall shear stress. Magn. Reson. Med. 2013;00:1–12. doi: 10.1002/mrm.24925.

28. Devos DGH, Rietzschel E, Heyse C, Vandemaele P, Van Bortel L, Babin D, Segers P, Westenberg JM, Achten R. MR pulse wave velocity increases with age faster in the thoracic aorta than in the abdominal aorta. J. Magn. Reson. Imaging 2014. doi: 10.1002/jmri.24592.

29. Zhang X, Petersen ET, Ghariq E, De Vis JB, Webb AG, Teeuwisse WM, Hendrikse J, van Osch MJP. In vivo blood T(1) measurements at 1.5 T, 3 T, and 7 T. Magn. Reson. Med. 2013;70:1082–6. doi: 10.1002/mrm.24550.

30. Adame IM, van der Geest RJ, Wasserman B a, Mohamed M a, Reiber JHC, Lelieveldt BPF. Automatic segmentation and plaque characterization in atherosclerotic carotid artery MR images. MAGMA 2004;16:227–34. doi: 10.1007/s10334-003-0030-8.

31. Abd-Elmoniem K, Gharib A, Pettigrew R. Coronary vessel wall 3-T MR imaging with time-resolved acquisition of phase-sensitive dual inversion-recovery (TRAPD) technique: initial results in patients. Radiology 2012;265:715–723. doi: 10.1148/radiol.12120068/-/DC1.

32. Malayeri A, Macedo R, Li D. Coronary vessel wall evaluation by magnetic resonance imaging in the multi-ethnic study of atherosclerosis: determinants of image quality. J. Comput. … 2009;33:1–7. doi: 10.1097/RCT.0b013e3181648606.Coronary.

33. Dragonu I, Geiger J, Jung B, Vicari M, Hennig J, Ludwig U. Optimized Dark-Blood Imaging for Evaluation of the Aorta and Subclavian Arteries in Patients with Giant Cell Arteritis. In: Proc. Intl. Soc. Mag. Reson. Med. 22. Vol. 22. ; 2014. p. 2539.

34. Katscher U, Börnert P. Parallel RF transmission in MRI. NMR Biomed. 2006;19:393–400. doi: 10.1002/nbm.1049.

Chapter 3

Combining a reduced field of excitation with SENSE-based parallel imaging for maximum imaging efficiency

This chapter has been published as:

Mooiweer, R., Sbrizzi, A., Raaijmakers, A. J.E., van den Berg, C. A.T., Luijten, P. R. and Hoogduin, H. (2017), *Combining a reduced field of excitation with SENSE-based parallel imaging for maximum imaging efficiency*. Magn Reson Med, 78: 88–96.

Abstract

Purpose: To show that a combination of parallel imaging using sensitivity encoding (SENSE) and inner volume imaging (IVI) combines the known benefits of both techniques. SENSE with a reduced field of excitation (rFOX) is termed rSENSE.

Theory and Methods: The noise level in SENSE reconstructions is reduced by removing voxels from the unfolding process that are rendered silent by using rFOX. The silent voxels need to be identified beforehand, this is done by using rFOX in the coil sensitivity maps. In vivo experiments were performed at 7T using a 32 channel receive coil.

Results: Good image quality could be obtained in vivo with rSENSE at acceleration factors that are higher than could be obtained using SENSE or IVI alone. With rSENSE we were also able to accelerate scans using an rFOX that was purposely designed to be imperfect or incompatible at all with IVI.

Conclusion: rSENSE has been demonstrated in vivo with 2D RF pulses. Besides allowing additional scan acceleration, it offers a greater robustness and flexibility than IVI. The proposed method can be used with other field strengths, anatomies and other rFOX techniques.

Introduction

Ever since the introduction of MRI, there has been a quest for methods that can shorten the image acquisition time. Both inner volume imaging (IVI) (2) and parallel imaging (PI) (3,4) are examples of non-sequence specific techniques that can be used to achieve this. In addition, these techniques improve image quality in sequences where T_2/T_2^* decay causes blurring and distortions, by shortening the readout times (5–7). Furthermore, using IVI, movement artifacts can be avoided by not exciting (moving) areas outside the region of interest (ROI) (8,9). These techniques are especially interesting for ultra-high field imaging (≥7T) where an increased signal to noise ratio (SNR) allows for high resolution imaging, accompanied with prolonged scan-times and an amplification of the aforementioned image artifacts.

In recent years, the realization arose that IVI, and in particular the signal-localization techniques that are used to facilitate this, could be used to improve PI. This is shown by a number of papers where an improved PI performance is described when the signal generating area was reduced in specific applications (10–15). Most notable is the work on zoomed GRAPPA (ZOOPPA) (10), where the signal in a part of the FOV is suppressed such that high GRAPPA acceleration factors can be used to achieve high resolution fMRI (12) and DWI (11) of the remaining areas. The authors of the former publication also noted that GRAPPA can be used to (retrospectively) reconstruct the full FOV from IVI images in cases where signal suppression was imperfect, which would otherwise lead to aliasing of this unwanted signal into the region of interest. An interesting take on the subject matter is provided by Taviani *et al.* who introduced the concept of virtual coil profiles for the combined use of a multi-band excitation pattern with PI (15).

To effectively discuss the decoupling of IVI from the enabling techniques that limit the signal generating area, we introduce the term reduced field of excitation (rFOX). In this terminology, IVI is the combined use of rFOX and a reduced field of view (rFOV) (**Figure 1e**). Here rFOV is any encoded FOV that is smaller than the full FOV, usually matching the size and shape of the rFOX. The full FOV is the fully encoded FOV such that no aliasing occurs when a regular (1D selective) excitation is used. The method by which the rFOX is created is not relevant for the definition of the concept.

Up to now, a detailed analysis of the interactions between rFOX and PI is missing, obscuring the potential applicability of the combination of these techniques. In the current work, we combine rFOX with SENSE (16,17). Since SENSE operates in the image domain instead of the k-space domain (GRAPPA (18)) it simplifies the conceptual and theoretical explanation of rFOX with PI.

We argue that instead of combining rFOX with rFOV into IVI, or even applying PI on the rFOV acquired by IVI, PI alone is the preferred method to be combined with rFOX. When used correctly, PI gives an increased robustness towards imperfect suppression of signal outside the targeted ROI and in general a greater flexibility by allowing accelerated imaging of rFOX shapes that are incompatible with rFOV imaging. In particular, the combination of rFOX and SENSE is dubbed rSENSE, and is explained in detail in this manuscript. Several examples of rSENSE accelerated scans are given using subject-specific two-dimensionally selective radiofrequency (2D RF) pulses (19,20) to create the rFOX. This study has been presented in part at the annual meeting of the ISMRM in Toronto, Canada, in 2015 (1).

Theory

The different ways in which a reduced field of excitation can be combined with a reduction of the acquired FOV or parallel imaging, are schematically reported in **Figure 1**. To understand the effect rFOX has on SENSE, we will briefly recapitulate the theory of SENSE (4). In particular, the way in which noise is propagated during SENSE reconstruction. The basic principle of SENSE is the unfolding of aliased voxel-values using coil sensitivity information. Compared to a fully (Nyquist) encoded FOV (**Figure 1a**), the density of the regularly sampled k-space lines is reduced by an acceleration factor *R*, shortening the acquisition by the same factor. Effectively, the encoded FOV is reduced by *R* as well, leading to *R* voxels aliasing (collapsing) onto each other, at every location in the reduced FOV (**Figure 1b**). This accumulated signal is detected by multiple coils simultaneously and needs to be unfolded in order to create an image of the full FOV (**Figure 1c**). The detected, aliased, signal per receive channel is assembled into a vector $\boldsymbol{\sigma}$ whose length is the number of receive coils (N_{coils}). It follows that $\boldsymbol{\sigma} = \mathbf{S}\,\boldsymbol{\rho}$, with $\mathbf{S}$ the N_{coils} *x* *R* coil sensitivity matrix and $\boldsymbol{\rho}$ the true signal originating from the aliasing voxels (vector of length *R*). The true signal can be retrieved in a least squares sense via $\boldsymbol{\rho} = (\mathbf{S}^{\mathrm{H}}\mathbf{S})^{-1}\mathbf{S}^{\mathrm{H}}\,\boldsymbol{\sigma}$. The condition number of the matrix $\mathbf{S}$ describes how much the calculated value $\boldsymbol{\rho}$ changes with a small change in $\boldsymbol{\sigma}$. Small changes in $\boldsymbol{\sigma}$ occur naturally and are randomly distributed across the image (noise), so an amplification of noise will occur when the problem is ill-conditioned. The level of noise amplification in each voxel depends on the spatial variation of the receive coil sensitivities and is represented by the geometry factor (g-factor). When the noise correlation matrix between receive coils $\boldsymbol{\Psi}$ is also taken into account, the g-factor is defined as $g_{\mathrm{j}}(\mathrm{R}) = \sqrt{[(\boldsymbol{S}^{\mathrm{H}}\boldsymbol{\Psi}^{-1}\boldsymbol{S})^{-1}]_{\mathrm{j,j}}(\boldsymbol{S}^{\mathrm{H}}\boldsymbol{\Psi}^{-1}\boldsymbol{S})_{\mathrm{j,j}}}$ (4), at voxel location *j*. The g-factor is related to the SNR in a SENSE-accelerated image, compared to a fully sampled acquisition via $SNR_{SENSE}(R) = SNR_{full}/(g\sqrt{R})$. The $\sqrt{R}$ term follows from the reduced number

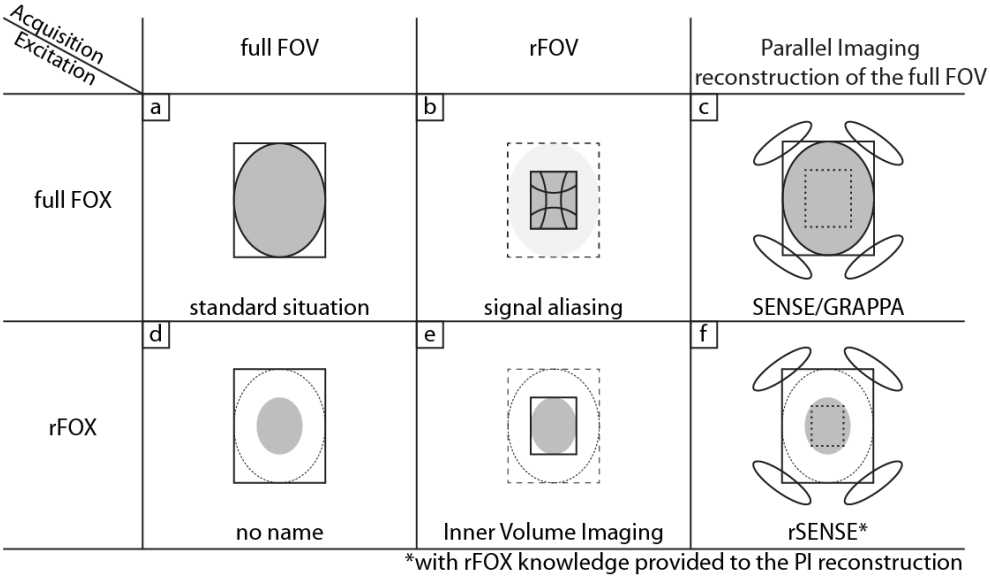

***Figure 1**. Summary of different combinations of full and reduced Field Of View (FOV), Field Of Excitation (FOX), and Parallel Imaging.*

of Fourier averaged samples contributing to the total SNR. This loss mechanism equally affects rFOV sequences without parallel imaging, such as IVI (**Figure 1e**): $SNR_{IVI}(R) = SNRfull/\sqrt{R}$. For ideal SENSE unfolding, so without amplification of noise, *g* equals 1. Since in practice *g* > 1, the SNR in a scan using IVI will be higher than when SENSE is used to achieve the same scan acceleration factor. In contrast to IVI, however, SENSE will reconstruct the full FOV and not just the rFOV.

In the here proposed rSENSE method (**Figure 1f**), rFOX is used to reduce the number of aliasing voxels at a given acceleration factor *R*. The reduced number of aliasing voxels (R_r) can be described using $R_r = R \times \frac{PE_{rFOX}}{PE_{fullFOX}}$, where PE_{rFOX} and $PE_{fullFOX}$ are the number of excited voxels in the phase encoded directions using rFOX and full FOX respectively. In the unfolding procedure, the voxels that do not contribute any signal can be assigned a zero value in $\boldsymbol{\rho}$ and the columns of $\boldsymbol{S}$ corresponding to the coil sensitivities of these suppressed voxels can be removed from the matrix. **Figure 2** illustrates this situation, where an rFOX is used to reduce the number of aliased voxels from four (A-D) to two (B and C only). Since the number of unknowns is reduced from $R = 4$ to $R_r = 2$, and the number of equations remains the same ($N_{coils} = 4$), the system of equations is typically better conditioned. This is expressed in a lower condition number and g-factors, and results thus into a higher local SNR compared to excitation of the full field of view. An ideal unfolding situation can even be obtained when the size of the rFOX is the same as the rFOV obtained during SENSE acceleration. In this situation of matched excitation reduction and acceleration factor there is no aliasing of signal, *g* equals 1, and the SNR of IVI and rSENSE should be equal. Acceleration beyond the ideal unfolding situation, while keeping the rFOX fixed, is possible using rSENSE (with an increased g-factor), though with IVI this would lead to signal aliasing without the ability to unfold it.

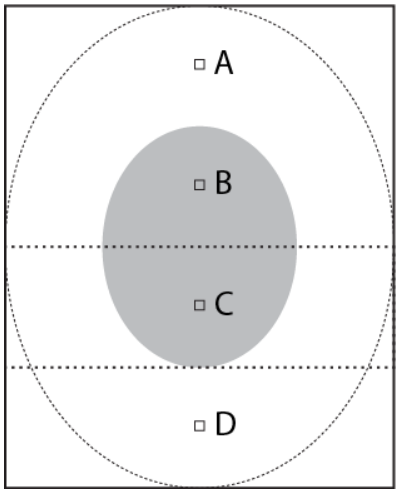

$$\begin{pmatrix}\sigma_1\\ \sigma_2\\ \sigma_3\\ \sigma_4\end{pmatrix} = \begin{pmatrix}S_{1A} & S_{1B} & S_{1C} & S_{1D}\\ S_{2A} & S_{2B} & S_{2C} & S_{2D}\\ S_{3A} & S_{3B} & S_{3C} & S_{3D}\\ S_{4A} & S_{4B} & S_{4C} & S_{4D}\end{pmatrix}\begin{pmatrix}\rho_A\\ \rho_B\\ \rho_C\\ \rho_D\end{pmatrix}$$

$$\begin{pmatrix}\sigma_1\\ \sigma_2\\ \sigma_3\\ \sigma_4\end{pmatrix} = \begin{pmatrix}\cancel{S_{1A}} & S_{1B} & S_{1C} & \cancel{S_{1D}}\\ \cancel{S_{2A}} & S_{2B} & S_{2C} & \cancel{S_{2D}}\\ \cancel{S_{3A}} & S_{3B} & S_{3C} & \cancel{S_{3D}}\\ \cancel{S_{4A}} & S_{4B} & S_{4C} & \cancel{S_{4D}}\end{pmatrix}\begin{pmatrix}0\\ \rho_B\\ \rho_C\\ 0\end{pmatrix}$$

$$\begin{pmatrix}\sigma_1\\ \sigma_2\\ \sigma_3\\ \sigma_4\end{pmatrix} = \begin{pmatrix}S_{1B} & S_{1C}\\ S_{2B} & S_{2C}\\ S_{3B} & S_{3C}\\ S_{4B} & S_{4C}\end{pmatrix}\begin{pmatrix}\rho_B\\ \rho_C\end{pmatrix}, \begin{pmatrix}\rho_A\\ \rho_D\end{pmatrix} = \begin{pmatrix}0\\ 0\end{pmatrix}$$

Figure 2. *Illustration and matrix representation of aliasing voxels (A,B,C,D) in a 4x under sampled acquisition with 4 receive coils (1,2,3,4). By changing the excitation from the full area (dotted ellipse) to a reduced field of excitation (filled grey ellipse) the signal contributions of voxels A and D vanish. In the corresponding matrix, ρ_A and ρ_D are set to 0, allowing the removal of columns $S_{[1-4],A}$ and $S_{[1-4],D}$ from the equation.*

Methods

Identification of voxels for exclusion

Since rSENSE works by excluding 'silent' voxels from the inversion problem, we need to identify these voxels beforehand. In fact, voxels that lie outside the imaged object are already excluded to improve SNR in regular SENSE (4). In the general implementation of SENSE, these voxels outside the body are easily identified on the separately acquired, 1D-selective, coil sensitivity maps. In our implementation of rSENSE low flip angle 2D RF pulses are used to create the rFOX. The coil sensitivity mapping scan is in fact a low flip angle gradient echo sequence. So we can simply use the same 2D RF pulses in the mapping sequence to create the rFOX and identify the signal-suppressed voxels inside the object in the same way as the voxels outside the body.

Experimental validation of rSENSE

A model situation was chosen to experimentally verify the rSENSE method, based on a 3D brain scan in sagittal orientation. An rFOX of 1/3rd the size of the head in both the phase encoding directions (AP and RL) was chosen (dubbed rFOX shape 1). This geometry allows the comparison of scan acceleration in two dimensions via rSENSE (**Figure 1f),** regular SENSE (**Figure 1c**) and IVI (**Figure 1e**). Additionally, rFOX was used in combination with SENSE unfolding using sensitivity maps of the full FOX, to show the incompatibility of this combination.

Different 2D acceleration factors were used in the acquisitions: 2 x 2 = 4, 3 x 3 = 9, 4 x 4 = 16 and 5 x 5 = 25. The IVI scan was acquired at an rFOV matching the rFOX, so at a 2D reduction factor of 3 x 3 = 9, compared to the full FOV. G-factor maps were generated to predict the performance of the SENSE and rSENSE accelerated scans.

To show the robustness of rSENSE towards an imperfect rFOX, compared to IVI, a separate experiment was performed. Here an extra excitation 'hotspot' was added to the design of the 2D RF pulses, outside rFOX shape 1, to simulate imperfect signal suppression (rFOX shape 2).

To show how rSENSE is flexible in accelerating acquisitions of different rFOX shapes that are incompatible with IVI, another additional experiment was performed. Here, the outer cortex was targeted as the ROI in RF pulse design, resulting in a ring-like rFOX with suppression of signal in the center of the brain (rFOX shape 3).

General scan parameters

All experiments were performed on a 7T MRI system (Philips Healthcare, Cleveland, OH, USA) using a 2-channel transmit coil and a 32-channel receive coil (both from Nova Medical, Wilmington, MA, USA). Healthy volunteers were scanned, after having provided informed consent. A modified version of the 3D whole brain protocol for 7T (21) was used. This gradient echo based sequence was chosen for its clinically relevant T_2*-weighted contrast and 0.5 mm isotropic resolution, to facilitate the visual detection of changes in image quality. An EPI acceleration factor of 9 was used to keep scan times short, so that multiple scans using

different acceleration methods could be acquired from the same subject. Other scan parameters were: sagittal orientation, FOV: 210 x 210 x 180 mm (FH x AP x RL), TR: 75 ms, TE: 25 ms, FA: 15˚. Care was taken to disable any oversampling in the phase encoding directions (AP and RL).

Details on rFOX generation and coil sensitivity mapping

The 2D selective RF pulses were designed on-site using the numerical pulse design method described by *Sbrizzi et al.* (22). B_1^+ and B_0 information of a transverse slice at about half the FH length of the brain was used. B_1^+ maps were acquired using the DREAM method (23), with STEAM flip angle 40˚. B_0 maps were acquired using a ΔTE of 1.0 ms. The 2D RF pulses for rFOX shapes 1 and 2 were designed on a spiral-in k-space trajectory with a maximum value of 3 cm/rad, and a duration of 4.3 ms. For rFOX shape 3 a maximum k-space value of 5 cm/rad was chosen, leading to a duration of 8.9 ms.

The sensitivity maps of the receive coils were based on coarse-resolution, proton density weighted, gradient echo scans. The maps were acquired in the standard 1D-selective way, and using the rFOX excitation pulses scaled down to FA = 1˚. Compared to the 1D selective scan, the TR was extended from 8 to 18 ms to fit the longer excitation pulses (39 ms for rFOX shape 3). To cross-check the efficacy of the 2D RF pulses in the sensitivity mapping sequence, we acquired a low-resolution $(1,5\ mm)^3$, T_2* weighted, image without SENSE acceleration (SENSE 1 x 1).

The coil sensitivity maps were conventionally acquired at an overly large FOV to facilitate a wide range of user-desired FOVs and over-sampling factors. To correctly calculate the g-factor maps for the FOV used in the (r)SENSE accelerated scans, a set of sensitivity maps was also acquired using this FOV and orientation.

Image reconstruction

Raw data of the T_2*-weighted scans was saved in the k-space domain and reconstructed offline using ReconFrame (GyroTools LLC, Winterthur, Switzerland). The standard pipeline for SENSE unfolding was used, which included regularization (24). Additionally, the 'Mask' option of ReconFrame was enabled during reconstruction of the rSENSE accelerated scans to make sure that the silent voxels obtained with rFOX were excluded from the unfolding process. The 'Mask' option is designed to mask out noise only regions from the sensitivity maps and was used without any adjustments.

Results

rSENSE acceleration of a centered rFOX

The efficacy of rFOX generation using 2D RF pulses is shown in **Figure 3**, for shape 1. In the SENSE reconstruction process, the summation of the receive coil sensitivity images is used to determine the voxels that are to be for excluded from reconstruction. Because of the matching signal generating areas in the T2* weighted scan and the summed coil sensitivity map, we expect adequate identification of the large number of silent voxels in rSENSE reconstruction.

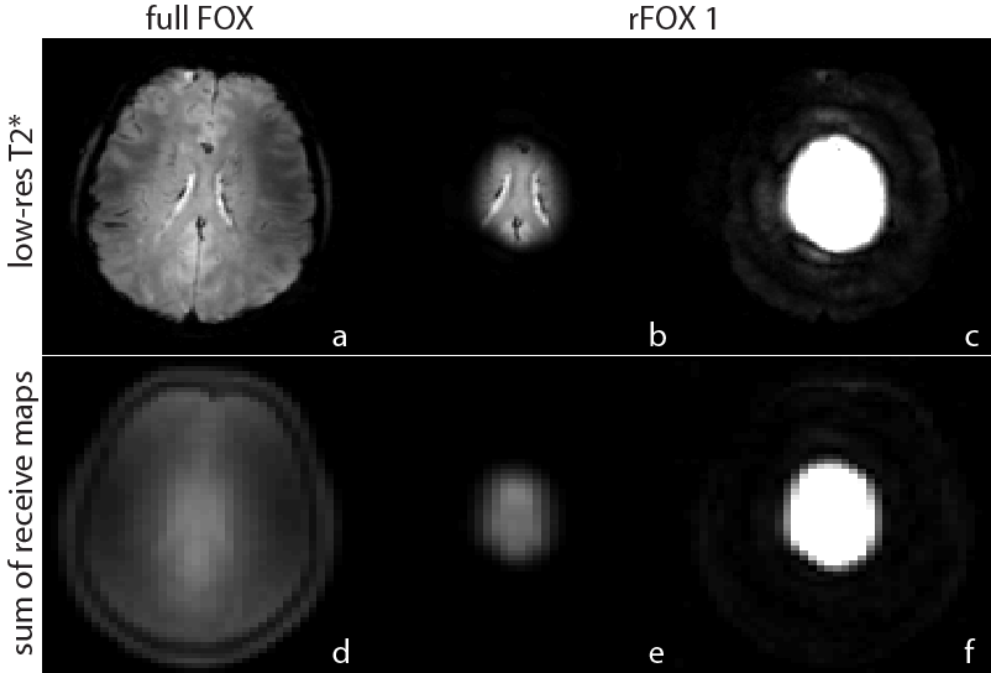

***Figure 3**. Full FOX (**a**, **d**) and rFOX 1 (**b**, **c**, **e**, **f**) applied to T_2*-weighted images (**a**,**b**,**c**) and the receive coil sensitivity maps (summed signal, figures **d**,**e**,**f**). Figures **c** and **f** show the same data as **b** and **e**, but with a different a intensity window to reveal low intensity signals.*

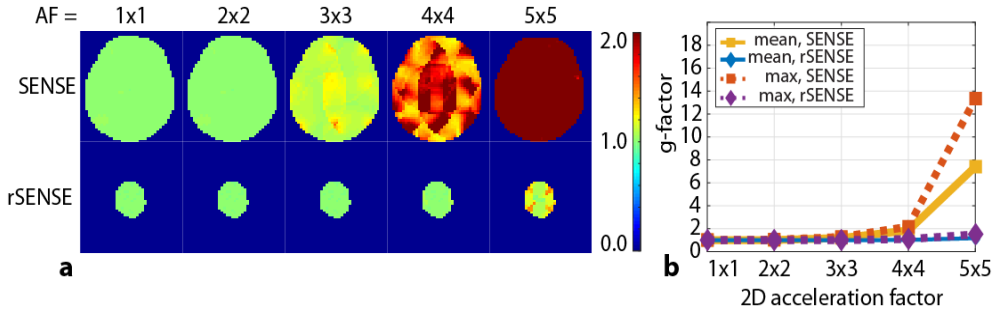

Figure 4. *G-factor maps (**a**) calculated for acceleration in both phase encoded directions, for SENSE and rSENSE with rFOX shape 1. The mean and maximum values inside the ROI are plotted (**b**).*

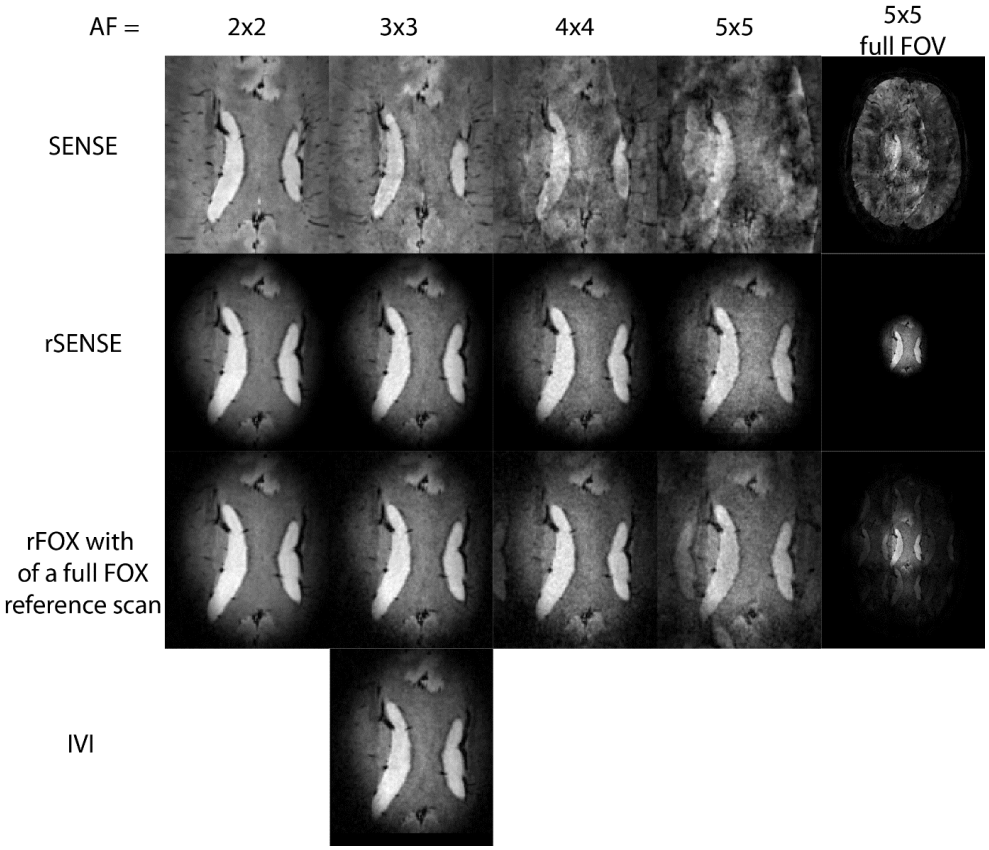

Figure 5. *Transversely reconstructed T_2*-weighted images, showing the corpus callosum in one volunteer. SENSE, rSENSE, and SENSE unfolding of rFOX using a full FOX reference scan are used at increasing acceleration factors. The column on the right shows the full FOV image for anatomical reference, the other columns are zoomed images to show the ROI. Inner Volume Imaging using an rFOV of 1/3rd x 1/3rd the size of the full FOV is also shown.*

Figure 4 shows the g-factor maps for increasing acceleration factors (AFs), using SENSE and rSENSE with rFOX shape 1. At AF = 2 x 2, the g-factor is still close to 1 for both methods. At AF = 3 x 3 a divergence between the g-factors can be seen, and slight difference in SNR can be expected. For AF = 4 x 4 and 5 x 5, *g* is much higher for SENSE compared to rSENSE. At these acceleration factors we expect to see substantial SNR differences, resulting in inadequate (using SENSE) and usable (using rSENSE) T_2* weighted images. These AFs can't be obtained when IVI is used with this rFOX: this would be limited to a FOV reduction of 3 x 3.

In **Figure 5** we see how the image quality of rSENSE accelerated images compares to the other acceleration methods of the T_2* weighted acquisitions. The regular SENSE accelerated scan shows signs of image quality degradation already at AF = 3 x 3, and artifacts are dominating the images' appearance at higher acceleration factors. When rFOX is used, the image quality at 3 x 3 times under-sampling is comparable for all techniques. This includes the IVI image, confirming that rSENSE and IVI are equivalent when the g = 1 situation is realized. Furthermore, no noticeable artifacts are introduced at rSENSE acceleration factors of 4 x 4 and 5 x 5, only an increase in noise can be observed, as is expected from the $1/\sqrt{R}$ relationship with SNR.

When rFOX is used in combination with SENSE unfolding using a full FOX reference scan, we see that signal is incorrectly allocated to locations outside the targeted rFOX, at AF = 4 x 4 and 5 x 5. This can be seen in the zoomed reproductions, and even more in the full FOV images.

Figure 6 shows that rSENSE constantly provides good image quality when the experiment is repeated in multiple volunteers. Some variation in size and shape of the rFOX can be seen, partly corresponding to variations in head size between volunteers and partly due to inconsistencies in the manual planning of the rFOX.

In **Figure 7** we see transverse slices reconstructed at a lower position in the brain, showing the red nuclei and substantia nigra. Noteworthy here is that the SENSE accelerated images have severe artifacts whereas in the rSENSE accelerated images the actual brain structures can be seen. The banding artifacts originate from the rapid susceptibility changes near the nasal cavities. Because of intentional aliasing followed by SENSE unfolding, the artifacts are repeated across the full FOV, also into the ROI. When rSENSE is used, the locations that generate the artifacts are mostly outside the rFOX, thus preventing signal generation in this area of rapid susceptibility changes in the first place. Useful images were created with rSENSE acceleration, even though these basal ganglia are in a very challenging location because of pulsating motion associated with the lower brain region.

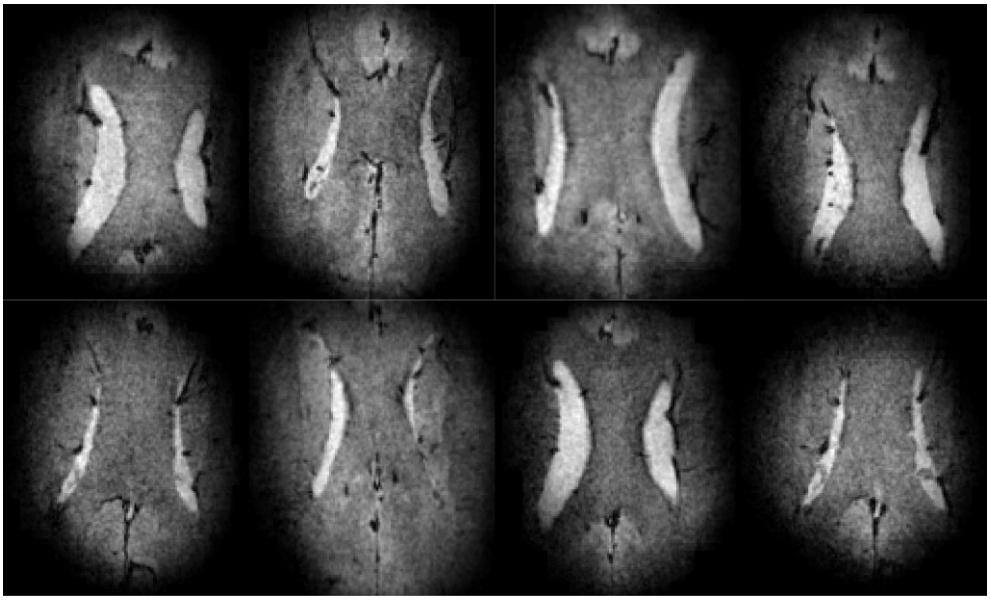

***Figure 6**. rSENSE accelerated, T_2*-weighted, images of the corpus callosum in 8 volunteers. AF = 5 x 5, rFOX shape 1 = 1/3 x 1/3 of full FOX. The images are transverse reconstructions form the sagitally acquired 3D scans, and zoomed to show the ROI.*

Testing the robustness and flexibility of rSENSE

To demonstrate the robustness of rSENSE towards an imperfect rFOX we designed rFOX shape 2 to have a separate excitation hotspot in addition to the first rFOX shape. In **Figure 8** we see that the purposely introduced signal hotspot leads to several artifacts due to signal folding in the IVI images. When rSENSE is used, the location of the hotspot is revealed, and most of the aliasing artifacts are avoided. One artifact is greatly reduced in visibility, but is still present in the rSENSE image (white arrow). The g-factor remains close to 1, indicating little to no SNR loss with respect to an rSENSE acquisition of rFOX shape 1.

An excitation pattern following the outer cortex (rFOX shape 3) is absolutely incompatible with IVI. **Figure 9** shows that rFOX can still be used to speed up the acquisition of this rFOX shape, whereas simply unfolding this scan using the default full FOX coil sensitivity map leads to obvious artifacts. In this situation the number of signal contributing voxels was halved with respect to the full FOX, but an rSENSE acceleration factor of 3 x 3 = 9 could be used.

Discussion

This work proposed to combine rFOX with SENSE into rSENSE. By using rFOX in the coil sensitivity mapping procedure, information on the actual aliasing voxels can be provided to the unfolding algorithms, resulting in high quality images at ultra-high acceleration factors.

The receive coil sensitivity scans combined well with the 2D spatially selective RF pulses that were used to create the rFOX. Voxels that were not excited were excluded from SENSE unfolding and the remaining voxels were successfully reconstructed. The extended TR in the

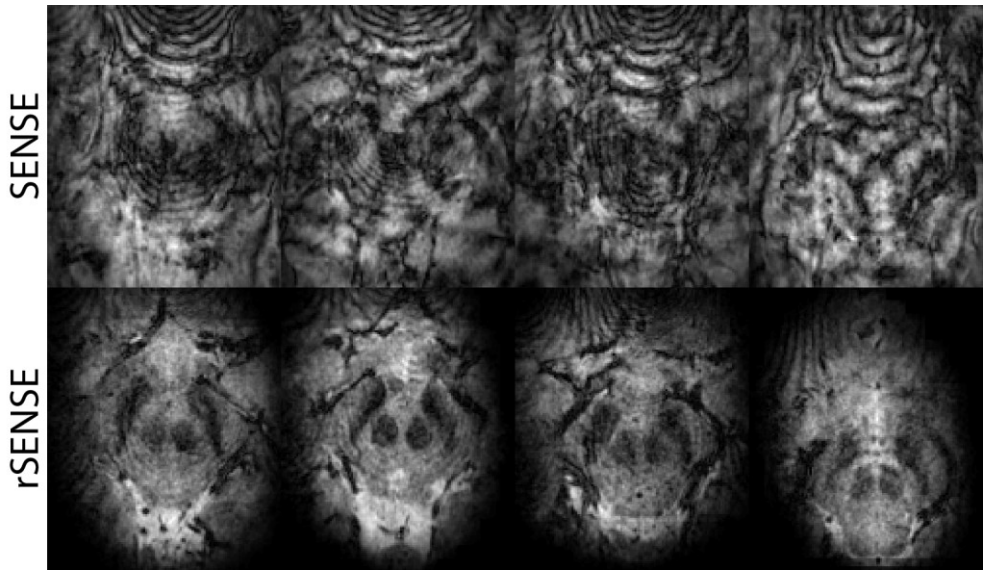

***Figure 7**. T_2*-weighted images using SENSE (top row) and rSENSE (bottom row) at 5 x 5 acceleration factor in 4 different volunteers. Transverse, zoomed in, slices are reproduced, showing the red nuclei and substantia nigra.*

sensitivity mapping scans lead to an increase in scan time of these scans, from 66 seconds in the regular 1D-selective scan to 148 seconds for rFOX shapes 1 and 2 and 324 seconds for rFOX shape 3. On one hand one could argue that an increased calibration scan time is permitted if the actual (functional) scan can be performed faster, or using shorter echo times. On the other hand other strategies for providing information of the rFOX could be envisaged that would require less scan time in the calibration phase of the scan protocol. For example, the targeted or simulated excitation pattern might be used as a mask on the regular full FOX coil sensitivity map.

The newly proposed rSENSE method clearly performed better than regular SENSE when imaging a limited region of interest, as was predicted by a drastically reduced g-factor. At acceleration factors above the rFOV limit, regular SENSE creates unusable images while rSENSE results in excellent images in the corpus callosum and usable images in the red nuclei.

When rFOX is combined with SENSE acceleration and a full FOX coil sensitivity scan, image quality is also improved significantly with respect to regular SENSE, but is not as good as rSENSE. This reduction in image quality is likely due to the incorrect unfolding of signal to voxels that did not contribute any to the aliased image.

When an imperfect rFOX was simulated, we saw that rSENSE was capable of unfolding most of the extra signal to its origin, where in IVI this lead to aliasing. This exemplifies the robustness of rSENSE compared to IVI, and is therefore the preferred method. A prerequisite for this to work is that the location of the imperfection is known in the unfolding process. It can be measured during the coil sensitivity mapping, the simulated excitation pattern might be

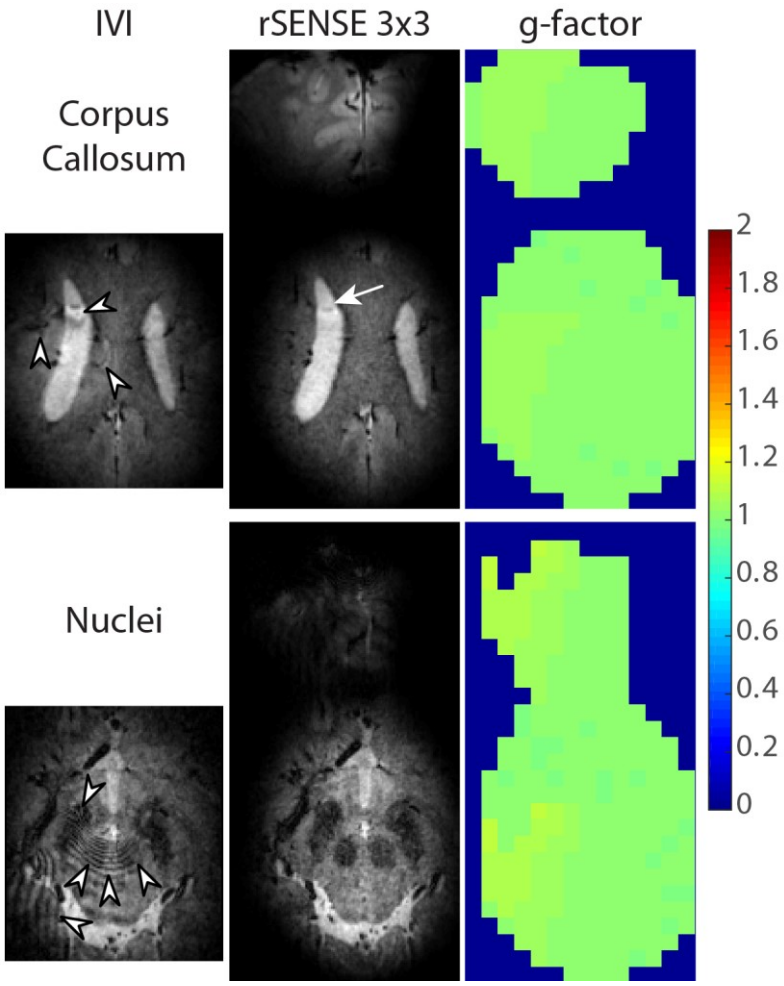

***Figure 8**. Images of rFOX shape 2 acquired using IVI and equivalent rSENSE acceleration factor. Transverse reconstructed slices showing the Corpus Callosum and Red Nuclei are shown, as well as g-factor maps for both locations. The rSENSE images and g-factor maps are cropped around the signal generating areas. Arrow and arrow heads point to aliasing artifacts.*

used as a mask on the regular full FOX coil sensitivity map. However, it remains to be determined to what extent a discrepancy between the simulated rFOX and the actual one could result in large reconstruction errors. In our example, one aliasing artifact was not completely removed. The spatial location of this signal was probably masked out in the reconstruction due to partial volume effects at the edge of the rFOX.

Several other methods of achieving a reduced field of excitation are available, such as refocusing slices orthogonal to excitation (2), outer volume suppression with spatial saturation (25) and signal localization via violation of the CPMG conditions (26). The rSENSE method should work with either of these rFOX generating methods, but providing the voxels exclusion

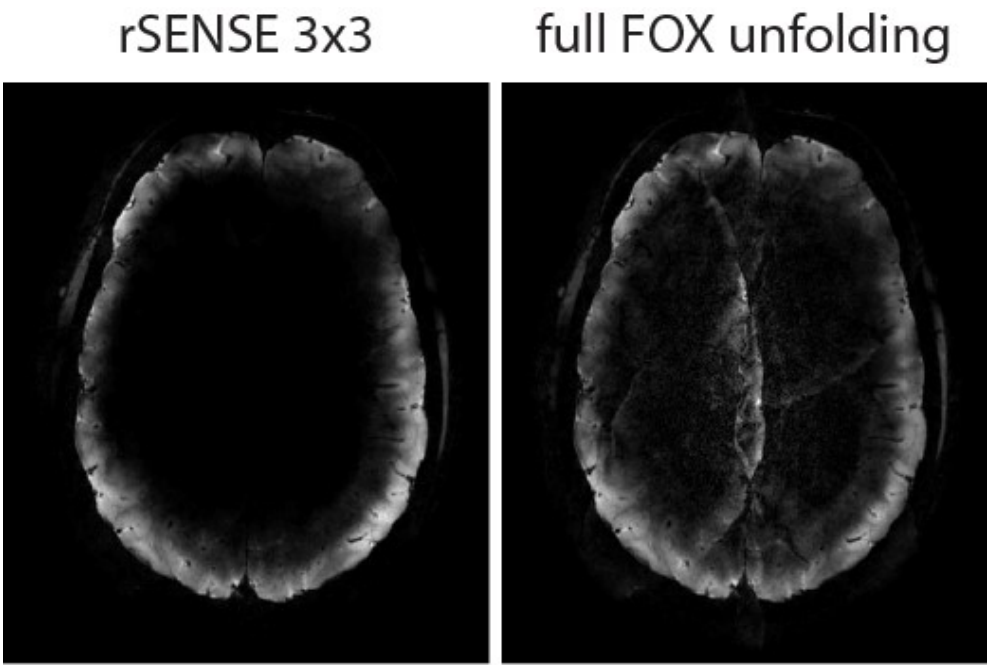

***Figure 9**. PI accelerated (AF = 3 x 3), T_2* weighted, transverse reconstructed images of rFOX shape 3, exciting the outer cortex. The images were reconstructed using rSENSE (left) and using the coil sensitivities of the full FOX (right).*

information may not be as straightforward as with 2D RF pulses. In these cases a regular 1D selective coil sensitivity map might be used that is masked by the targeted or simulated rFOX.

GRAPPA uses auto-calibration of the coil sensitivity during each sequence, possibly simplifying the process of performing rFOX-matched reconstructions. However, since GRAPPA operates in the k-space domain, an exact exclusion of silent voxels is not possible and the benefits of having fewer contributing voxels are not immediately clear. Still, certain benefits have been shown empirically (11–13).

A previously explored strategy of using SENSE acceleration after applying IVI (27) should be identical to rSENSE when the rFOX perfectly matches the rFOV. In this approach there is no need to provide additional rFOX knowledge to the SENSE reconstruction, since this is implicitly supplied by defining the rFOV. However, one can no longer benefit from the robustness towards excitation errors offered by rSENSE and one is limited to rFOX shapes that perfectly match the (usually square shaped) rFOV.

When rSENSE is considered to be used for accelerating an existing scan protocol, a short optimization of this protocol should be performed by determining the excitation target area, obtaining coil sensitivity maps and calculating g-factors for different acceleration factors. This is an additional effort to be performed before starting a new study that focusses on a particular region of interest, but results in a more effective scan protocol of which the cumulative benefits will be paramount when applied to a large number of examinations.

In practice, voxel exclusion in SENSE unfolding is achieved through regularization instead of masking, as is clearly explained by Omer *et al.* (28). There are no obvious reasons why this would not be compatible with rFOX inclusion in the coil sensitivity maps. In fact, the performance of rSENSE might benefit from this method because it lacks a sharp transition between excluded and included voxels, as is the case with masking.

In conclusion, we have shown how an rFOX is imaged most effectively: by combining rFOX and SENSE into rSENSE. Compared to SENSE of the full FOX, higher acceleration factors can be obtained. Compared to IVI, the rSENSE method offers greater geometrical flexibility and additional scan acceleration facilitated by PI.

References

1. Mooiweer R, Sbrizzi A, Raaijmakers A, van den Berg C a T, Luijten PR, Hoogduin H. Squashing the g-factor: Ultra high scan acceleration factors in reduced Field of Excitation imaging. In: Proc. Intl. Soc. Mag. Reson. Med. ; 2015. p. 3620.

2. Feinberg D, Hoenninger JC, Crooks L, Kaufman L, Watts J, Arakawa M. Inner volume MR imaging: technical concepts and their application. Radiology 1985;156:743–747.

3. Sodickson DK, Manning WJ. Simultaneous acquisition of spatial harmonics (SMASH): Fast imaging with radiofrequency coil arrays. Magn. Reson. Med. 1997;38:591–603. doi: 10.1002/mrm.1910380414.

4. Pruessmann KP, Weiger M, Scheidegger MB, Boesiger P. SENSE: sensitivity encoding for fast MRI. Magn. Reson. Med. 1999;42:952–62.

5. Pfeuffer J, Van De Moortele P-F, Yacoub E, Shmuel A, Adriany G, Andersen P, Merkle H, Garwood M, Ugurbil K, Hu X. Zoomed functional imaging in the human brain at 7 Tesla with simultaneous high spatial and high temporal resolution. Neuroimage 2002;17:272–286. doi: 10.1006/nimg.2002.1103.

6. Griswold MA, Jakob PM, Chen Q, Goldfarb JW, Manning WJ, Edelman RR, Sodickson DK. Resolution enhancement in single-shot imaging using simultaneous acquisition of spatial harmonics (SMASH). Magn. Reson. Med. 1999;41:1236–1245. doi: 10.1002/(SICI)1522-2594(199906)41:6<1236::AID-MRM21>3.0.CO;2-T.

7. Rieseberg S, Frahm J, Finsterbusch J. Two-dimensional spatially-selective RF excitation pulses in echo-planar imaging. Magn. Reson. Med. 2002;47:1186–93. doi: 10.1002/mrm.10157.

8. Schneider R, Haueisen J, Pfeuffer J. Shaped saturation with inherent radiofrequency-power-efficient trajectory design in parallel transmission. Magn. Reson. Med. 2014;72:1015–27. doi: 10.1002/mrm.25016.

9. Mooiweer R, Sbrizzi A, El Aidi H, Eikendal ALM, Raaijmakers A, Visser F, van den Berg CAT, Leiner T, Luijten PR, Hoogduin H. Fast 3D isotropic imaging of the aortic vessel wall by application of 2D spatially selective excitation and a new way of inversion recovery for black blood imaging. Magn. Reson. Med. 2016;75:547–555. doi: 10.1002/mrm.25599.

10. Heidemann R, Fasano F, Vogler M, Leuze C, Pfeuffer J, Turner R. Improving Image Quality by Combining Outer Volume Supression and Parallel Imaging: zoomed EPI with GRAPPA at 7T. Proc. 16th Sci. Meet. Int. Soc. Magn. Reson. Med. 2008;Toronto:1284.

11. Heidemann RM, Anwander A, Feiweier T, Knösche TR, Turner R. k-space and q-space: combining ultra-high spatial and angular resolution in diffusion imaging using ZOOPPA at 7 T. Neuroimage 2012;60:967–78. doi: 10.1016/j.neuroimage.2011.12.081.

12. Heidemann RM, Ivanov D, Trampel R, Fasano F, Meyer H, Pfeuffer J, Turner R. Isotropic submillimeter fMRI in the human brain at 7 T: Combining reduced field-of-view imaging and partially parallel acquisitions. Magn. Reson. Med. 2012;68:1506–16. doi: 10.1002/mrm.24156.

13. Coristine AJ, van Heeswijk RB, Stuber M. Combined T 2 -preparation and two-dimensional pencil-beam inner volume selection. Magn. Reson. Med. 2015;74:529–536. doi: 10.1002/mrm.25442.

14. Gallichan D, Marques JP, Gruetter R. Retrospective correction of involuntary microscopic head movement using highly accelerated fat image navigators (3D FatNavs) at 7T. Magn. Reson. Med. 2015;00:n/a–n/a. doi: 10.1002/mrm.25670.

15. Taviani V, Alley MT, Banerjee S, Nishimura DG, Daniel BL, Vasanawala SS, Hargreaves BA. High-resolution diffusion-weighted imaging of the breast with multiband 2D radiofrequency pulses and a generalized parallel imaging reconstruction. Magn. Reson. Med. 2016;00:n/a–n/a. doi: 10.1002/mrm.26110.

16. van den Brink JS, Watanabe Y, Kuhl CK, et al. Implications of SENSE MR in routine clinical practice. Eur. J. Radiol. 2003;46:3–27. doi: 10.1016/S0720-048X(02)00333-9.

17. Weiger M, Pruessmann KP, Boesiger P. 2D SENSE for faster 3D MRI. MAGMA 2002;14:10–19.

18. Griswold M a, Jakob PM, Heidemann RM, Nittka M, Jellus V, Wang J, Kiefer B, Haase A. Generalized autocalibrating partially parallel acquisitions (GRAPPA). Magn. Reson. Med. 2002;47:1202–10. doi: 10.1002/mrm.10171.

19. Pauly J, Nishimura D, Macovski A. A k-space analysis of small-tip-angle excitation. J. Magn. Reson. 1989;81:43–56. doi: 10.1016/0022-2364(89)90265-5.

20. Grissom W, Yip C, Zhang Z, Stenger VA, Fessler J a, Noll DC. Spatial domain method for the design of RF pulses in multicoil parallel excitation. Magn. Reson. Med. 2006;56:620–9. doi: 10.1002/mrm.20978.

21. Zwanenburg JJM, Versluis MJ, Luijten PR, Petridou N. Fast high resolution whole brain T2* weighted imaging using echo planar imaging at 7T. Neuroimage 2011;56:1902–1907. doi: 10.1016/j.neuroimage.2011.03.046.

22. Sbrizzi A, Hoogduin H, Lagendijk JJ, Luijten P, Sleijpen GLG, van den Berg C a T. Time efficient design of multi dimensional RF pulses: application of a multi shift CGLS algorithm. Magn. Reson. Med. 2011;66:879–85. doi: 10.1002/mrm.22863.

23. Nehrke K, Versluis MJ, Webb A, Börnert P. Volumetric B 1 + Mapping of the Brain at 7T using DREAM. Magn. Reson. Med. 2014;71:246–256. doi: 10.1002/mrm.24667.

24. Lin F-H, Kwong KK, Belliveau JW, Wald LL. Parallel imaging reconstruction using automatic regularization. Magn. Reson. Med. 2004;51:559–567. doi: 10.1002/mrm.10718.

25. Le Roux P, Gilles RJ, McKinnon GC, Carlier PG. Optimized outer volume suppression for single-shot fast spin-echo cardiac imaging. J. Magn. Reson. Imaging 1998;8:1022–1032. doi: 10.1002/jmri.1880080505.

26. Malik SJ, Hajnal J V. Phase relaxed localized excitation pulses for inner volume fast spin echo imaging. Magn. Reson. Med. 2015;3:n/a–n/a. doi: 10.1002/mrm.25996.

27. Wargo CJ, Gore JC. Rapid Acquisition of Targeted High Resolution Human Brain Images Using a Combined SENSE , Inner Volume Imaging , and Multi-Shot EPI Spin Echo Sequence at 7T. In: Proc. Intl. Soc. Mag. Reson. Med. Vol. 19. ; 2011. p. 2358.

28. Omer H, Dickinson R. Regularization in parallel MR image reconstruction. Concepts Magn. Reson. Part A 2011;38A:52–60. doi: 10.1002/cmr.a.20206.

Chapter 4

Phase matched RF Pulse design for imaging a reduced field of excitation with a fast TSE acquisition

Ronald Mooiweer, Alessandro Sbrizzi, Alexander J.E. Raaijmakers, Cornelis A.T. van den Berg, Peter R. Luijten, Hans Hoogduin

This chapter has been submitted for publication.

Abstract

A method is described to design parallel transmit (PTX) excitation pulses that are compatible with turbo spin echo (TSE) sequences, based on information available from conventional per-channel B_1^+ mapping. The excitation phase of PTX pulses that generate a reduced field of excitation (rFOX) is matched to the phase the quadrature mode of a PTX coil. This enables TSE imaging of a PTX-enabled rFOX excitation combined with standard nonselective refocusing pulses transmitted in the quadrature mode. *In-vivo* imaging experiments were performed at 7T using a dual channel parallel transmit head coil. In combination with simulations, the CPMG-required excitation phase was confirmed in TSE sequences with refocusing pulses of variable flip angle. Further experiments showed that the same rFOX was generated in TSE and gradient echo sequences, enabling high-resolution imaging with parallel imaging acceleration of the rFOX.

Introduction

Tailored radio frequency (RF) excitation pulses [1] can create a personalized reduced field of excitation (rFOX), allowing acquisitions shortening [2] and avoiding motion artifacts from outside the region of interest [3]. These qualities are increasingly important at (ultra) high field, where the long scan times that are associated with high-resolution imaging increase the risk of motion artifacts. Parallel transmission (PTX) can be used to shorten tailored RF pulses [4].

Application of tailored excitation pulses is simple for gradient echo (GRE) sequences: through amplitude scaling any flip angle up to 90°can be obtained [5]. In turbo spin echo (TSE) sequences however, the CPMG conditions [6,7] constrain the phase of the tailored pulse: the excitation phase should offset the refocusing pulse's phase by π/2, at every location of the imaged volume. This is particularly important when the refocusing pulses are nonselective and of variable flip angle (VFA) [8]. With these short, less than 180°, refocusing pulses, more than 100 echoes can be solicited from a single rFOX-generating tailored excitation pulse. The spiral-in transmit k-space trajectory is especially suited for this sequence: the center of k-space is sampled at the end of the pulse, allowing the first pulse of the refocusing train to follow rapidly and consecutive pulses with short spacing. Although tailored excitation in combination with a default-mode (turbo) spin echo acquisition has been reported in the past [9,10], this has been done without describing how the phase of the personalized pulse should be treated.

For the acceleration of rFOX-featuring sequences, rSENSE [3] has been shown to be more efficient than only reducing the field of view (FOV), allowing rFOX shapes that are non-rectangular and discontinuous. This method works by excluding voxels from parallel imaging reconstruction, after identifying these voxels based on a receive coil reference scan acquired with the same rFOX. Since the reference scan is acquired with GRE sequences, tailored pulses that generate a sequence-nonspecific rFOX are advantageous for rSENSE acceleration of rFOX-TSE acquisitions.

The aim of this paper is to provide this missing link between tailored pulses and nonselective refocusing pulses, thereby expanding their application to VFA-TSE sequences. Previous applications of rFOV imaging with TSE [9,10] illustrate the desire for such a combination, however the phase issue of CPMG was not addressed adequately. To allow the same pulse to be used in different sequence types, including rSENSE calibration scans, phase-matching is preferably achieved without sequence-specificity. Furthermore, we aim to achieve this by using the information that is already known from B_1^+ maps used for PTX radiofrequency pulse design (RFPD).

Materials and Methods

Phase-matching conditions

Tailored excitation pulses can in principle shape the magnetization pattern to any complex-valued target. The RF waveforms are numerically optimized, in combination with predefined gradient waveforms, and taking into account measured field distributions (B_0 and B_1^+). Conversely, the nonselective refocusing pulses that follow the excitation pulse in VFA-TSE

sequences produce a spatial phase pattern that is governed solely by the transmit phase of the driving mode.

The phase profile of the magnetization after excitation ($\varphi_{magnetization}(r)$) should be CPMG-matched to the phase of the refocusing pulses:

$$\varphi_{magnetization}(r) = \pi/2 + \angle\left[\sum_{j=1}^{N} c_j A_j(\mathrm{r}) e^{i\varphi_{tx,j}(\mathrm{r})}\right],$$

where $A_j(r)$ and $\varphi_{tx,j}(\mathrm{r})$ are the amplitude and absolute phase of the B_1^+ field per transmit channel j, at location r, for N channel, and the complex weights ($c_j = C_j e^{i\varphi_{c,j}}$) govern the combination of individual transmit channels. As $A_j(r)$ is measured using a B_1^+-mapping method, and c_j is defined, both of these are known. The transmit phase $\varphi_{tx,j}(r)$ is not known explicitly, but is nonetheless contained in any recorded signal, combined with additional contributions from the receive system and the specific sequence that was used to measure the signal.

In B_1^+-mapping methods that measure each channel sequentially (for example: AFI [11], DREAM [12,13]), the additional phase terms are identical for the measured signal[1] of each transmit channel. This measured signal phase can be used, instead of the unknown absolute transmit phase, to define the transmit coil sensitivities in RFPD. Since the additional phase terms are equal for all channels, they will result in an offset in the magnetization phase with respect to any arbitrary target:

$$\varphi_{magnetization}(r) = \varphi_{target}(r) - \varphi_{sequence+receive}(r).$$

For the magnetization to satisfy CPMG after excitation, the target phase requires pre-correction for this phase offset:

$$\varphi_{target}(r) = \pi/2 + \angle[\sum_{j=1}^{N} c_j A_j(\mathrm{r}) e^{i\varphi_{tx,j}(\mathrm{r})}] + \varphi_{sequence+receive}(r).$$

Even though the individual phase elements are still undetermined, the total expression is found if we calculate the phase of the refocusing mode using the measured B1+ maps, where again the phase of the measured signals replaces the absolute transmit phase:

$$\angle\left[\sum_{j=1}^{N} c_j A_j(\mathrm{r}) e^{i\,(\varphi_{tx,j}(\mathrm{r}) + \varphi_{sequence+receive}(r))}\right] = \angle[\sum_{j=1}^{N} c_j A_j(\mathrm{r}) e^{i\varphi_{tx,j}(\mathrm{r})}] + \varphi_{sequence+receive}(r).$$

The phase is as an *additional* requirement next to the targeted magnitude profile that describes the rFOX. The resulting rFOX is therefore expected to be the same in both TSE and GRE sequences.

Experiments

All experiments were conducted with a birdcage head coil (Nova Medical, Wilmington, MA) of which the two ports could be driven either in quadrature mode or independently, using the two transmit channels of the scanner (7T Achieva, Philips Healthcare, Cleveland, OH). When

[1] For example the stimulated echo and the free induction decay in DREAM [12]

tailored excitation pulses were used, the two channels were driven independently (PTX). During B_1^+-mapping, one channel was active at a time. All other RF pulses were emitted using the quadrature mode.

Healthy volunteers were scanned, after having provided informed consent. Calibration scans were performed as follows. First a B_0-map (multi-echo 3D GRE, ΔTE = 1 ms) was acquired for image based shimming on the brain with up to 3rd order shims. These shim settings were used for all subsequent scans of the same subject. A second B_0-map was acquired to determine the remaining static field variations for RFPD. For parallel imaging, the receive coil sensitivities (32 channel head coil, Nova Medical, Wilmington, MA) were measured using a 3D spoiled GRE sequence at 1° flip angle. A signal was recorded once using the individual receive channels and (in lieu of a body coil as external reference source) once using the two-channel head coil in quadrature mode. B_1^+ maps of the individual transmit channels were acquired using DREAM [13] (FID first, STEAM angle 40°).

Tailored pulses were computed on-site [14], using the B_0 and B_1^+ maps of one transverse slice, to generate a two-dimensionally selective rFOX. The complex RF waveforms were numerically optimized for a spiral k-space trajectory, of which the maximum k-space value to be sampled was adjusted for each experiment. Local SAR was monitored using a look-up-table of maximum local SAR values for each combination of amplitude ratio and relative phase of the two channels, summed over all samples of the PTX RF pulses [15].

Parallel imaging acceleration of scans featuring an rFOX was done using rFOX-adapted SENSE: rSENSE [3]. A full FOV is reconstructed, but the reconstruction is informed of the rFOX so that voxels outside the rFOX can be 'blanked'. For this, the receive coil sensitivity mapping was repeated with the same rFOX-generating pulses, scaled to 1° flip angle.

Experiment 1: phase matching in a CPMG sequence, full brain excitation

The first experiment was designed to test phase matching in a sequence in which the CPMG conditions are essential: VFA-TSE with 213 echoes per excitation. To facilitate analysis over a large area, the tailored pulse was targeted to excite the entire brain on a transverse slice. A second pulse was designed to target a spatially constant phase, reflecting a situation in which the transmit phase is (assumed to be) corrected for the phase of the quadrature mode. A third image was acquired using the scanner's default non-selective excitation pulse.

Pilot experiments (not shown) revealed a maximum achievable flip angle of 40°; higher values would exceed the hardware limit of 20 µT RF amplitude for these tailored excitation pulses (duration: 2.7 ms). This excitation flip angle was chosen for all scans in this experiment. Acquisition parameters are listed in **Table 1**.

Table 1. Scan Parameters

	TSE Exp. 1 & 2	TSE Exp. 3	GRE Exp. 3	Receive coil mapping
Scan type	3D VFA-TSE T2	3D VFA-TSE T2	3D GRE-EPI T2*	3D spoiled GRE
FOV (mm^3) (AP x RL x FH)	250 x 191 x 250	220 x 190 x 150	229 x 200 x 150	300 x 300 x 450
Scan orientation	sagittal	sagittal	sagittal	transverse
Resolution (mm)	1 x 1 x 1	0.6 x 0.6 x 0.6	0.35 x 0.35 x 0.35	4.7 x 4.7 x 4.7
Undersampling factor	1.2 x 2.8	2.3 x 3.3	2.5 x 2.5	-
Excitation flip angle (˚)	40[A] / 85[B] / 90[C]	90	22	1
Shot length	213	162	9	-
TSE echo spacing (ms)	2.3	3.5	-	-
TSE VFA range (˚)	[10,90]	[10,90]	-	-
TE (ms)	281 (effective)	295 (effective)	27	0.79[E] / 0.71[F]
TR (ms)	3,158	3,158	66[E] / 65[F]	8[E] / 39[F]
Fat Suppression	SPAIR[D]	SPAIR[D]	-	-
Signal averages	2	2	1	2[G]
Scan time (m:s)	9:45.6	10:16	7:20[A] / 7:17[B]	5:24

A: Experiment 1, rFOX and standard excitation
B: Experiment 2, rFOX
C: Experiment 3, standard excitation
D: SPAIR: Spectral Attenuated Inversion Recovery
E: When a standard excitation pulse is used
F: When a tailored rFOX pulse is used
G: Two scans with different receive coil setups

Experiment 2: phase-matched excitation pulses in GRE and TSE sequences, excitation of the visual cortex

The second experiment tested if the same rFOX is created in GRE and TSE sequences. To this end, a tailored pulse was used in the low-resolution GRE-based sequence for receive coil sensitivity mapping. Subsequently, VFA-TSE images were acquired using the same excitation pulse, and using the coil sensitivity maps for rSENSE unfolding. A consistent rFOX between the calibration scan (GRE) and accelerated images (TSE) is important for this technique, otherwise signal unfolding artifacts could occur [3]. The rFOX target was the visual cortex and the hardware-limited flip angle was 85°. This was a small deviation from the 90° excitation in the reference VFA-TSE image with non-selective excitation and otherwise identical parameters. The receive coil mapping parameters were the same as the standard protocol, but with a longer TR to incorporate the tailored pulse (duration: 9.7 ms), see **Table 1**.

Experiment 3: high resolution imaging of the temporal lobe using GRE and TSE

In experiment 3, phase-matching was tested in an area that generally suffers from poor B_1^+ performance at 7T, the temporal lobe. This rFOX was imaged at high resolution using both VFA-TSE and GRE with multishot EPI (GRE-EPI). Because of the small rFOX area, a higher SENSE factor could be chosen compared to the full brain excitation in Experiment 1. Pulse duration was 9.7 ms, scan parameters are in **Table 1**.

Results

Experiment 1: phase matching in a CPMG sequence, full brain excitation

Figures 1a-d show the B_1^+ maps and targets (**Figures 1e** and 1**g)** that were generated in this experiment. The phase-matched RF pulse had a maximum amplitude of only 11.7 µT, versus 19.7 µT for the constant-phase-targeted pulse (**Figures 1f** and **1h**).

The TSE images with phase-matched excitation (**Figures 2b** and **2e**) match the appearance of those acquired with standard excitation (**Figures 2a** and **2b**). Patterns of reduced signal intensity are seen in the images with constant-phase excitation (**Figures 2c** and **2f**). Bloch simulations[16] (**Figure 2h**) show the excitation phase is off-CPMG in the same area, confirming the sequence's sensitivity to the CPMG conditions.

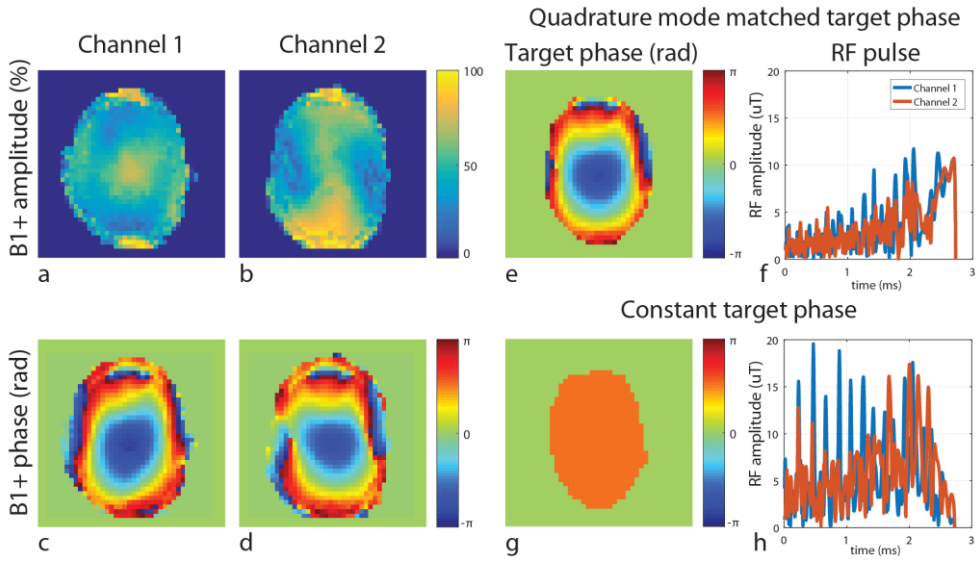

Figure 1. *Experiment 1: Full brain excitation. Measured B_1^+ maps for both channels,* ***a****,****b****: amplitude and* ***c,d****: phase from the stimulated echo (STE) signal.* ***e,g****: Target magnetization phase pattern masked by the shape of the target magnetization amplitude, for the phase matched (****c****) and spatially constant phase pattern (****g****). Corresponding PTX RF amplitude waveforms (****f****,****h****).*

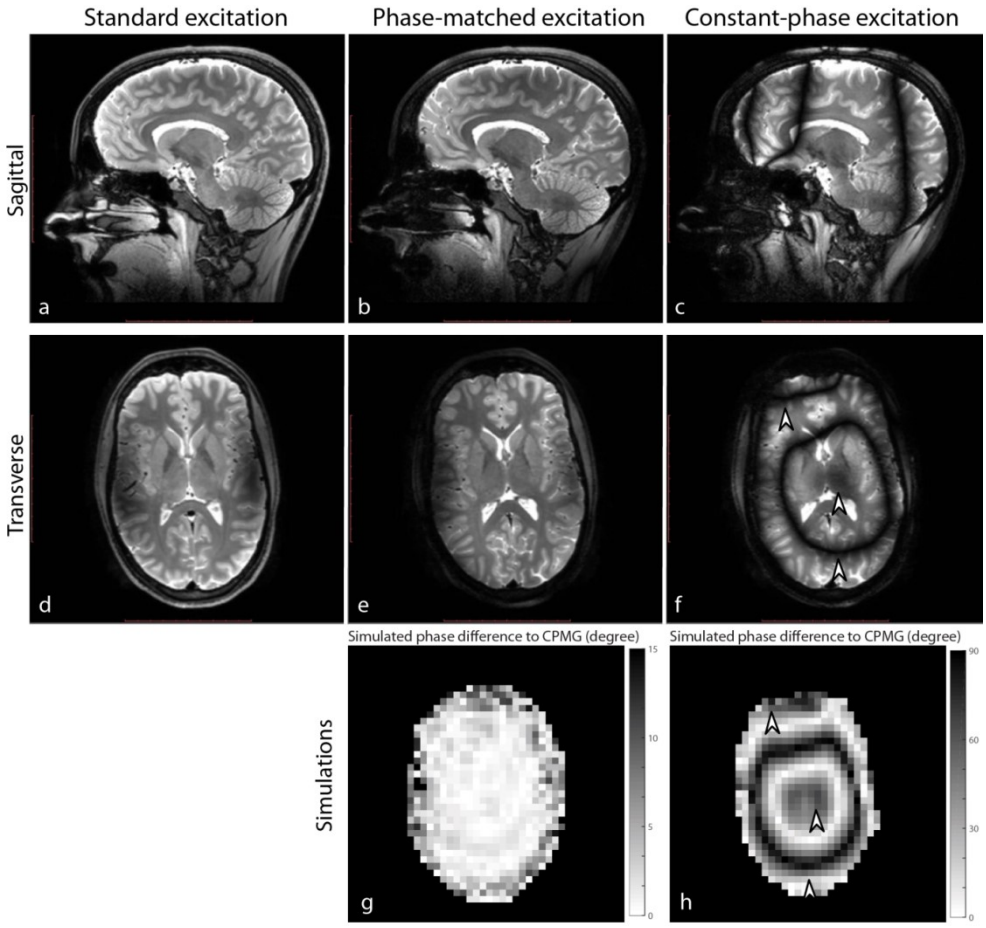

Figure 2. *Experiment 1, full brain excitation.* ***a-f:*** *3D VFA-TSE images acquired using different excitation pulses in combination with nonselective refocusing pulses.* ***a,d****: Non-selective standard excitation pulse,* ***b,e****: quadrature phase matched tailored pulse with full brain target,* ***c,f****: constant phase tailored pulse with nearly full brain target.* ***a-c****: (native) sagittal orientation.* ***d-f****: transverse reconstructions at the position of the target slice, where the measured information was used in RFPD.* ***g,h****: Simulated difference between the phase of the tailored pulse and the phase pattern prescribed by CPMG, at the same transverse slice . Note that the in* ***h*** *the full range of values is shown, while in* ***g*** *the window of values is reduced to 1/4th to show any contrast. The pattern (marked with arrowheads) of locations with a large phase deviation (****h****) is similar to the signal loss in the TSE images in* ***f.*** *In the transverse plane, it mainly manifests as a ring-like structure, and extends in the feet-head direction, as can be seen in* ***c****.*

Experiment 2: phase-matched excitation in GRE and TSE sequences, visual cortex

The rFOX was successfully created in the GRE scan (**Figures 3b** and **3d**), and similarly in the TSE scan (**Figures 3e** and **3g**). No artifacts are observed when the zoomed-in rFOX-TSE and reference images (**Figures 3i** and **3j**) are compared, confirming that rSENSE was applied successfully .

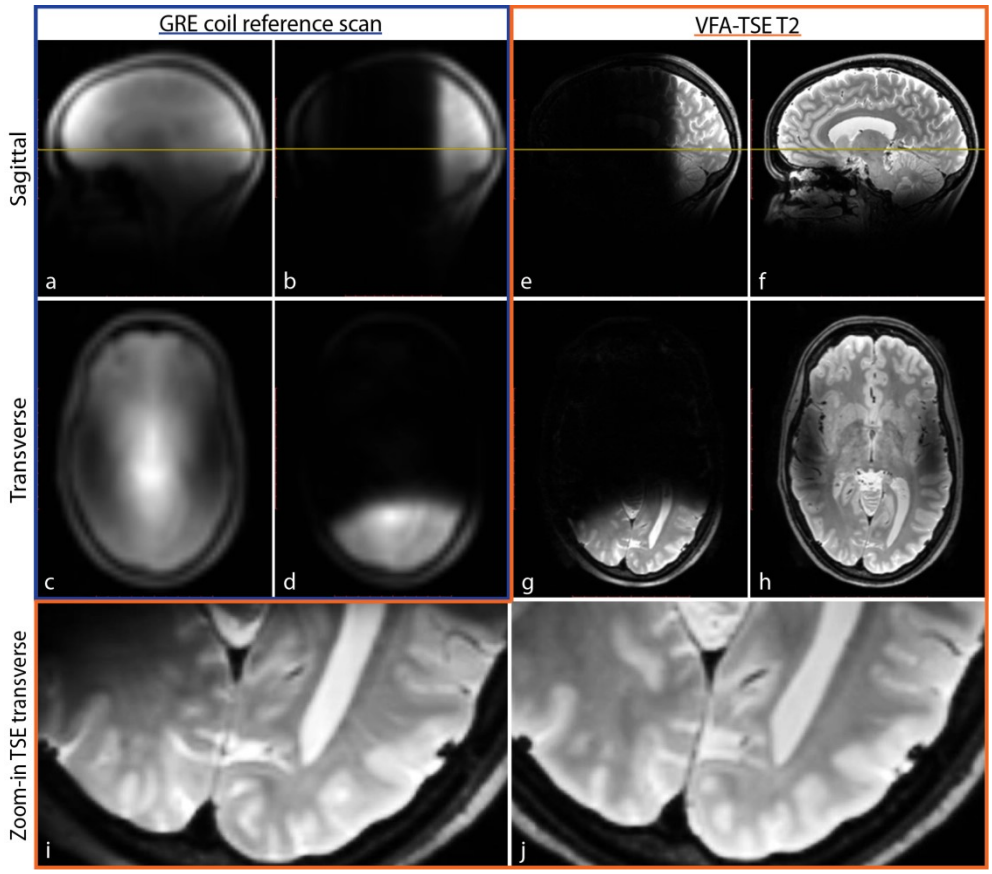

Figure 3. *Experiment 2, excitation of the visual cortex.* ***a,b,c,d****: Low resolution GRE images used for receive coil sensitivity mapping.* ***e,f,g,h****: TSE images using a 3D VFA acquisition and (r)SENSE acceleration.* ***a,c****: GRE with standard excitation for whole brain,* ***b,d****: GRE with phase matched rFOX,* ***e,g****: TSE with phase matched rFOX,* ***f,h****: TSE with standard excitation.* ***Top row****: sagittal (native) view,* ***middle row****: transverse (reformatted) view.* ***Bottom row****: zoomed-in sections of* ***g,h****.* ***i:*** *Phase matched rFOX,* ***j:*** *standard excitation.*

Experiment 3: high resolution imaging of the temporal lobe using GRE and TSE

High resolution images were successfully obtained (**Figure 4**). Some improvements in image quality can be seen in the rFOX images: the TSE image appears more homogeneous (**Figures 4h** vs. **4j**) and the GRE-EPI displays a lower noise level towards the center of the brain (**Figures 4g** vs **4i**). The first observation is attributed to a locally homogeneous excitation, the second to a lower g-factor from using rFOX with SENSE.

Discussion

This study has been performed as a proof of principle to show that subject specific multidimensional selective excitation can be performed with VFA-TSE and GRE acquisitions. The acquisitions with rFOX were accelerated using rSENSE: instead of reducing the

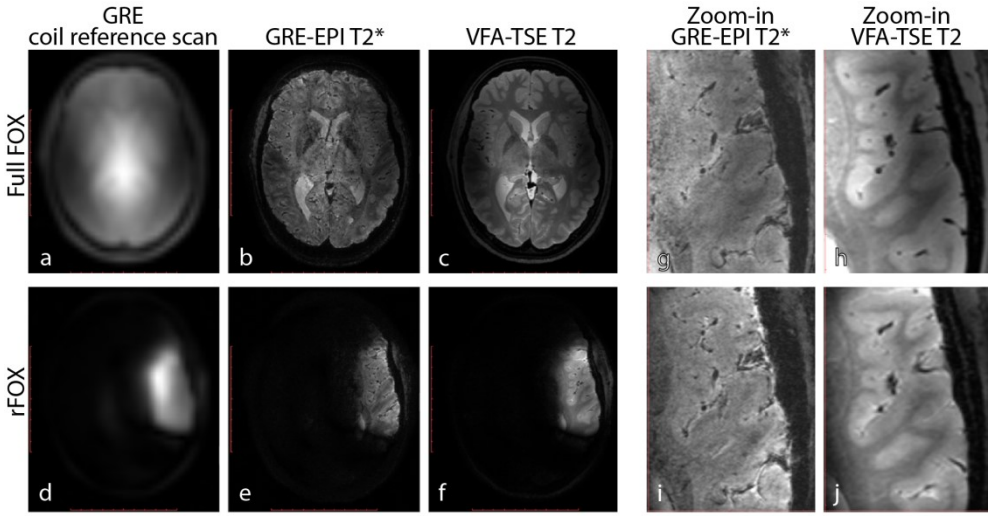

Figure 4. *Experiment 3, excitation of the temporal lobe with high resolution imaging.* ***a,d****: Low resolution GRE coil reference scan,* ***b,e****: T2* GRE-EPI at (0.35 mm)^3,* ***c,f****: T2 VFA-TSE at (0.6 mm)^3.* ***g,h,i,j****: Zoomed versions of the high resolution images (****b,c,e,f*** *respectively).* ***Top row****: standard excitation,* ***bottom row****: phase-matched rFOX.*

prescribed FOV, the SENSE reconstruction is improved by the reduced number of voxels that require unfolding.

Earlier work that featured tailored excitation in combination with VFA-TSE [10] used interferometrically acquired B_1^+ maps of which the phase-implications are not described. We speculate that the sensitivity maps are pre-calibrated with respect to default excitation mode and the transceive phase, explaining the successful TSE experiments.

For phase-matching, the phases of any B_1^+-mapping method or other combination of signals can be used, provided that the transmit phase is the only phase contribution that varies between the individual signals. The presented method is developed from a PTX point-of-view, but is equally valid for single channel systems. However, transmit phase maps are no longer required here and the transmit phase and target phase could simply be defined as, respectively, zero and π/2 at every location. The phase can't be ignored completely (as in a pure magnitude least squares optimization), since this would violate the CPMG conditions.

A 90° flip angle was not always accomplished. RF amplitude-limiting techniques such as VERSE [17] may be used to reduce the amplitude, and possibly also the length [18], of the tailored pulses. The RF amplitude needed to excite the same rFOX was reduced when the target phase was matched to quadrature mode, compared to a constant target phase. This reduction is a noteworthy advantage over an improperly chosen target phase and advocates the use of phase-matching even for non-TSE imaging. We did not systematically investigate the possible improvements of existing TSE protocols, and for TSE imaging the benefits of using rFOX remain to be seen – applications could include imaging near structures in motion.

In conclusion, phase matched excitation pulses allow VFA-TSE imaging with standard refocusing pulses. This was achieved by using phase information from a signal that is acquired as part of conventional B_1^+-mapping. The applicability of these pulses remained uncompromised in GRE sequences, allowing coil sensitivity mapping of the same rFOX, and ultimately rSENSE acceleration of the TSE acquisition.

References

[1] Grissom W, Yip C, Zhang Z, Stenger VA, Fessler J a, Noll DC. Spatial domain method for the design of RF pulses in multicoil parallel excitation. Magn Reson Med 2006;56:620–9. doi:10.1002/mrm.20978.

[2] Schneider JT, Kalayciyan R, Haas M, Herrmann SR, Ruhm W, Hennig J, et al. Inner-volume imaging in vivo using three-dimensional parallel spatially selective excitation. Magn Reson Med 2013;69:1367–78. doi:10.1002/mrm.24381.

[3] Mooiweer R, Sbrizzi A, Raaijmakers AJE, van den Berg CAT, Luijten PR, Hoogduin H. Combining a reduced field of excitation with SENSE-based parallel imaging for maximum imaging efficiency. Magn Reson Med 2016;0:1–9. doi:10.1002/mrm.26346.

[4] Katscher U, Börnert P, Leussler C, van den Brink JS. Transmit SENSE. Magn Reson Med 2003;49:144–50. doi:10.1002/mrm.10353.

[5] Pauly J, Nishimura D, Macovski A. A k-space analysis of small-tip-angle excitation. J Magn Reson 1989;81:43–56. doi:10.1016/0022-2364(89)90265-5.

[6] Carr HY, Purcell EM. Effects of Diffusion on Free Precession in Nuclear Magnetic Resonance Experiments. Phys Rev 1954;94:630–8. doi:10.1103/PhysRev.94.630.

[7] Meiboom S, Gill D. Modified spin-echo method for measuring nuclear relaxation times. Rev Sci Instrum 1958;29:688–91. doi:10.1063/1.1716296.

[8] Busse RF, Hariharan H, Vu A, Brittain JH. Fast spin echo sequences with very long echo trains: design of variable refocusing flip angle schedules and generation of clinical T2 contrast. Magn Reson Med 2006;55:1030–7. doi:10.1002/mrm.20863.

[9] Ullmann P, Junge S, Wick M, Seifert F, Ruhm W, Hennig J. Experimental analysis of parallel excitation using dedicated coil setups and simultaneous RF transmission on multiple channels. Magn Reson Med 2005;54:994–1001. doi:10.1002/mrm.20646.

[10] Malik SJ, Hajnal J V. Phase relaxed localized excitation pulses for inner volume fast spin echo imaging. Magn Reson Med 2015;3:848–61. doi:10.1002/mrm.25996.

[11] Yarnykh VL. Actual flip-angle imaging in the pulsed steady state: a method for rapid three-dimensional mapping of the transmitted radiofrequency field. Magn Reson Med 2007;57:192–200. doi:10.1002/mrm.21120.

[12] Nehrke K, Börnert P. DREAM-a novel approach for robust, ultrafast, multislice B_1 mapping. Magn Reson Med 2012;68:1517–26. doi:10.1002/mrm.24158.

[13] Nehrke K, Versluis MJ, Webb A, Börnert P. Volumetric B_1^+ Mapping of the Brain at 7T using DREAM. Magn Reson Med 2014;71:246–56. doi:10.1002/mrm.24667.

[14] Sbrizzi A, Hoogduin H, Lagendijk JJ, Luijten P, Sleijpen GLG, van den Berg C a T. Time efficient design of multi dimensional RF pulses: Application of a multi shift CGLS algorithm. Magn Reson Med 2011;66:879–85. doi:10.1002/mrm.22863.

[15] Hoogduin H, Mooiweer R, Mens G, Hajnal J V, Luijten P, Malik SJ. Initial experience with SPIral Non Selective (SPINS) RF pulses for homogeneous excitation at 7T. Proc. Intl. Soc. Mag. Reson. Med, 2014, p. 4914.

[16] Hargreaves B. Bloch Equation Simulator n.d. http://mrsrl.stanford.edu/~brian/blochsim/ (accessed February 1, 2012).

[17] Lee D, Grissom W a., Lustig M, Kerr AB, Stang PP, Pauly JM. VERSE-guided numerical RF pulse design: A fast method for peak RF power control. Magn Reson Med 2012;67:353–62. doi:10.1002/mrm.23010.

[18] Lee D, Lustig M, Grissom WA, Pauly JM. Time-optimal design for multidimensional and parallel transmit variable-rate selective excitation. Magn Reson Med 2009;61:1471–9. doi:10.1002/mrm.21950.

Chapter 5

Ultra-high isotropic resolution imaging of the hippocampus through a reduced field of excitation

Ronald Mooiweer, Alessandro Sbrizzi, Alexander J.E. Raaijmakers, Nico A.T. van den Berg, Peter R. Luijten, Hans Hoogduin

This chapter has been submitted for publication.

Abstract

By using a reduced field of excitation (rFOX), the hippocampus could be imaged at an ultra-high isotropic resolution of 0.35^3 mm^3, in a scan time that allows for multiple acquisitions on the same subject: 10 minutes. Subject-specific rFOX-generating pulses require additional calibration steps, but reduce the noise levels compared to conventional excitation strategies. With isotropic voxel sizes, the hippocampus can be viewed in any orientation.

Introduction

The hippocampus is a brain structure belonging to the limbic system. It is important in the creation and processing of memories and is therefore subject of many memory related studies. Two hippocampal structures reside in the medial temporal lobes; one in each hemisphere, neighboring the midbrain. With a total typical length of several centimeters, subfields of the hippocampus have been identified with only sub-millimeter dimensionality (1,2). A matching high spatial resolution is desirable to image these structures (3,4), as coarse (>1mm) resolution voxels might obscure these substructures. Moreover the accuracy of volumetric measurements, a commonly used tool in the study of the hippocampus, can benefit from an increasingly higher imaging resolution through an increased precision.

With the introduction and development of 7T MRI, higher imaging resolutions have become feasible, resulting from the increased signal levels compared to lower field strengths. An overview of the frontiers of ultra-high resolution imaging up to 7T field strength is included in the Appendix, **Table A1**. The protocols featuring the smallest in-plane voxel dimensions (5,6) make use of a much coarser resolution in the through-plane direction. This approach boosts the SNR with respect to isotropic ultra-high resolution. However, the benefits of having a high resolution are partly annulled by choosing highly anisotropic voxels. Isotropic voxels are also desirable since they offer the ability of reformatting the images and viewing the anatomy from any angle after the images have been acquired. Protocols that do offer ultra-high isotropic resolution (5,7) require such a long scan time that no other scans can be performed on the same subject within a timeframe that is considered acceptable for scanning volunteers (1 hour).

Two dimensionally selective excitation has since long been associated with a promise of imaging at more detailed resolution and/or in a reduced scan time. For EPI-based functional imaging, in which long echo trains distort the acquired images, this has been confirmed on several occasions (8–10). This paper describes a study into utilizing the potential benefits of two dimensionally selective excitation for structural imaging of the hippocampus. Using more general terminology, a reduced field of excitation (rFOX) is created that limits the excited area in two dimensions to the contour of the hippocampus. The time spent on the acquisition can then be reduced by using a reduced field of view (rFOV) or a reduced parallel imaging reconstruction (11,12). The latter has been shown to offer the same or superior scan time advantages compared to rFOV imaging, as non-rectangular rFOX shapes and receive coil encoding can be exploited (12). Additionally, rFOX can also prevent surrounding tissues from generating artifacts, which otherwise might deteriorate the image quality inside the ROI (13).

Imaging with T2* contrast is time-efficient (14,15) and the contrast is particularly pronounced at 7T (16–18). By using multi-shot EPI, T2* weighted acquisitions can be performed rapidly, even though relatively long TE and TR are used for a strong T2* contrast (15). Instead of a typical single shot 2D EPI (as is used in fMRI), multishot EPI uses a moderate shot length to acquire multiple echoes (approximately 10) per TR without the distortions that are associated with the former. Moreover, while traditional EPI is predominately used for (multi-) slice encoding, multi-shot EPI supports 3D encoding and is therefore compatible with imaging at high isotropic resolution. In our experiments we compared images that were acquired using multishot EPI with parallel imaging alone, as well as in combination with rFOX. To arrive at a

protocol that has practical feasibility, i.e. allowing multiple scans of different types to be performed on the same subject, the acquisition time was limited to 10 minutes per scan.

Material and methods

Experiments: protocol setup

Based on the T2* weighted 3D gradient echo sequence with multi-shot EPI (15), protocol optimization was performed on several volunteers to image the hippocampus at ultra-high resolution (0.35^3 mm^3). While initially shorter scan times were considered (19), a 10 minute long protocol using rFOX and an acquisition bandwidth similar to the original sequence was established and scanned in a healthy volunteer (protocol A, **Table 1**). Here, a FOV enclosing the full brain was used in combination with SENSE parallel imaging in two dimensions and rFOX in two dimensions to improve the image quality. The rFOX was obtained by using numerically designed excitation pulses (20,21) that were two-dimensionally selective in the transverse plane (**Figure 1b**). The protocol was optimized for the combination with the 2D selective excitation by aligning the frequency encoding direction with the nonselective direction of the excitation pulse: feet to head (sagittal 3D acquisition). SENSE acceleration was applied in the AP and RL directions. Prior to this T2*-weighted scan, the receive coil sensitivity was mapped using the same 2D selective excitation pulse (refscan A in **Table 1**), to enable SENSE acceleration of the rFOX (rSENSE)(12). Inclusion of the tailored excitation pulse resulted in a longer scan time of 5:24 compared to 1:05 of the original receive coil reference scan.

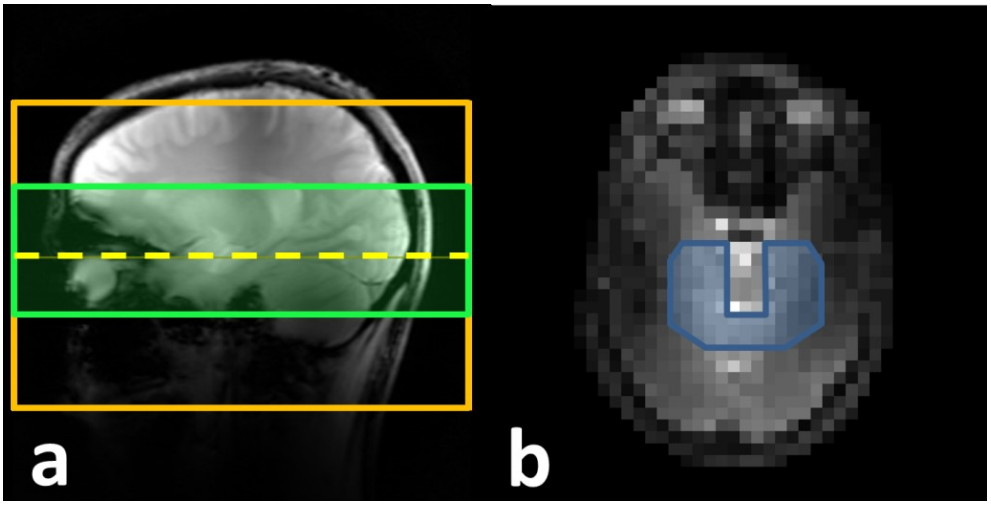

Figure 1. a) *Localizer image showing the coverage of protocol A and B before oversampling with an orange rectangle, and that of protocol C in green. The location of the transverse slice through the hippocampus that is used for RFPD is marked with a yellow dashed line.* ***b)*** *Magnitude image of one of the signals collected in the B_0-mapping scan that is used for planning the rFOX (blue U-shape).*

Table 1. Imaging parameters.

	Protocol A	Protocol B	Protocol C	Refscan A	Refscan B
Excitation pulse selectivity	2D-hippocampal	1D-slab	1D-slab	2D-hippocampal	1D-slab
3DFOV (FH x AP x RL) (mm)	150 x 229.2 x 200.6	150 x 229.2 x 200.6	65.1 x 240 x 192.6	300 x 300 x 450	300 x 300 x 450
Matrix (FE x PE1 x PE2 (slice))	428 x 649 x 573	428 x 649 x 573	684 x 550 x 186	96 x 64 x 64	96 x 64 x 64
Resolution (mm)	0.35 x 0.35 x 0.35	0.35 x 0.35 x 0.35	0.350 x 0.35 x 0.350	4.69 x 4.69 x 4.69	4.69 x 4.69 x 4.69
Frequency encoding direction	FH	FH	AP	RL	RL
Phase encoding direction 1 x 2	AP x RL	AP x RL	RL x FH	AP x FH	AP x FH
Flip angle (˚)	23	23	25*	1	1
TR / TE (ms)	90 / 27	90 / 27	112* x 27	39.0 / 0.71	8.0 / 0.79
BW readout direction (Hz / pixel)	36.9	36.9	39.0	2071.3	2071.3
BW phase encoding direction (Hz / pixel)	504.4	504.4	593.8	-	-
EPI factor	11	11	11	-	-
Slice-oversampling factor	1	1	default	default	default
k-space shutter	no	no	default	default	default
SENSE PE1 x PE2	2.3 x 2.3	2.3 x 2.3	2.3 x 1	-	-
P oversampling factor	1	1	1	-	-
Fat Suppression	no	no	SPIR	-	-
Scan time (m:s)	9:45.6	9:45.6	9:49.4	5:23.8	1:05.8

FOV: field-of-view, AP: anterior–posterior, RL: right–left, FH: feet–head, FE: frequency encoding (read-out), PE: phase encoding (2 PE directions in 3D AQ), TR: repetition time, TE: echo time, BW: bandwidth, SENSE: parallel imaging acceleration factor (sensitivity encoding), SPIR: spectral presaturation by inversion recovery. *FA of protocol C is slightly higher than A and B to match the longer TR, which was the shortest possible for this geometry.

For a direct evaluation on the effect of the 2D localized excitation, protocol B was designed to have identical parameters to protocol A but with non-selective excitation pulses and preceded by a regular SENSE reference scan (refscan B in **Table 1**). Finally, a third protocol was optimized to best image the hippocampus without the use of numerically designed RF pulses. A transverse 3D acquisition was chosen to minimize the number of required slices using conventional slab-selective excitation. SENSE was applied in one direction only (protocol C in **Table 1**, **Figure 1a**). The three different protocols were all evaluated in three additional subjects to enable a side-by-side comparison.

The full brain FOV in combination with an ultra-high isotropic resolution resulted in very large data sets. To reduce this, the prescribed FH coverage of these scans was limited to 150 mm (**Figure 1a**), making use of the standardly applied over-sampling in the readout direction. With over-sampling, a larger FOV is encoded than prescribed, to prevent aliasing of the signal, but the excess information is disregarded after reconstruction.

All experiments were performed on a 7T scanner (Philips) using a dual channel transmit coil (Nova) and a 32 channel receive coil (Nova). Healthy volunteers were scanned, after they provided informed consent to participation in the study.

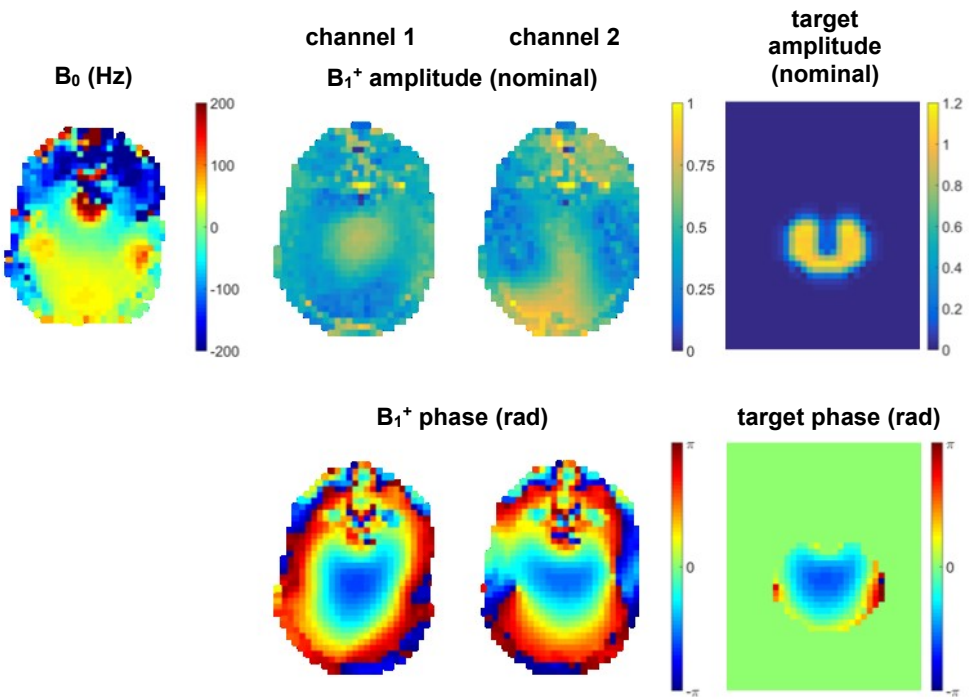

***Figure 2**. Typical field maps and target pattern used as input for RF pulse design. The measured maps are masked to show tissue containing voxels only.*

Workflow and calibration scans

The rFOX-generating excitation pulses were designed for every subject, on a transverse slice and taking into account the spatial variations in B_0 and B_1^+. First, image based B_0 shimming was performed on the brain before all scans, after which the measured resonance frequency was fixed. Then, B_0 and B_1^+ maps were acquired. The transverse slice that was used for the design of the excitation pulses was positioned at the level of the hippocampus, in the middle of its structure (**Figure 1a**). B_0-maps were acquired using a double TE GRE image (ΔTE = 1 ms , scan time 21 s) and B_1^+ maps using DREAM (scan time 33 s) (22).

Figure 2 shows the information that was used as input for the pulse design software, for one subject. The pulse design software was accessed off-line as a graphical user interface in a commercial software package (MATLAB, The Mathworks Inc., Nantick, MA). Guided by the localizer images and one of the images of the B_0-maps (**Figure 1**b), a region of interest covering both of the hippocampi was drawn around the brain stem, resulting in a U-shaped excitation target. The brain stem was excluded in the design of the rFOX to minimize the signal-generating volume and to avoid possible artifacts coming from this pulsating region. A spiral-in transmit k-space with a maximum value of 5 rad/cm was chosen and the ROI was filtered in the k-space domain to fit within this prescribed trajectory. This resulted in a small transition zone between the rFOX and tissue that should not be excited, in image space. Since parallel transmission was used, the local and global SAR of the dual-channel RF pulses was

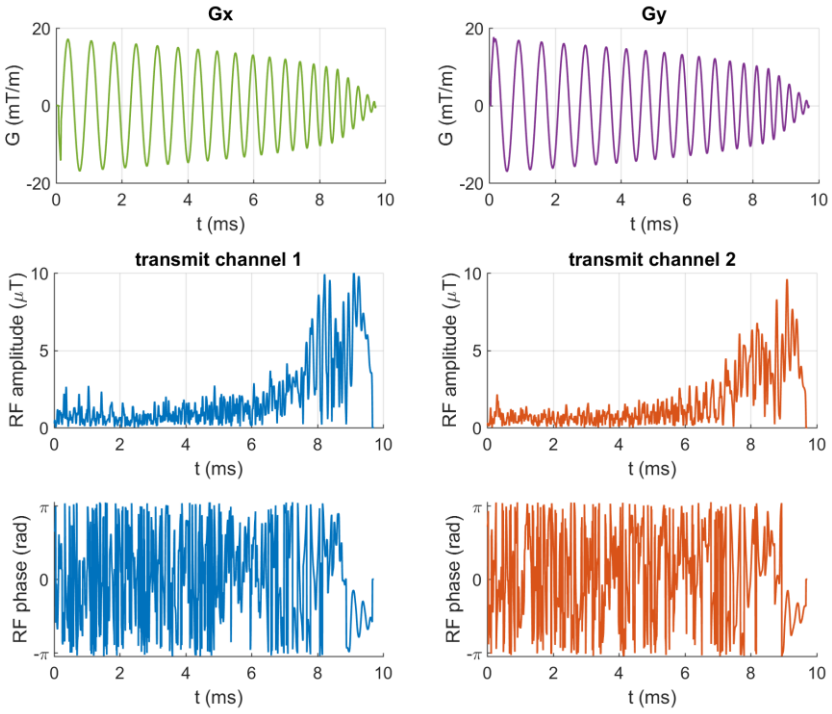

***Figure 3**. Waveforms for 2D selective excitation, which are output from RF pulse design for one subject.*

supervised via lookup-table approach, integrated into the scanner software (23). As the tailored excitation pulses were designed in the low tip angle approximation, amplitude scaling could be used to achieve different flip angles for the T2* protocol (23˚) and the receive coil sensitivity map (1˚). The resulting gradient and RF waveforms are shown in **Figure 3** for the same subject.

Multiplanar reconstructions

Multiplanar reconstructions were made in a DICOM viewer (RadiAnt 4.0.3.16415, Medixant, Poznań, Poland). A 2D slice through the original 3D data was angulated twice to show as much of the hippocampal structure in a single image, along its the long axis. Images perpendicular to this plane were also reconstructed.

Results

The effective rFOX in **Figure 4** shows the intended U-shape in the transverse plane and no restriction of the excitation in the feet-head direction. Excitation is not always limited to within sharp contours of the target, which is acceptable in the rSENSE method. Still, a large volume fraction of the head is not generating signal, which should lead to clear improvements in parallel imaging performance compared to the protocol with nonselective excitation. Indeed, the images of protocol B in **Figure 3** display a poor SNR in the center of the brain, which can be related to a reduced g-factor in the 2D SENSE unfolding.

The transverse image of method B in subject 2 (**Figure 4**) displays a slight central darkening instead of the central brightness seen in subjects 1 and 3. In fact, receive coil sensitivity correction (CLEAR / bias correction) has not been applied during this image's reconstruction. This is a linear scaling of the signal intensity and does not influence the local SNR.

The images resulting from protocol A (rFOX) and C (the best alternative, with fewer slices and SENSE in 1 direction) are compared in **Figure 5**, showing zoomed and reformatted images. In most images, the SNR of these ultra-high resolution images is sufficient to show the folded structure of the hippocampus together with small vessels entwined within the structure. In the head of the hippocampus however, the images of the highly folded structure are plagued by noise in protocol C, with noise levels increasing towards the center of the brain. With protocol A, less noisy images were obtained here in 5 out of 6 images shown. Only the rFOX image of the left hippocampal head in subject 1 appears more blurry than with the alternative method. In the middle and tail sections of the hippocampus the same trend of less noisy rFOX images can be observed, although the effect is less pronounced. In several of the rFOX images the signal drops off rapidly near the edge of the hippocampus, possibly obscuring part of the hippocampal formation as well. This could be due to the rFOX having been chosen overly restrictive, or because of a slight displacement of the subject after planning of the rFOX.

The isotropy of the data was exploited to create images along and perpendicular to the long axis of the hippocampus in **Figure 6**. These images again show the complex features and numerous vessels

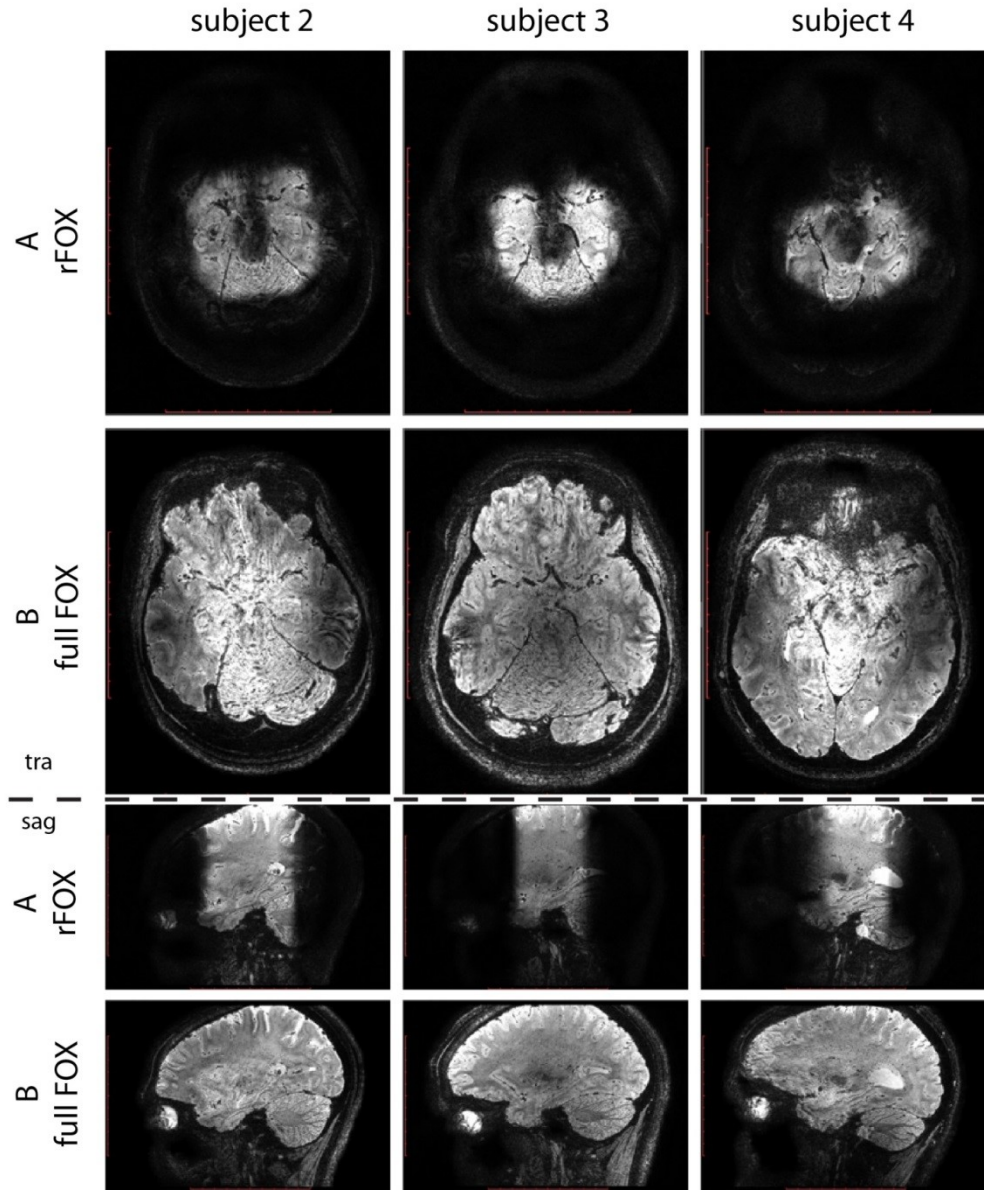

Figure 4. *Comparison of protocol A and B, showing the effective rFOX in the 3 subjects. Top panels: transverse view, bottom: sagittal (native) view.*

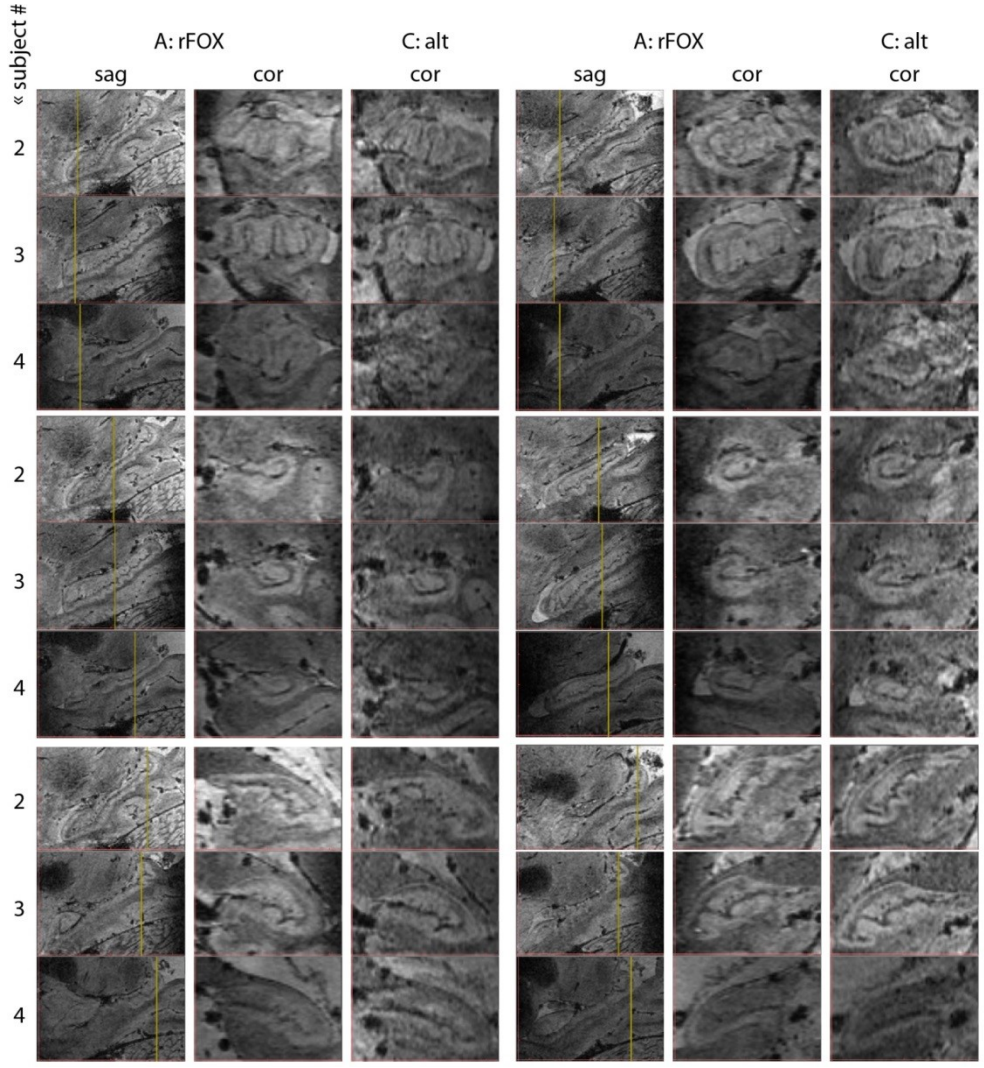

***Figure 5**. Zoomed images of the right and left hippocampal formations of three volunteers, for the rFOX method (protocol A, sagittal and coronal) and best alternative (protocol C, coronal). The coronal images are zoomed in to a more detailed level than the sagittal views. Three levels are shown; first 3 rows: head, second 3 rows: middle, and third 3 rows: tail of the hippocampus. The positions of the coronal slices are marked with a yellow lines on the sagittal images. Contrast windows are the same in all images to avoid bias through manual optimization.*

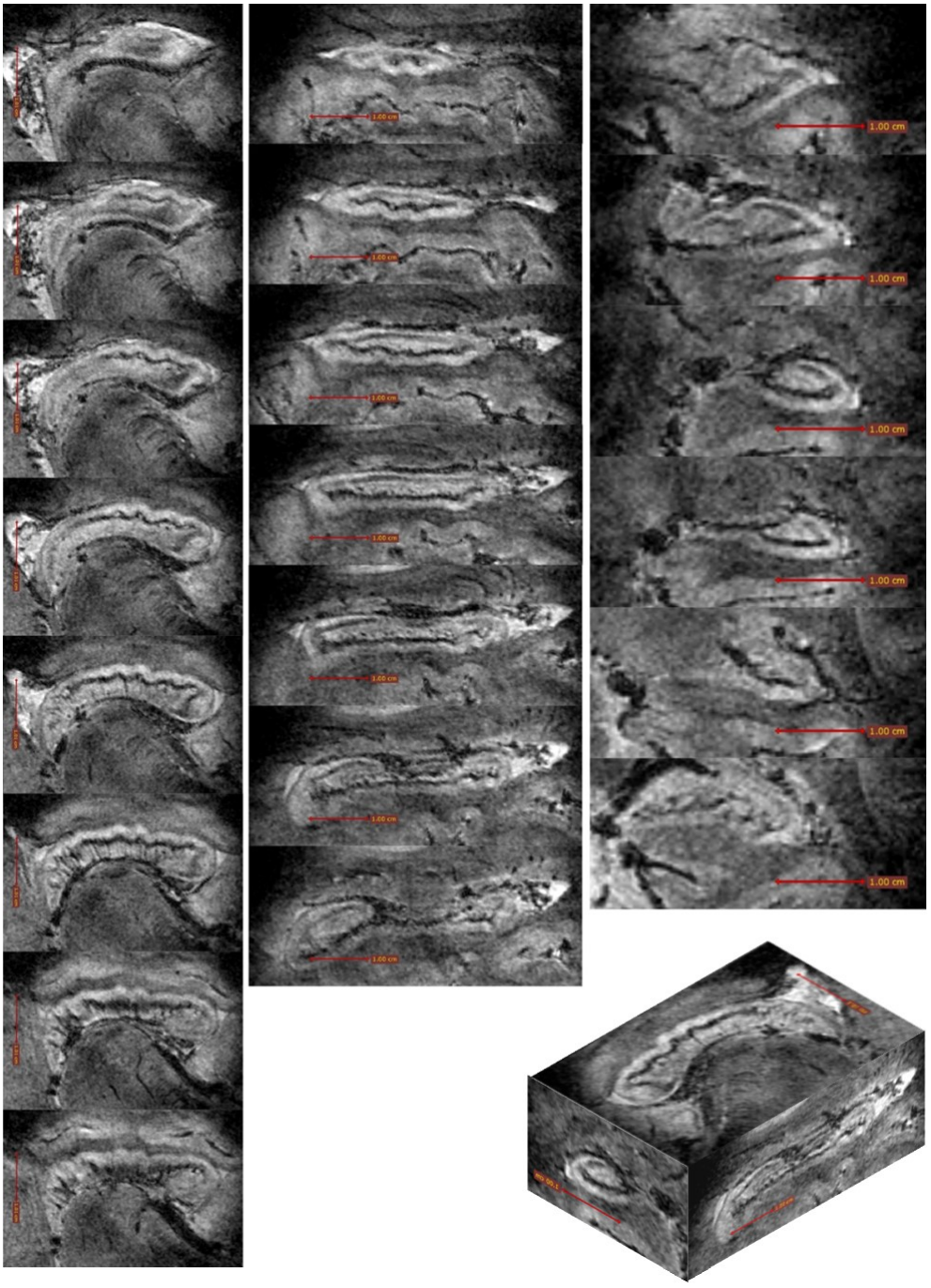

Figure 6 *(previous page). Reconstructed images of hippocampus (Right) in an orientation that matches the general orientation of the structure. The images in the left column are twice angulated transversal, with an interval of 1 slice (every 3rd slice is shown). The images in the middle column are twice angulated sagittal, with an interval of 3 slices (every 5th is shown). Right column: twice angulated coronal, at irregular interval, showing the head, middle section and tail of the hippocampus. The red scale bars are 1 cm in each image. The inset shows how the images relate to each other in 3D.*

Discussion and conclusion

T2* weighted imaging of the hippocampus was shown to be feasible at 0.35 mm isotropic resolution (43 nL) in a 10 minute acquisition by using two-dimensionally selective rFOX. The subject specifically designed excitation pulses had a duration of 10 ms. In the T2*weighted scans the 10 ms long, subject-specifically designed, excitation pulses did not lead to timing conflicts, as the TR was sufficiently long to accommodate these. However, the TR of the receive coil calibration scans had to be extended, resulting in a scan time of 5 minutes compared to 1 minute for the standard nonselective scan. No attempt has been made to reduce the calibration scan time, but possible solutions could be to use multi-shot EPI (15) for the calibration scan, or to reduce the pulse length through time-optimum gradient design (24,25). Alternatively, it has been suggested to use the standard (full FOX) receive coil reference scan in combination with a rFOX obtained through simulation (12). A lengthy calibration scan might also be acceptable if the obtained information could be used for several scans, for example to obtain different contrast types of the same object of interest.

The rFOX obtained with the subject specific excitation pulses was not always capturing the entire shape of the hippocampus. Accurate planning remains a challenging aspect of rFOX imaging; a more detailed image to plan the rFOX might be of benefit here. Superfluous excitation outside our targeted region of interest might have resulted in fold-over artifacts if an rFOV was prescribed, by using rSENSE this has been avoided. For a greater level of artifact reduction, 3D selective excitation could also be beneficial (26).

Motion-compensation (7) and post-acquisition alignment of segmented acquisitions (5) are used in other ultra-high resolution experiments with long acquisition times. While motion compensation might provide additional robustness in the rFOX protocol, by limiting the acquisition time the need for this is inherently reduced.

This study has been performed as a proof of principle to show how subject-specific rFOX pulses can be used to push the limits of imaging at high resolution: structural imaging of the hippocampus at unprecedented detail per imaging time has been demonstrated. A 2D selective rFOX was used to maintain a good image quality in this highly challenging situation. In future studies, one might consider integrating the pulse design software on the scanner console to further improve the workflow. Volumetric analysis and subfield registration can also be performed, although automated approaches might not yet be suitable for this type of data with rFOX.

Acknowledgements

The authors would like to thank to Jaco Zwanenburg and Fredy Visser for their help in optimizing the imaging sequences.

References

1. Hyman B, Van Hoesen G, Damasio A, Barnes C. Alzheimer's disease: cell-specific pathology isolates the hippocampal formation. Science (80-.). 1984;225:1168–1170. doi: 10.1126/science.6474172.

2. Langston RF, Stevenson CH, Wilson CL, Saunders I, Wood ER. The role of hippocampal subregions in memory for stimulus associations. Behav. Brain Res. 2010;215:275–291. doi: 10.1016/j.bbr.2010.07.006.

3. van Strien NM, Widerøe M, van de Berg WDJ, Uylings HBM. Imaging hippocampal subregions with in vivo MRI: advances and limitations. Nat. Rev. Neurosci. 2012;13:70. doi: 10.1038/nrn3085-c1.

4. Giuliano A, Donatelli G, Cosottini M, Tosetti M, Retico A, Fantacci ME. Hippocampal subfields at ultra high field MRI: An overview of segmentation and measurement methods. Hippocampus 2017;27:481–494. doi: 10.1002/hipo.22717.

5. Zeineh MM, Parekh MB, Zaharchuk G, Su JH, Rosenberg J, Fischbein NJ, Rutt BK. Ultrahigh-Resolution Imaging of the Human Brain with Phase-Cycled Balanced Steady-State Free Precession at 7 T. Invest. Radiol. 2014;49:278–289. doi: 10.1097/RLI.0000000000000015.

6. Prudent V, Kumar A, Liu S, Wiggins G, Malaspina D, Gonen O. Human hippocampal subfields in young adults at 7.0 T: feasibility of imaging. Radiology 2010;254:900–6. doi: 10.1148/radiol.09090897.

7. Federau C, Gallichan D. Motion-Correction Enabled Ultra-High Resolution In-Vivo 7T-MRI of the Brain. PLoS One 2016;11:e0154974. doi: 10.1371/journal.pone.0154974.

8. Rieseberg S, Frahm J, Finsterbusch J. Two-dimensional spatially-selective RF excitation pulses in echo-planar imaging. Magn. Reson. Med. 2002;47:1186–1193. doi: 10.1002/mrm.10157.

9. Saritas EU, Cunningham CH, Lee JH, Han ET, Nishimura DG. DWI of the spinal cord with reduced FOV single-shot EPI. Magn. Reson. Med. 2008;60:468–473. doi: 10.1002/mrm.21640.

10. Finsterbusch J. Functional neuroimaging of inner fields-of-view with 2D-selective RF excitations. Magn. Reson. Imaging 2013. doi: 10.1016/j.mri.2013.03.005.

11. Heidemann RM, Anwander A, Feiweier T, Knösche TR, Turner R. k-space and q-space: combining ultra-high spatial and angular resolution in diffusion imaging using ZOOPPA at 7 T. Neuroimage 2012;60:967–78. doi: 10.1016/j.neuroimage.2011.12.081.

12. Mooiweer R, Sbrizzi A, Raaijmakers AJE, van den Berg CAT, Luijten PR, Hoogduin H. Combining a reduced field of excitation with SENSE-based parallel imaging for maximum imaging efficiency. Magn. Reson. Med. 2016;0:1–9. doi: 10.1002/mrm.26346.

13. Mooiweer R, Sbrizzi A, El Aidi H, Eikendal ALM, Raaijmakers A, Visser F, van den Berg CAT, Leiner T, Luijten PR, Hoogduin H. Fast 3D isotropic imaging of the aortic vessel wall by application of 2D spatially selective excitation and a new way of inversion recovery for black blood imaging. Magn. Reson. Med. 2016;75:547–555. doi: 10.1002/mrm.25599.

14. Cho Z, Han J, Hwang S, Kim D, Kim K-N, Kim N-B, Kim SJ, Chi J, Park C, Kim Y. Quantitative analysis of the hippocampus using images obtained from 7.0 T MRI. Neuroimage 2010;49:2134–2140. doi: 10.1016/j.neuroimage.2009.11.002.

15. Zwanenburg JJM, Versluis MJ, Luijten PR, Petridou N. Fast high resolution whole brain T2* weighted imaging using echo planar imaging at 7T. Neuroimage 2011;56:1902–1907. doi: 10.1016/j.neuroimage.2011.03.046.

16. Trattnig S, Springer E, Bogner W, Hangel G, Strasser B, Dymerska B, Cardoso PL, Robinson SD. Key clinical benefits of neuroimaging at 7T. Neuroimage 2016. doi: 10.1016/j.neuroimage.2016.11.031.

17. van der Kolk AG, Hendrikse J, Brundel M, Biessels GJ, Smit EJ, Visser F, Luijten PR, Zwanenburg JJM. Multi-sequence whole-brain intracranial vessel wall imaging at 7.0 tesla. Eur. Radiol. 2013;23:2996–3004. doi: 10.1007/s00330-013-2905-z.

18. van der Zwaag W, Schäfer A, Marques JP, Turner R, Trampel R. Recent applications of UHF-MRI in the study of human brain function and structure: a review. NMR Biomed. 2016;29:1274–1288. doi: 10.1002/nbm.3275.

19. Mooiweer R, Sbrizzi A, Visser F, van den Berg C a T, Luijten PR, Hoogduin H. High resolution imaging of the hippocampus with spatially selective excitation and a reduced FOV readout at 7T. In: Proc. Intl. Soc. Mag. Reson. Med. Vol. 21. ; 2013. p. 3016.

20. Grissom W, Yip C, Zhang Z, Stenger VA, Fessler J a, Noll DC. Spatial domain method for the design of RF pulses in multicoil parallel excitation. Magn. Reson. Med. 2006;56:620–629. doi: 10.1002/mrm.20978.

21. Sbrizzi A, Hoogduin H, Lagendijk JJ, Luijten P, Sleijpen GLG, van den Berg C a T. Time efficient design of multi dimensional RF pulses: Application of a multi shift CGLS algorithm. Magn. Reson. Med. 2011;66:879–885. doi: 10.1002/mrm.22863.

22. Nehrke K, Börnert P. DREAM-a novel approach for robust, ultrafast, multislice B_1 mapping. Magn. Reson. Med. 2012;68:1517–1526. doi: 10.1002/mrm.24158.

23. Hoogduin H, Mooiweer R, Mens G, Hajnal J V, Luijten P, Malik SJ. Initial experience with SPIral Non Selective (SPINS) RF pulses for homogeneous excitation at 7T. In: Proc. Intl. Soc. Mag. Reson. Med. ; 2014. p. 4914.

24. Lee D, Lustig M, Grissom WA, Pauly JM. Time-optimal design for multidimensional and parallel transmit variable-rate selective excitation. Magn. Reson. Med. 2009;61:1471–1479. doi: 10.1002/mrm.21950.

25. Lee D, Grissom W a., Lustig M, Kerr AB, Stang PP, Pauly JM. VERSE-guided numerical

RF pulse design: A fast method for peak RF power control. Magn. Reson. Med. 2012;67:353–362. doi: 10.1002/mrm.23010.

26. Malik SJ, Hajnal J V. Phase relaxed localized excitation pulses for inner volume fast spin echo imaging. Magn. Reson. Med. 2015;3:848–861. doi: 10.1002/mrm.25996.

27. Bonnici HM, Chadwick MJ, Kumaran D, Hassabis D, Weiskopf N, Maguire E a. Multi-voxel pattern analysis in human hippocampal subfields. Front. Hum. Neurosci. 2012;6:1–13. doi: 10.3389/fnhum.2012.00290.

28. Suthana NA, Donix M, Wozny DR, et al. High-resolution 7T fMRI of Human Hippocampal Subfields during Associative Learning. J. Cogn. Neurosci. 2015;27:1194–1206. doi: 10.1162/jocn_a_00772.

29. Wisse LEM, Kuijf HJ, Honingh AM, Wang H, Pluta JB, Das SR, Wolk DA, Zwanenburg JJM, Yushkevich PA, Geerlings MI. Automated Hippocampal Subfield Segmentation at 7T MRI. Am. J. Neuroradiol. 2016. doi: 10.3174/ajnr.A4659.

30. Yushkevich P a, Wang H, Pluta J, Das SR, Craige C, Avants BB, Weiner MW, Mueller S. Nearly automatic segmentation of hippocampal subfields in in vivo focal T2-weighted MRI. Neuroimage 2010;53:1208–24. doi: 10.1016/j.neuroimage.2010.06.040.

31. Theysohn JM, Kraff O, Maderwald S, Schlamann MU, de Greiff A, Forsting M, Ladd SC, Ladd ME, Gizewski ER. The human hippocampus at 7 T-In vivo MRI. Hippocampus 2009;19:1–7. doi: 10.1002/hipo.20487.

32. Santyr BG, Goubran M, Lau JC, et al. Investigation of hippocampal substructures in focal temporal lobe epilepsy with and without hippocampal sclerosis at 7T. J. Magn. Reson. Imaging 2016:1–12. doi: 10.1002/jmri.25447.

33. Thomas BP, Welch EB, Niederhauser BD, Whetsell WO, Anderson AW, Gore JC, Avison MJ, Creasy JL. High-resolution 7T MRI of the human hippocampus in vivo. J. Magn. Reson. Imaging 2008;28:1266–1272. doi: 10.1002/jmri.21576.

34. Parekh MB, Rutt BK, Purcell R, Chen Y, Zeineh MM. Ultra-high resolution in-vivo 7.0T structural imaging of the human hippocampus reveals the endfolial pathway. Neuroimage 2015;112:1–6. doi: 10.1016/j.neuroimage.2015.02.029.

Appendix

Entry #	In-plane resolution (mm x mm)	Through plane resolution (mm)	Voxel volume (nL)	AQ time (minute)
1	0.22 x 0.22	1.5 + 0.5 gap	73	10-12
2	0.38 x 0.38*1.33[2]	0.38*1.33 = 0.51	98	29*2 = 58
3	0.52 x 0.52	0.5	135	4*12 = 48
4	0.35 x 0.35	2.0	245	7:38
4	0.7 x 0.7	0.7	343	9:09
5	0.7 x 0.7	0.7	343	10:15
6	0.4 x 0.5	2.0	400	3:23
7	0.35 x 0.35*1.33	0.35*1.33 = 0.47	77	31*4 = 124
8	0.50 x 0.50	0.65	163	7:23
9	0.58 x 0.43	1.0	249	5:42
10	0.23 x 0.23	10	54	14
11	0.35 x 0.35*1.33[3]	0.35*1.33 = 0.47	76	14:27
12	0.35 x 0.35*1.33	0.35*1.33 = 0.47	77	42
13	0.5 x 0.5	0.5	125	5:50
14	0.5 x 0.5	1.0	250	4:20
15	0.5 x 0.5	1.5	375	12
16	0.8 x 0.8	0.8	512	6:15
17	0.44 x0.44[4]	3	581	4:20
18	0.4 x 0.4[5]	0.4	64	5:11*8 = 41:28

***Table A1 (continues on opposite page)**. Overview of high resolution protocols, up to 7T. All entries were performed on 7T, unless stated otherwise. General brain studies and studies focusing on the hippocampus are included. Resolution numbers are given as they are acquired, without interpolation / zero-filling.*

[2] Point Spread Function broadening due to 3/4 Partial Fourier in both phase encoding directions: 33% increase

[3] 3/4 Partial Fourier

[4] Before interpolation of factor 2

[5] 58% Partial Fourier in both phase encoding directions, 0.33 x 0.33 x 0.4 after zero filling interpolation

Appendix

Entry #	Coverage (FOV, cm)	Contrast type / Method	Year	Ref.
1	17 x 17 x 3.2	2D TSE	2014	(5)
2	19.4 x12.2 x 17.0	T2 3D TSE	2016	(7)
3	20.0 x 17.1 x 5.2	3T, 3D TSE, NSA = 4	2012	(27)
4	22.4 x 100 x 4.2	TSE	2015	(28)
4	17.9 x 17.9 x 18.6	3D T2 TSE	2014	(5)
5	24.9 x 25.0 x 19.0	T2 3D TSE	2016	(29)
6	full FOV[6] x 4.8	4T, TSE	2010	(30)
7	19.3 x 15.4 x 14.6	T1w 3D MP2RAGE	2016	(7)
8	25.6 x 25.6 x 16.6	MPRAGE	2009	(31)
9	14.8 x 22.0 x 17.2	T1 MPRAGE	2016	(32)
10	23.8 x 23.8 x 1.7	T2*2D GRE		(6)
11	17.9 x 20.2 x 2.1	T2* 3D GRE		(14)
12	17.9 x 15.5 x 11.2	T2*3D GRE	2016	(7)
13	24.0 x 19.2 x 15.0[7]	T2* 3D EPI	2014	(15)
14	24.0 x 18.0 x 15.0	SWI (T2* 3D GRE)	2008	(33)
15	12.8 x 18.0 x 12.0	T2* GRE	2016	(32)
16	20 x 20 x 14.9	3D GRE	2014	(5)
17	22.6 x 17.3 x 4.5	T2*	2009	(31)
18	17.0 x 17.0 x 19.2	3D bSSPP	2014	(5,34)

***Table A1 (continued from opposite page)**. Overview of high resolution protocols, up to 7T. All entries were performed on 7T, unless stated otherwise. General brain studies and studies focusing on the hippocampus are included. Resolution numbers are given as they are acquired, without interpolation / zero-filling.*

[6] Size of FOV not specified

[7] 1.28 slice over sampling factor

Chapter 6

Summary and general discussion

Summary

The overall aim of this work has been to study 3D structural imaging with tailored 2D spatially selective excitation pulses. We focused on spiral excitation trajectories that can reduce the field of excitation in two dimensions without creating excitation side lobes. In these two directions, the number of phase encoding steps could be reduced compared to nonselective excitation. The third dimension, in which no restriction is enforced on the excitation, was rapidly encoded using frequency encoding. This approach lent itself well for 3D isotropic imaging.

In Chapter 2, an efficient imaging protocol was developed for 3D imaging of the aorta vessel wall, aimed at improving the detection of atherosclerosis. The nonselective direction of the 2D SSE was aligned with the aorta and an rFOV acquisition was used at isotropic resolution. Some generalizations were applied in the design of the pulses, as measured field maps in the thorax were imperfect and not necessarily representative for the field values down the length of the aorta, which was imaged in a single acquisition. Black blood contrast was generated by partially inverting the magnetization in the heart, before acquisition in the descending aorta. Compared to the standard method (multiple 2D slices) a larger coverage could be imaged at higher resolution. Compared to a similar 3D acquisition without 2D SSE, artifacts from peripheral tissues were reduced.

The standard way to acquire an image with 2D SSE is to use a reduced field of view (rFOV). In Chapter 3 we showed that 2D SSE (or any reduced field of excitation - rFOX) is most efficiently acquired when this is combined with SENSE into rSENSE. With rSENSE, voxels that are not excited are excluded from the parallel imaging reconstruction, improving the reconstruction. Higher acceleration factors are possible than with rFOV or SENSE alone. Moreover, this acceleration technique is not limited to rectangular rFOX shapes, typically associated with rFOV imaging. In-vivo experiments were performed at 7T, using a 32-channel receive coil.

For rSENSE to work, the location of the voxels in the rFOX must be known before the undersampled image is reconstructed. In the first implementation of rSENSE, in Chapter 3 this was done by acquiring the receive coil sensitivity mapping scan with the same 2D SSE pulse as the undersampled image. This increased the length of the calibration more than two-fold. Strategies to bring this calibration time down could help in the applicability of rSENSE.

In Chapter 4 we looked at expanding the applicability of 2D SSE from gradient echo to turbo spin echo (TSE) sequences, a routinely used imaging method. In principle, the excitation selectivity of these sequences can be defined by just the excitation pulse, without adjustments to the refocusing pulse train. This is interesting as in 3D TSE the refocusing train is highly efficient with the use of nonselective pulses of variable flip angles. For the combination of a custom 2D SSE pulse (with PTX) and default refocusing pulses (in quadrature mode), the custom excitation should match the phase of the quadrature mode, as prescribed by the CPMG conditions. We showed how this phase-matching can be achieved, using the phase information of the signals that are used to map the transmit coil sensitivities. In-vivo experiments at 7T confirmed that the CPMG conditions were being met, and that the phase-

matched pulses could still be used in gradient echo sequences. TSE imaging with 2D SSE and rSENSE acceleration was shown, opening up the way for further exploration.

PTX-enabled 2D SSE with rSENSE acceleration was used to image the hippocampus at unprecedented resolution versus imaging time in Chapter 5. Three-dimensional images at 0.35^3 mm^3 isotropic resolution could be achieved in a 10 minute scan time on a 7T MR system. In line with the original rSENSE implementation of Chapter 3, the time needed for calibration was increased.

General discussion

Planning of the rFOX

Planning a 3D acquisition with 2D SSE requires taking into account several factors that are different from planning a conventional excitation. A 2D plane has to be identified on which the field of excitation is to be reduced in both dimensions, keeping in mind that the excitation is unrestricted in the 3rd dimension. Initially, the most obvious geometry would be to limit the rFOX in the plane where surface ratio between the object of interest and the surrounding tissue is at its minimum. Alternatively, one can choose to avoid certain regions that are expected to cause artifacts in the phase encoded imaging directions.

One must also consider whether reliable field maps can be acquired in the plane of 2D SSE, for the most accurate rFOX generation on this slice, and whether the obtained values are representative for other locations along the whole length of the ROI in the 3rd dimension. If this is not the case, approximations to 3D field maps might be used, as was shown in Chapter 2. Furthermore, if acceleration by parallel imaging is to be used (beyond the rFOV limit), one must make sure that there is sufficient variation in receive coil sensitivity.

After an orientation and a slice have been determined on which the 2D SSE is going to be designed, the excitation target can be determined. The target should be sufficiently large to cover the anatomy of interest throughout the orthogonal dimension. The rFOX target planning for the hippocampus and aorta is shown in **Figure 1**.

Shortening of 2D SSE pulses

Shortening of excitation pulses is generally desirable as the resulting excitation would be less affected by T_2* degradation and less susceptible to (local) off-resonances. It could also be directly beneficial to sequences with short TR's that are limited by the long excitation pulse, such as the SENSE reference scan with rFOX in the rSENSE method (as seen in Chapters 3, 4, and 5).

The RF pulses that were generated throughout this work all follow the same general shape (**Figure 2**). The pulses' amplitudes remains low during the first ~60% of the pulse, where the high spatial frequencies are encoded, and amplitudes exceeding half the maximum amplitude are only found in the final ~40%, encoding the center of k-space. This trend suggests that there could be room for reducing the length of these pulses: shorter pulses with higher average amplitudes might be able to achieve the same excitation profile. Such a time-optimization of the excitation pulse could be achieved through the iterative VERSE method [1,2]. In this

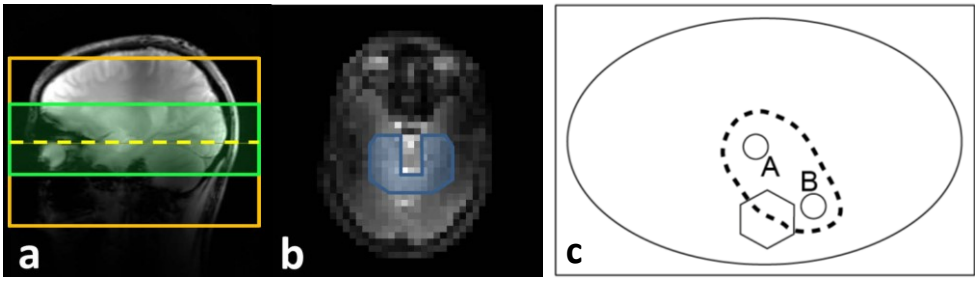

Figure 1. *Planning of the rFOX. The yellow dashed line in localizer image* ***a*** *marks the transverse slice on which the 2D SSE pulse is designed to excite the hippocampus. On image* ***b*** *the excitation target (blue shape) and don't care region (head contour) were defined. The excitation target was determined as an estimated projection of the hippocampus' location across the feet-head direction. The excitation target determination for the aorta is schematically shown in* ***c****, where the ellipse represents the body contour and the hexagon the spine. The target is shown with a dashed line, covering a projection of the location of the aorta transverse slices at different heights: A and B.*

method, individual fragments of the k-space trajectory are stretched and shortened, and RF pulses redesigned, to improve the time-efficiency of the pulse while respecting the hardware limits of the gradient and RF systems. As the spiral-in k-space trajectory is already very time-efficient in covering transmit k-space, any pulse shortening might be paired with an altered k-space trajectory, possibly reducing the fidelity of the excitation pattern.

Another obvious choice to shorten the excitation pulses would be to use k-space undersampling via Transmit SENSE [3,4], which was originally developed with shortening of 2D SSE pulses in mind. It uses the encoding power of the individual transmit coils to mitigate the aliasing effects of undersampling, similar to traditional SENSE [5]. As transmit SENSE operates using a different form of information redundancy than reVERSE, the two techniques should be complementary. We have not used k-space undersampling in our experiments as we limited ourselves to clinically available setups of maximum two transmit channels. These would only offer modest undersampling factors before degrading the excitation pattern. We did however use PTX B_1^+ maps to calculate separate RF pulses per channel (Chapters 3, 4, and 5), without undersampling (Transmit SENSE reduction factor = 1). By including these transmit sensitivities of the individual channels of the birdcage coil, the encoding power was still enhanced with respect to using one B_1^+ map of the two channels combined in a fixed combination (quadrature mode), which should have added to the excitation fidelity.

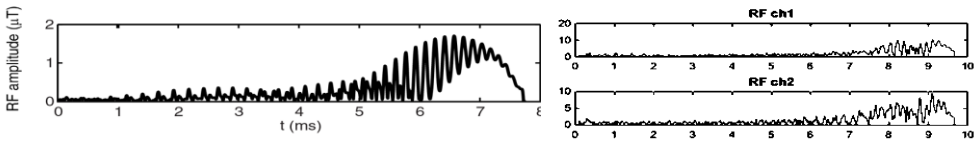

Figure 2. *Amplitudes of RF waveforms that were used for 2D SSE of the aorta in Chapter 2 (****left****) and the hippocampus in Chapter 5 (****right****, 2ch PTX).*

3D SSE pulses

A seemingly natural extension of our work would be to move to 3D-selective excitation pulses, removing the complexities related to the non-restricted excitation direction of 2D SSE. As organs rarely retain their shape along one dimension, 3D SSE could follow an organ's shape in all spatial dimensions, thereby minimizing the rFOX size. This might further improve imaging efficiency and could provide additional artifact suppression. It has also been suggested that by taking into account the measured 3D field information, deviations from the targeted rFOX patterns could be avoided. These can emerge in sequences with 2D SSE as pulses are calculated on a single slice only. However, we have shown that 2D SSE can be quite robust against these through-slice deviations, exemplified by the large-coverage imaging of the aorta in Chapter 2. Several results suggest a similar through-slice consistency in the head: **Figure 3e** in Chapter 4 and **Figure 4** in Chapter 5. Moreover, even if the rFOX pattern is not constant on every slice axial to the unrestricted dimension, the rSENSE method (Chapter 3) can image it efficiently as long as a similar rFOX is measured in the reference scan. This is in contrast to conventional rFOV imaging, where additional signal generation results in aliasing artifacts. Controlling the rFOX in 3D can still be beneficial over 2D, as it provides increased freedom in choosing the directions for frequency encoding , phase encoding, and parallel imaging.

The methods that were used to calculate pulses for 2D SSE are not inherently limited to 2D. Similar numerical optimization in the small tip angle regime can just as well be used for 3D SSE, if an appropriate 3D k-space trajectory is selected [6]. The rSENSE (Chapter 3) and phase-matching (Chapter 4) methods that were developed in this thesis can also be applied. Parallel transmit systems seem to be a necessity for 3D SSE though, as PTX-enabled undersampling factors of 3 to 5.6 were used in the past to bring the pulse length down to 5 and 12.5 ms respectively [6,7]. Additionally, it remains to be seen if the SNR reduction associated with highly shortened acquisitions still leads to useable images.

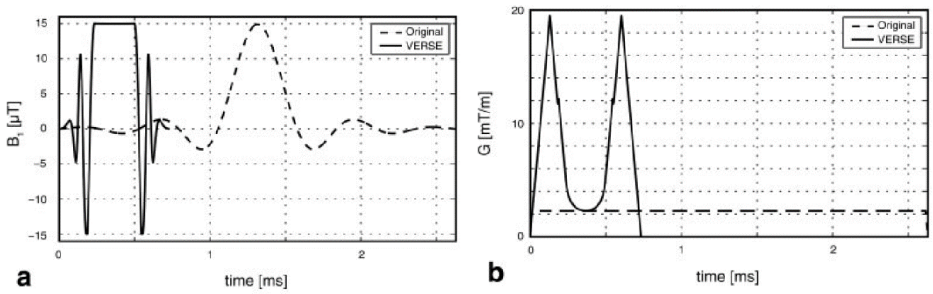

Figure 3. *RF (**a**) and gradient (**b**) pulses of a slab selective excitation, before and after minimum-time VERSE. By increasing the time fraction at which the RF pulse is activated at maximum amplitude, and matching with an increased gradient amplitude, the length of the pulse was reduced to 28% of its original duration. Image reproduced with permission of the rights holder, copyright © 2009 Wiley-Liss, Inc. [1].*

Imaging acceleration using transmit and receive control

Parallel to our study on 2D SSE, another novel excitation approach aiming at faster acquisitions has been developed: Simultaneous Multislice Imaging (SMS). Using a multi-band excitation pulse, several slices are excited simultaneously. The signals originating from these slices are collected as one, after which techniques similar to parallel imaging unfolding are used to disentangle the images of the slices [8]. Fundamentally, this approach does not suffer from the SNR loss associated with rFOV imaging, but consequently it is also not suitable to avoid artifact generation from excitation of unwanted structures. Besides, SMS is a slice-based (2D) imaging technique and therefore not very suitable for 3D isotropic imaging. It is however interesting to see how SMS takes into account excitation and signal reception from a different point of view.

Another novel technique that crosses the boundaries between transmit and receive encoding is controlled aliasing (CAIPI), aimed at reducing the noise that originates from uncertainties in parallel imaging (PI) reconstruction [9]. Here, additional spatial encoding gradients are used to deviate from the standard rectilinear filling of imaging k-space, affecting the locations of signals that collapse onto each other due to undersampling. These locations are chosen for maximum differences in receive coil sensitivities, favorable for parallel imaging unfolding. Undersampling in one direction can even be made to cause aliasing in the other PI direction, when a 3D acquisition is used, allowing greater flexibility in optimizing the aliasing pattern. The same principles could be combined with rSENSE imaging, but given that many voxels are already excluded from PI, the overall effect might be small.

Scan accelerations that utilize the transmit and receive systems benefit from the intrinsically higher RF encoding capacity from coil profiles at higher field strengths. Also, the trend to use larger numbers of coils in parallel can add to the encoding power, on both the transmit and receive side.

Remarks on the use of PTX

PTX is becoming more widely available in new and upgraded high field systems, and for good reasons. The added flexibility in transmit field control is the first line of defense against the inhomogeneity of the excitation at increasingly higher main magnetic field strengths. A simple RF shim optimization can already steer the excitation towards the desired region, in the abdomen for example. More advanced solutions can be obtained through waveform design for the individual channels in combination with appropriate gradients, such as in the spokes [10] and SPINS [11] methods. On the largest time-scale, sequence-level optimization can adjust the RF shims of individual pulses towards homogenization of the signal level over the entire pulse sequence [12].

Instead of seeing the inhomogeneity of the transmit field as something that needs repairing, it can be seen as an encoding power. This has been shown for example in Magnetic Resonance Fingerprinting [13], a novel way of performing MR measurements. Instead of generating images through well-defined encoding steps, the tissue's properties are found by fitting a pseudo-randomly generated signal to a database of pre-calculated signal responses [14]. Perhaps the same principle of creating additional flip angle variation can one day be used in MRF's database-less counterpart: MR-STAT [15].

In the common situation of volume coil excitation without channel-dependent waveforms the global SAR needs to be restricted to prevent excessive heating in patients, according to the international safety standards [16]. Global SAR can directly be controlled through the overall RF power and is effectively dealt with on clinically approved MR scanners. When local transmit coils are used, the power deposition in small tissue volumes must also be understood and monitored: local SAR. This is also required when the independent channels of a volume coil are used for PTX. It is becoming increasingly clear, however, that a good understanding of PTX is not only crucial to monitoring the (local) SAR, but can even be used to reduce it [17]. SAR reduction can be used to shorten the scan times of existing applications, in cases where the repetition times are limited because of their SAR levels [18]. The inclusion of local SAR in a pulse or sequence optimization algorithm can be quite time-consuming, due to the large number of small subvolumes that make up a body model. This can be speed up by using virtual observation points [19]; voxels that respond similarly in electromagnetic modeling are grouped together and evaluated as one.

Concluding remarks on the applicability of 2D SSE

The promise of 2D SSE has always been to allow more detailed resolution and/or shorter acquisition times, which was explored for structural imaging in this thesis. Our studies confirmed that indeed a better ratio of resolution versus imaging time can be obtained than with conventional methods. However, as current structural imaging protocols are generally artifact-free, and 2D parallel imaging can also be used for acceleration of 3D sequences, the additional advantages of 2D SSE are not always immediately clear. In functional imaging, where 2D SSE has been shown beneficial in multiple occasions, the detrimental effects of single shot acquisitions are much more pronounced, and benefits of 2D SSE are more obvious. The expanded understanding of rFOX with parallel imaging, and phase control in pulse design, might be used to further advance the developments in this area.

The unique advantage of 2D SSE for structural imaging is its capability to avoid artifacts that originate outside the region of interest, allowing scan orientations that might otherwise not be feasible. With this in mind, 2D SSE can serve a niche where specific structures are studied, the surrounding tissue is of no interest at all and actually impairing the optimal acquisition of the object of interest. Currently, however, the effort to implement 2D SSE are considerable both in practical and technical sense. Integration of tailored pulse generation directly into the software driving the MRI scanner can take away part of these hurdles. With more integrated rFOX planning facilities, and following the guidelines described at the beginning of this chapter, experiments with 2D SSE could enter a new phase where the technique's merits in clinical and research settings can be studied with increased user-friendliness and accuracy.

References

1. Lee D, Lustig M, Grissom WA, Pauly JM. Time-optimal design for multidimensional and parallel transmit variable-rate selective excitation. Magn. Reson. Med. 2009;61:1471–1479. doi: 10.1002/mrm.21950.

2. Lee D, Grissom W a., Lustig M, Kerr AB, Stang PP, Pauly JM. VERSE-guided numerical RF pulse design: A fast method for peak RF power control. Magn. Reson. Med. 2012;67:353–362. doi: 10.1002/mrm.23010.

3. Katscher U, Börnert P, Leussler C, van den Brink JS. Transmit SENSE. Magn. Reson. Med. 2003;49:144–150. doi: 10.1002/mrm.10353.

4. Grissom W, Yip C, Zhang Z, Stenger VA, Fessler J a, Noll DC. Spatial domain method for the design of RF pulses in multicoil parallel excitation. Magn. Reson. Med. 2006;56:620–629. doi: 10.1002/mrm.20978.

5. Pruessmann KP, Weiger M, Scheidegger MB, Boesiger P. SENSE: sensitivity encoding for fast MRI. Magn. Reson. Med. 1999;42:952–62.

6. Schneider JT, Kalayciyan R, Haas M, Herrmann SR, Ruhm W, Hennig J, Ullmann P. Inner-volume imaging in vivo using three-dimensional parallel spatially selective excitation. Magn. Reson. Med. 2013;69:1367–1378. doi: 10.1002/mrm.24381.

7. Malik SJ, Hajnal J V. Phase relaxed localized excitation pulses for inner volume fast spin echo imaging. Magn. Reson. Med. 2015;3:848–861. doi: 10.1002/mrm.25996.

8. Larkman DJ, Hajnal J V., Herlihy AH, Coutts GA, Young IR, Ehnholm G. Use of multicoil arrays for separation of signal from multiple slices simultaneously excited. J. Magn. Reson. Imaging 2001;13:313–317. doi: 10.1002/1522-2586(200102)13:2<313::AID-JMRI1045>3.0.CO;2-W.

9. Breuer F a, Blaimer M, Mueller MF, Seiberlich N, Heidemann RM, Griswold M a, Jakob PM. Controlled aliasing in volumetric parallel imaging (2D CAIPIRINHA). Magn. Reson. Med. 2006;55:549–556. doi: 10.1002/mrm.20787.

10. Grissom WA, Khalighi MM, Sacolick LI, Rutt BK, Vogel MW. Small-tip-angle spokes pulse design using interleaved greedy and local optimization methods. Magn. Reson. Med. 2012;68:1553–1562. doi: 10.1002/mrm.24165.

11. Malik SJ, Keihaninejad S, Hammers A, Hajnal J V. Tailored excitation in 3D with spiral nonselective (SPINS) RF pulses. Magn. Reson. Med. 2012;67:1303–1315. doi: 10.1002/mrm.23118.

12. Malik SJ, Beqiri A, Padormo F, Hajnal J V. Direct signal control of the steady-state response of 3D-FSE sequences. Magn. Reson. Med. 2015;73:951–963. doi: 10.1002/mrm.25192.

13. Cloos MA, Knoll F, Zhao T, Block K, Bruno M, Wiggins C, Sodickson D. Multiparamatric imaging with heterogenous radiofrequency fields. Nat. Commun. 2016;in press:1–10. doi: 10.1038/ncomms12445.

14. Ma D, Gulani V, Seiberlich N, Liu K, Sunshine JL, Duerk JL, Griswold MA. Magnetic resonance fingerprinting. Nature 2013;495:187–192. doi: 10.1038/nature11971.

15. Sbrizzi A, van der Heide O, Cloos M, van der Toorn A, Hoogduin H, Luijten PR, Berg CAT van den. Fast quantitative MRI as a nonlinear tomography problem. Magn. Reson. Imaging 2017;46:56–63. doi: 10.1016/j.mri.2017.10.015.

16. International, Commission E. IEC. Medical electrical equipment. Part 2–33: particular requirements for the safety of magnetic resonance equipment for medical diagnosis. 2015.

17. Sbrizzi A, Hoogduin H, Lagendijk JJ, Luijten P, Sleijpen GLG, van den Berg C a T. Fast design of local N-gram-specific absorption rate-optimized radiofrequency pulses for parallel

transmit systems. Magn. Reson. Med. 2012;67:824–834. doi: 10.1002/mrm.23049.

18. Beqiri A, Price AN, Padormo F, Hajnal J V., Malik SJ. Extended RF shimming: Sequence-level parallel transmission optimization applied to steady-state free precession MRI of the heart. NMR Biomed. 2017:e3701. doi: 10.1002/nbm.3701.

19. Eichfelder G, Gebhardt M. Local specific absorption rate control for parallel transmission by virtual observation points. Magn. Reson. Med. 2011;66:1468–76. doi: 10.1002/mrm.22927.

Chapter 7

Nederlandse samenvatting

Chapter 7

Dit proefschrift onderzoekt het gebruik van tweedimensionaal-selectieve excitatiepulsen (2D SSE) voor driedimensionale, structurele, beeldvorming. Het onderzoek richtte zich met name op excitatiepulsen met een spiraalvormig excitatiepad, om het excitatieveld in twee richtingen te beperken zonder dat daarbij secundaire banden geëxciteerd worden. In deze twee richtingen kon voor de beeldvorming het aantal fasecoderingsstappen verlaagd worden, vergeleken met niet-selectieve excitatie. De derde dimensie, waarin de excitatie geen beperking is opgelegd, kon snel gecodeerd worden door middel van frequentiecodering. Deze aanpak was zeer geschikt voor 3D isotrope beeldvorming.

In hoofdstuk 2 werd een efficiënt afbeeldingsprotocol ontwikkeld voor het 3D afbeelden van de vaatwand van de aorta, gericht op een verbeterde opsporing van aderverkalking. De niet-selectieve richting van 2D SSE werd langs de lange as van de aorta gericht en een gereduceerd afbeeldingsveld (‘reduced field of view’ – rFOV) kon worden toegepast in de andere twee richtingen. Een isotrope resolutie kon worden verkregen. Enige veralgemeniseringen werden toegepast tijdens het ontwerpen van de pulsen, aangezien de gemeten velddistributies in de thorax imperfecties vertoonden en niet noodzakelijkerwijs de veldwaarden beschreven die langs de gehele lengte van de aorta - welke in een enkele opname afgebeeld werd- gevonden kunnen worden. Zwart bloed contrast werd bereikt door de magnetisatie in het hart gedeeltelijk te inverteren, voordat deze afgebeeld werd in de neerdalende aorta. Vergeleken met de standaard methode (meerdere 2D plakken) kon een groter bereik worden afgebeeld, met een hogere resolutie. In vergelijking met een overeenkomstige 3D opname zonder 2D SSE kon van perifeer weefsel afkomstige beeldverstoringen worden verminderd.

De gebruikelijke manier om een afbeelding te vormen met 2D SSE is door een rFOV van overeenkomstige afmetingen te specificeren. Hoofdstuk 3 laat echter zien dat 2D SSE (of elk ander gereduceerd excitatieveld (‘reduced field of excitation’ – rFOX)) het meest efficiënt afgebeeld kan worden wanneer dit gecombineerd word met SENSE in rSENSE. In de rSENSE methode worden voxels die niet geëxciteerd worden vermeden in de parallelle-opname-afbeeldingsreconstructie, waardoor deze reconstructie verbeterd wordt. Hogere versnellingsfactoren zijn mogelijk dan wanneer enkel rFOV of SENSE toegepast worden. Deze versnellingstechniek is bovendien niet beperkt tot rechthoekige rFOX-vormen, welke veelal met rFOV geassocieerd worden. In-vivo-experimenten werden op 7T uitgevoerd, gebruikmakend van een 32-kanaals ontvangstspoel.

De locatie van de voxels die zich binnen het rFOX bevinden moeten in de rSENSE-methode bekend zijn vóórdat het onvoldoende bemonsterd beeld gereconstrueerd kan worden. In de eerste implementatie van rSENSE, in hoofdstuk 3, wordt dit bewerkstelligd door de sequentie die de gevoeligheid van de ontvangstspoel meet uit te voeren met dezelfde 2D SSE puls die in de onvoldoende bemonsterde opname gebruikt word. Hierdoor werd de duur van deze kalibratie meer dan verdubbeld. Methodes om de duur van de kalibratie te verkorten zouden de toepasbaarheid rSENSE kunnen vergroten.

Hoofdstuk 4 beschouwt de uitbreiding van 2D SSE-toepassingen van gradiënt echo naar turbo spin echo (TSE) sequenties, een veelgebruikte afbeeldingsmethode. In principe kan de excitatieselectiviteit in deze sequentie door enkel de excitatiepuls bepaald worden, zonder dat de daarop volgende refocusseringspulstrein aangepast hoeft te worden. Dit is van belang, aangezien in 3D TSE de refocusseringspulstrein erg efficiënt is door het gebruik van niet-

selectieve pulsen en variabele fliphoeken. Om gepersonaliseerde 2D SSE pulsen (waarbij van parallelle zendspoelen ('parallel transmit'- PTX) gebruikgemaakt wordt) te combineren met standaard refocusseringspulsen (welke in kwadratuurmodus worden uitgezonden) zal de gepersonaliseerde excitatie het fasepatroon van de kwadratuurmodus moeten volgen, zoals voorgeschreven wordt door de CPMG-voorwaarden. Wij hebben aangetoond hoe deze fase-paring verkregen kan worden, daarbij gebruikmakend van de fase-informatie van de signalen die gebruikt worden om de gevoeligheid van de zendspoelen te meten. Door middel van in-vivo experimenten, uitgevoerd op 7T, werd bevestigd dat aan de CPMG-voorwaarden voldaan werd en dat de pulsen met fase-paring in ongewijzigde vorm ook gebruikt konden worden in gradiënt echo sequenties. TSE beeldvorming met 2D SSE en rSENSE-versnelling kon worden getoond, de weg vrijmakend voor verder onderzoek.

In hoofdstuk 5 werd van PTX gebruikmakende 2D SSE in combinatie met rSENSE-versnelling gebruikt om de hippocampus af te beelden, in een niet eerder vertoonde verhouding van resolutie en scantijd. Driedimensionale afbeeldingen met een isotrope resolutie van 0.35^3 mm^3 konden worden verkregen in een scantijd van 10 minuten, op een 7T MRI scanner. Overeenkomstig met de originele rSENSE implementatie van hoofdstuk 3 was de tijd die nodig was voor kalibratie toegenomen.

Afsluitende opmerkingen aangaande de toepasbaarheid van 2D SSE

Van 2D SSE werd altijd verwacht dat het een meer gedetailleerde resolutie en/of kortere scantijd mogelijk kan maken, wat in dit proefschrift onderzocht is voor structurele beeldvorming. Ons onderzoek bevestigde dat inderdaad een betere verhouding van resolutie per scantijd verkregen kon worden, vergeleken met conventionele methodes. Echter, aangezien de huidige protocollen voor structurele beeldvorming over het algemeen geen beeldverstoringen vertonen, en 2D parallelle opnames (zoals bijvoorbeeld 'sensitivity encoding'- SENSE) ook gebruikt kan worden om 3D sequenties te versnellen, is de toegevoegde waarde van 2D SSE niet altijd meteen duidelijk. In functionele beeldvorming, waar meermaals is aangetoond dat 2D SSE voordelen biedt, zijn de schadelijke effecten van opnames in een enkel schot veel meer aanwezig en is het nut van 2D SSE meer voor de hand liggend. Het vergrootte begrip van de combinatie van 2D SSE met parallelle opnames, en fase-paring in het ontwerp van de pulsen, zouden gebruikt kunnen worden voor verdere ontwikkelingen in dit toepassingsgebied.

Het unieke voordeel van 2D SSE in structurele beeldvorming is dat het beeldverstoringen kan voorkomen die buiten het interessegebied veroorzaakt worden. Hierdoor kunnen scanrichtingen gebruikt worden die anders niet mogelijk zijn. Dit in overweging nemende kan 2D SSE een niche bedienen waar specifieke structuren bestudeerd worden waarbij het omliggende weefsel niet van belang is en zelfs een geoptimaliseerde beeldvorming van het interessegebied in de weg staat. In de huidige situatie kost het echter aanzienlijke moeite om 2D SSE toe te passen, zowel op praktisch als op technisch gebied. Een deel van deze belemmeringen zouden weggenomen kunnen worden door het creëren van de gepersonaliseerde pulsen te integreren in de software die de MRI scanner aanstuurt. Met een meer geïntegreerde rFOX planning, en met inachtname van de adviezen die in het vorige hoofdstuk beschreven zijn, zouden experimenten met 2D SSE een nieuwe fase in kunnen gaan. De baten van de techniek in klinische en onderzoeksgerelateerde situaties zouden met een groter gebruikersgemak en toegenomen nauwkeurigheid onderzocht kunnen worden.

List of publications

Journal articles

El-Dardiry, R.G.S., **Mooiweer, R**., and Lagendijk, A., *Experimental phase diagram for random laser spectra*, New Journal of Physics (2012), 14: 113031

Mooiweer, R., Sbrizzi, A., El Aidi, H., Eikendal, A. L.M., Raaijmakers, A., Visser, F., van den Berg, C. A.T., Leiner, T., Luijten, P. R. and Hoogduin, H., *Fast 3D isotropic imaging of the aortic vessel wall by application of 2D spatially selective excitation and a new way of inversion recovery for black blood imaging*, Magnetic Resonance in Medicine (2016), 75: 547–555

Mooiweer, R., Sbrizzi, A., Raaijmakers, A. J.E., van den Berg, C. A.T., Luijten, P. R. and Hoogduin, H., *Combining a reduced field of excitation with SENSE-based parallel imaging for maximum imaging efficiency*, Magnetic Resonance in Medicine (2017), 78: 88–96

Çavuşoğlu M., **Mooiweer R**., Pruessmann K.P., *Malik S.J., VERSE-guided parallel RF excitations using dynamic field correction*, NMR in Biomedicine (2017), 30:e3697

Ronald Mooiweer, Alessandro Sbrizzi, Alexander J.E. Raaijmakers, Cornelis A.T. van den Berg, Peter R. Luijten, Hans Hoogduin, *Phase matched RF pulse design for imaging a reduced field of excitation with a fast TSE acquisition*, submitted for publication

Ronald Mooiweer, Alessandro Sbrizzi, Alexander J.E. Raaijmakers, Nico A.T. van den Berg, Peter R. Luijten, Hans Hoogduin, *Ultra-high isotropic resolution imaging of the hippocampus through a reduced field of excitation*, submitted for publication

Conference proceedings

Ronald Mooiweer, Alessandro Sbrizzi, Cornelis A. T. van den Berg, Fredy Visser, Peter Luijten, Mark R. Stoesz, Paul Harvey, Giel Mens, Hans Hoogduin, *Initial in vivo experiments with spatially selective RF excitation on a clinical 3T scanner*, Proc. ESMRMB Lisbon 2012

Ronald Mooiweer, Alessandro Sbrizzi, Fredy Visser, Cornelis A. T. van den Berg, Peter R. Luijten, and Hans Hoogduin, *High Resolution Imaging of the Hippocampus with Spatially Selective Excitation & a Reduced FOV Readout at 7T*, Proc. ISMRM Ultra High Field Workshop Noordwijk aan Zee 2013

Ronald Mooiweer, Alessandro Sbrizzi, Fredy Visser, Cornelis A.T. van den Berg, Peter R. Luijten, Hans Hoogduin, *High Resolution Imaging of the Hippocampus with Spatially Selective Excitation and a Reduced FOV Readout at 7T*, Proc. Intl. Soc. Mag. Reson. Med. 21 (2013): 3016.

Ronald Mooiweer, Alessandro Sbrizzi, Hamza el Aidi, Cornelis A.T. van den Berg, Fredy Visser, Tim Leiner, Peter R. Luijten, Hans Hoogduin, *Spatially Selective Excitation Applied to Aortic Vessel Wall Imaging*, Proc. Intl. Soc. Mag. Reson. Med. 21 (2013): 4244.

Hans Hoogduin, **Ronald Mooiweer**, Giel Mens, Joseph V Hajnal, Peter Luijten, and Shaihan J Malik, *Initial experience with SPIral Non Selective (SPINS) RF pulses for homogeneous excitation at 7T*, Proc. Intl. Soc. Mag. Reson. Med. 22 (2014): 4914.

Tessa N van de Lindt, **Ronald Mooiweer**, Peter R Luijten, Dennis W J Klomp, and Vincent O Boer, *Fast water suppression for high resolution MRSI by frequency selective spokes pulses at 7T*, Proc. Intl. Soc. Mag. Reson. Med. 22 (2014): 3766

Ronald Mooiweer, Alessandro Sbrizzi, Hamza El Aidi, Alexander Raaijmakers, Cornelis A. T. van den Berg, Fredy Visser, Tim Leiner, Peter R. Luijten, and Hans Hoogduin, *Large coverage 3D black blood imaging of the aorta using 2D spatially selective excitation and a reduced field of view readout*., 26th Annual Conference of the International MRA Working Group (2014)

Mooiweer, Ronald, Sbrizzi, Alessandro, Raaijmakers, Alexander, van den Berg, Cornelis A. T., Luijten, Peter R., Hoogduin, Hans, *Squashing the g-factor: Ultra high scan acceleration factors in reduced Field of Excitation imaging*, Proc. Intl. Soc. Mag. Reson. Med. 23 (2015): 3620.

Mooiweer, Ronald, Sbrizzi, Alessandro, Raaijmakers, Alexander, van den Berg, Cornelis A. T., Luijten, Peter R., Hoogduin, Hans, *Squashing the g-factor: Ultra high scan acceleration factors in reduced Field of Excitation imaging*, ISMRM Benelux Chapter Meeting (2015) Ghent BE

Restivo, Matthew, **Mooiweer, Ronald**, van den Berg, C.A.T, Raaijmakers, Alexander, Simonis, Frank, Luijten, Peter R., Hoogduin, Hans, *A Phantom Designed Specifically for Local SAR Validation*, Proc. Intl. Soc. Mag. Reson. Med. 23 (2015): 3219.

Ronald Mooiweer, Shaihan J Malik, Joseph V Hajnal, Nico van den Berg, Peter R Luijten, and Hans Hoogduin, *SPINS excitation versus DSC dynamic RF shimming for homogenising high field strength TSE imaging*, Proc. Intl. Soc. Mag. Reson. Med. 24 (2016): 1893

Ronald Mooiweer, Joseph V Hajnal, and Shaihan J Malik, *A single-channel universal SPINS pulse for calibration-free homogeneous excitation without PTX*, Proc. Intl. Soc. Mag. Reson. Med. 25 (2017): 0390

Felipe Godinez, Joseph Hajnal, Greig Scott, **Ronald Mooiweer**, Francesco Padormo, and Shaihan Malik, *Tissue and device visualization using parallel transmission for interventional MRI*, Proc. Intl. Soc. Mag. Reson. Med. 25 (2017): 0740

Felipe Godinez, Joseph Hajnal, Greig Scott, **Ronald Mooiweer**, and Shaihan Malik, *'Pulse-acquire' method for obtaining the guidewire coupling modes of a PTx transmit array*, Proc. Intl. Soc. Mag. Reson. Med. 25 (2017): 5554

Acknowledgements

There have are many people that have been very supportive, in many different ways, during this adventurous time called ‘doing a PhD’. First and foremost: Hans. From my first day and first time at a scanner, via weekly meetings, many more scan sessions, endless manuscript iterations and, in the end, regular Skype sessions, you’ve been there with me through it all. Thank you so much for your never-ending support. Nico, my second supervisor, together with Alessandro and Alexander of our Multix team, thank you for the countless discussions in which we sharpened our ideas and deepened our understanding of MR physics and - almost more often - linear algebra. I would like to thank Peter for putting together the great collection of people that make up the 7T group as well as making the official bits of my PhD possible.

Tim, Hamza, and Anouk: your enthusiasm for trying out our exotic new method for imaging the aorta was very motivational to me. Also many thanks for the help with scanning, scoring, and teaching this physics kid how to use an ECG. Here I also would like to mention the support and practical advice offered by the team of technicians, especially Niels and Guus. In fact, there have been many people at the UMCU that have been fantastically supportive. Starting with Sylvia and extending through other offices like the ´bedrijfsbureau´ and IT support.

Of course I will remember the great times we’ve had with everyone involved in the 7T group and adjoining groups: drinks at The Basket, chilled out BBQs, cosy Christmas dinners, and enjoying the many conferences I’ve had the pleasure to attend. I believe there even was some scientific help now and then. There´s no way I can make a definitive list, but here´s an attempt: Dennis, Fredy, Jaco, Natalia, Jannie, Jeroen, Martijn, Vincent, Wouter, Anouk, Anja, Alexandra, Esben, Wybe, Bertine, Catalina, Mariska, Ingmar, Mark, Michel, Irene, Hanke, Tijl, Joep, Frank, Tim, Bjorn, Anita, Nikki, Erwin, Roos, Wieke, Lennart, Lisa, Alex, Vitaliy, Matthew, Stefano, Tessa, Mariska, Janot, Arjan, etc, etc: thank you and I hope to see you soon again!

In London, I would like to thank Jo and Shaihan for taking me in into their fantastic group. Arian, Fran, Rui, Samy, and everyone else at perinatal imaging: thank you for the support, nonsensical tea/coffee brakes, and legendary pub nights at the Walrus. Of course, also a very big thank you to all the volunteers in Utrecht and London, many of them colleagues and friends, who had their various body parts scanned in the name of science.

On a more personal level I would like to thank my family, friends, and flat mates for continuous support and distractions. A special mention for the nerds of the weekly lunch-followed-by-coffee breaks: Tristan, Marcel, and Pim. Three of us ended up doing a PhD in the same hospital, the fourth came because he could.

Ben, Mieke, Laurens&Eva: thank you for everything!

My dear Sila. Finishing the thesis wasn’t always easy for me, but luckily I had you by my side: thank you for sticking by me! I’m looking forward to the good times we can now enjoy.

Curriculum vitae

Ronald was born in Zwolle, The Netherlands, on September 20th 1987. His family moved to Herwen, from where he attended the Liemers College in Zevenaar. After obtaining his VWO diploma in 2005 he studied “Physics and Astronomy” at Utrecht University, from which he received his Bachelor’s degree in 2010. During his Master’s “Nanomaterials: Chemistry and Physics” at the same university, he studied for one semester at Copenhagen University in Denmark as part of the Erasmus exchange programme. He carried out his year-long Master’s research project, on random scattering lasers, at the FOM Institute for Atomic and Molecular Physics (AMOLF) in Amsterdam.

In 2012, Ronald started his PhD in the 7T group of Professor Peter Luijten at the University Medical Center Utrecht. Under supervision of Hans Hoogduin and Nico van den Berg, he studied the use of 2D spatially selective excitation for structural imaging at high field strength MRI. He did an internship in 2015 in the parallel transmit MRI group of Professor Jo Hajnal and Shaihan Malik at King’s College London (KCL). He returned to KCL in 2016 to work as a Research Assistant in the same group, now exploring universal excitation pulses. From London he finished writing this thesis, in which the most important results of his PhD are presented. Ronald is now a Research Associate in the Biomedical Engineering Department of KCL, investigating MRI guidance for cardiac interventions.

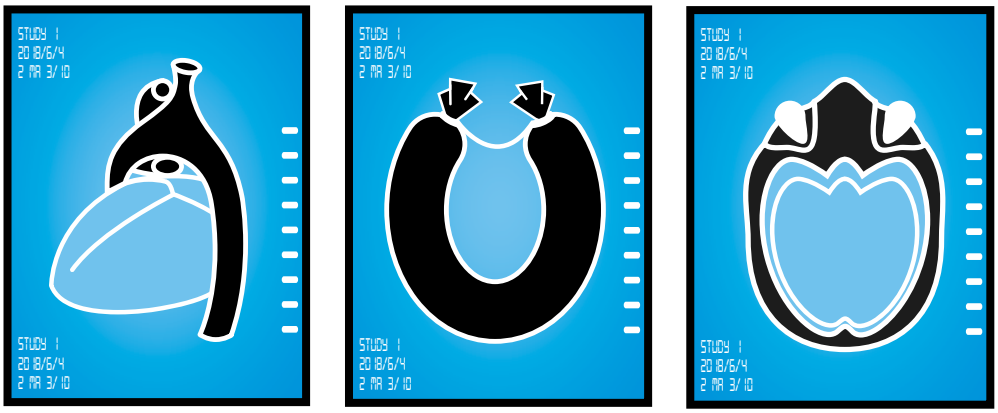

Brain Center Rudolf Magnus
Universiteit Utrecht
ISBN 978-94-6299-933-6